THE BELL SYSTEM TECHNICAL JOURNAL

An Analysis of Inherent Distortion in Asynchronous Frequency-Shift Modulators

By L. R. BOWYER and W. H. HIGHLEYMAN

(Manuscript received May 15, 1962)

In many commonly used frequency-shift modulators, a phase error occurs at the time of switching. If a demodulator is used which utilizes only the zero-crossing information, then this phase error will cause time jitter in the received data transitions.

The magnitude of the peak time jitter for various modulators is derived, assuming an ideal zero-crossing detector. The modulators considered include the reactance tube and variable reactance modulators, the basic switched reactance modulators, and the multivibrator modulator. It is found that the switched reactance modulators cause the most jitter, and that the multivibrator modulator may be designed to cause as small a jitter as desired. The theory agrees well with some experimental measurements made on existing data sets, which show that this jitter accounts for most of the back-to-back data distortion in many wideband data systems.

Finally, a set of sufficient conditions is derived for jitter-free frequency-shift modulation, and an implementation of a modulator satisfying these conditions is described.

I. SUMMARY

For the reader who may be more interested in the results of this paper than in their derivation, the following summary is presented.

Data communication systems using frequency-shift channels commonly suffer from a form of fortuitous distortion called jitter. This is

particularly significant in systems in which the bit rate is not small compared to the carrier frequency. Jitter is the variation about the correct position of the transition between marking and spacing signals at the receiver output. It is desirable to keep the magnitude of the jitter small compared to the bit length.

This paper studies the jitter which is inherent in various types of frequency-shift modulators. For purposes of this analysis, it is assumed that the data source is jitter free, that the transmission channel is distortionless, and that the receiver is an ideal zero-crossing detector. The modulators to be studied shift frequency instantaneously at the time the data source goes through a mark-space transition. In an ideal frequency-shift modulator, this shift in frequency takes place with phase continuity. However, many commonly used modulators do not maintain phase continuity at the switching instant.

In an ideal frequency demodulator (i.e., one whose output is proportional to the instantaneous rate of change of phase at its input), such a phase discontinuity would not cause a time error in the output data transition; it would simply cause an impulse to be added at the time of transition to the otherwise correct transition. However, most present-day demodulators utilize only the information contained in the zero crossings of the received wave, since the first operation in the receiver is to limit, or clip, the wave. In such a receiver, phase discontinuities at the switching instant in the received wave may indeed cause a time error in the mark-space transition at the receiver output.

Such a receiver is modeled by an ideal zero-crossing detector. (An ideal zero-crossing detector approaches an ideal FM detector as the bandwidth becomes small with respect to the carrier frequency.) The analysis proceeds by first relating the phase error in the received wave to the transition time error at the output of an ideal zero-crossing detector. Then the peak phase error that may occur for each type of modulator is determined, and this is related to the peak time error, or jitter, by the above model.

The frequency-shift modulators to be studied include the switched reactance modulator (in which a reactance is switched into and out of the tank of an oscillator to modify its frequency), the reactance tube modulator (in which the effective output reactance of an active circuit is changed by changing the gain of the active element and this reactance is used to control the frequency of a separate oscillator), the variable reactance oscillator (in which the functions of variable reactance and oscillation are combined into a single active circuit), and the multivibrator.

It is shown that of the LC oscillators, the reactance tube and variable reactance type of oscillators have the minimum jitter. For all cases of practical interest, this time error has a peak value roughly one-twelfth of the period of the frequency midway between the marking and spacing frequencies, and may take on both positive and negative values with respect to the true transition time.

The switched reactance type of oscillators which are analyzed include all four ways of switching a single reactive element into a simple LC tank, i.e., an inductor or a capacitor switched in parallel with, or in series with, the tank. In all cases, the peak jitter is described by the same equation, although there are two distinctly different phenomena giving rise to the jitter. For a transition in one direction, the peak jitter is exactly that obtained with the reactance tube and variable reactance type of modulators. For the opposite transition, however, undesired dc quantities increase the jitter. This increase in jitter is sensitive to bit rate if there is a decay mechanism for the undesired dc quantity. In the worst case, the increase in jitter is almost an order of magnitude over that of the low jitter transition. As the bit rate becomes lower and lower, the peak jitter associated with the worse transition approaches that of the opposite transition.

The peak time error $\tau_{\epsilon m}$ for the various LC modulators is plotted in Fig. 7(a) as a function of the frequency-shift ratio $A = \omega_1/\omega_2 < 1$, where ω_1 and ω_2 are the two modulator frequencies. T_o is the period of the frequency midway between the marking and spacing frequencies. The parameter r applies to the switched reactance modulators. It is the ratio of the bit length to the time constant of the undesired dc quantity.

It is shown that the multivibrator may in principle be designed to be jitter-free. However, practical multivibrators do have some inherent jitter. The amount of jitter is dependent upon a linearity factor which is determined by the multivibrator circuit. The jitter associated with a multivibrator is usually less than the jitter associated with any of the above LC modulators.

In Fig. 13 is shown the peak jitter, $\tau_{\epsilon m}$, for the multivibrator modulator as a function of the frequency-shift ratio A. T_o is as defined in Fig. 7. The linearity factor, β, is the ratio of the supply voltage to the maximum control (voltage V_s and V_c respectively in Fig. 10a). The maximum control voltage corresponds to the highest frequency.

These theoretical results are supported by experimental jitter measurements made on various types of voice band data sets, as summarized in Table I. The agreement with the theory is good.

Finally, it is shown that a sufficient condition for jitter-free frequency-

shift modulation (when using a zero-crossing detector) is to switch the parameters of an oscillating tank circuit in such a way that

1. the tank current and voltage are maintained at the instant of switching, and

2. the characteristic impedance of the tank is held constant.

A means for implementing such an oscillator is described using a pair of variable reactance oscillators in a balanced arrangement. Some experimental waveforms for this circuit are shown in Fig. 16.

II. INTRODUCTION

A large part of present-day data communications systems utilize binary frequency-shift channels for transmission. In such systems, particularly in the wideband systems (i.e., systems in which the bit rate is not small compared to the carrier frequency), the problem of "jitter" is important. Jitter is the error in the reproduction of the exact time of transition between marking and spacing signals at the receiver output.

This problem is indicated in Fig. 1, in which it is assumed that the indicated data-source waveform is jitter-free and is transmitted repetitively. The received waveforms are shown overlapping one another. Note that, in addition to a usually harmless transmission delay, the receiver transitions do not all occur at the same relative time, but are instead distributed about the correct transition. The measure of jitter which will be used in this paper will be the maximum time error which may occur in the system, denoted by $\tau_{\epsilon m}$ in Fig. 1. (In all systems con-
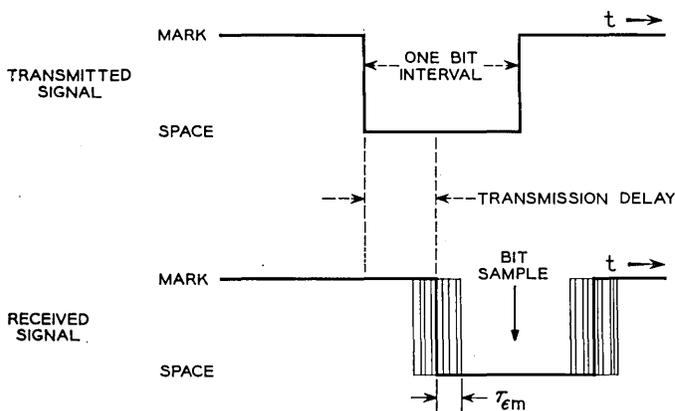

Fig. 1 — The problem of jitter.

sidered but one, the jitter is symmetric about the correct transition. However, the maximum jitter associated with a transition in one direction is not necessarily the same as that associated with the opposite transition. In these cases, a different $\tau_{\epsilon m}$ will be associated with each of the two transitions. The one exception to the above statement is the multivibrator modulator, in which the jitter occurs on only one side of the correct transition.)

As $\tau_{\epsilon m}$ increases, the time interval during which the received wave may be reliably sampled during each bit interval decreases. Thus it is important to keep this jitter to a minimum. Jitter may be induced from several sources. The data source itself may have inherent jitter. Jitter may be further induced in the modulation process. Distortion and noise present in the transmission channel will modify the modulated waveform, thus perhaps changing the apparent transition times. Finally, the receiver may contribute to the jitter.

This paper will analyze that jitter inherent in various asynchronous* frequency-shift modulation techniques. It will be assumed that the data source is jitter free, that the channel is ideal (i.e., noiseless and distortionless), and that the system utilizes an ideal zero-crossing type of detector. This detection process will be described more fully in the next section.

All the modulators to be studied shift frequency instantaneously at the time the data source goes through a mark-space transition. That is, the waveshape before the transition is given by

$$V_1 \cos (\omega_1 t + \theta_1)$$

and after the transition by

$$V_2 \cos (\omega_2 t + \theta_2).$$

The angular frequency before the transition is given by ω_1 and after the transition by ω_2. The expressions $\omega_1 t + \theta_1$ and $\omega_2 t + \theta_2$ are defined as the *phase* of the wave, before and after the transition, respectively. Ideally, the shift in frequency should take place with phase continuity; i.e. $\omega_1 t + \theta_1$ should equal $\omega_2 t + \theta_2$ at the time of transition. However, it will be shown that many commonly used modulators have an inherent phase error that results in an inherent time jitter.

The modulators to be studied include the switched reactance modulator (in which a reactance is switched into and out of the tank of an oscillator to modify its frequency), the variable reactance oscillator,[1] the

* That is, the frequency may be suddenly shifted during any portion of the cycle.

reactance tube modulator,[2] and the multivibrator.[3] It will be shown that the switched-reactance type of modulator has the most jitter. For example, at a data rate corresponding to one cycle of carrier per bit, the switched reactance modulator has a minimum peak jitter equivalent to 7.96 per cent data distortion. The variable reactance oscillator and reactance tube type of modulators are equivalent and have less jitter. The multivibrator may in principle be designed to have negligible jitter, but produces a square rather than a sinusoidal wave. These theoretical results are then supported by experimental data.

III. THE IDEAL ZERO-CROSSING DETECTOR

Before pursuing the jitter analysis further, it is necessary to define in some detail the assumed detection process. An ideal FM detector is one which measures the instantaneous rate of change of phase of the received wave. For the types of modulators considered in this paper, there would be no jitter in the received wave using such a detector. Rather, the phase discontinuity at switching would simply cause an impulse to be added at the time of transition to the otherwise correct transition. However, most present-day detectors utilize only the zero-crossing information in the received wave. For example, consider the receiving portion of the 43A1 carrier telegraph system.[4] The incoming signals are first passed through a filter to reject out-of-band noise, and then amplified. The next step is to limit the wave. The purpose of this is to remove any amplitude modulation, but in addition it removes any information other than that carried by the zero-crossings. The wave is next passed through a discriminator to convert the frequency modulation to baseband information, followed by a dc amplifier. The output is then a square wave which duplicates closely the wave originally presented to the modulator. Although other data sets use different methods of demodulation, a limiter to remove amplitude modulation is part of many of these. Thus is it of practical interest to study the performance of frequency-shift modulators when working with a zero-crossing type of detector. A zero-crossing detector approaches an ideal FM detector as the bandwidth of the transmitted signal becomes small with respect to the carrier frequency. This relation is described more fully by Stumpers.[5]

The characteristics of the zero-crossing detector are shown graphically in Fig. 2. Let it be receiving a constant frequency sine wave with zero phase at the time origin. Each zero crossing is identified by the zero-crossing detector as an advancement of π radians in the received wave. It thus knows the rate of change of phase, and hence the frequency, of the incoming sinusoidal wave. This is represented by the solid line in
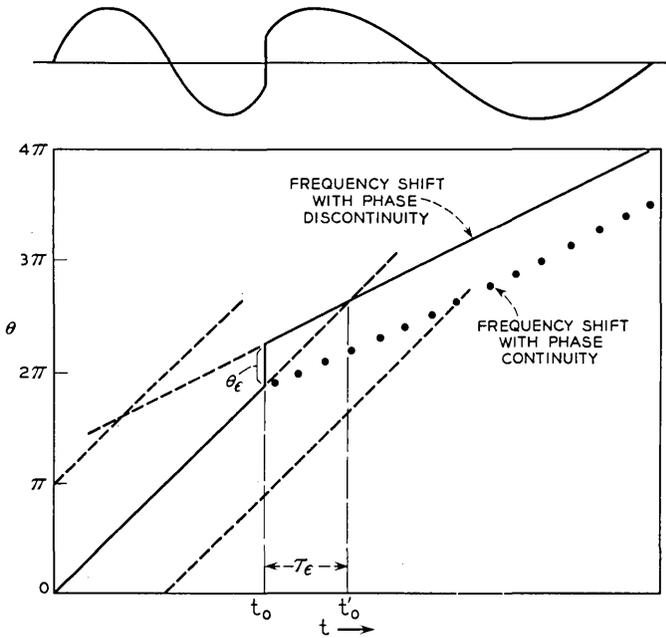
Fig. 2 — Graphical representation of the zero-crossing detector.

Fig. 2. However, the detector knows the phase of the wave only within an uncertainty factor of $n\pi$; the wave may equally well be represented by lines parallel to the solid line in Fig. 2, but of ordinate distance $n\pi$ away, where n is any integer. Two such lines are shown dashed.

If, at $t = t_o$, the frequency of the incoming wave is suddenly changed, the rate of zero crossings will be suitably changed. If the transition is made with phase continuity in the received wave, then the slope of the path in Fig. 2 simply changes suddenly, and the detector knows that the transition between frequencies occurred at the time of the break point. This case is illustrated by the dotted line in Fig. 2.

The problem of jitter is introduced when phase continuity is not preserved. In Fig. 2 is also shown a plot of the phase when the frequency is suddenly changed with an associated phase discontinuity of magnitude θ_ϵ. The detector has no knowledge of instantaneous phase except the zero-crossing information. It therefore assumes phase continuity, and determines the time t_o' at which a transition with phase continuity would have occurred to maintain the observed zero crossings. This time is determined graphically in Fig. 2 by the intersection of the two constant frequency lines determined by the detector. Since there is an indeter-

minacy of $n\pi$ in the absolute phase, there will be a multiplicity of such intersections, two of which are shown. It is assumed that the intersection yielding the minimum time error is chosen by the detector. Thus it is seen that a phase error of $n\pi$ radians causes no error in the detected transition time, as one would intuitively suspect. Furthermore, the phase error causing maximum time error is $\pi/2$ radians, or odd multiples thereof.

One problem has not been resolved. The zero-crossing detector is designed only for the two modulator frequencies at its input; it therefore is presumably incapable of recognizing zero crossings occurring at intervals closer than one-half a period of the upper frequency, since such zero crossings could not occur in a phase-continuous input wave. But with phase discontinuities, it is possible to get zero crossings closer than this interval. It is assumed that the zero-crossing detector ignores such zero crossings.

The relation between phase error and time error may be easily determined from Fig. 3 by noting that the slope of a line segment is the angular frequency, ω, of the input wave. Let the two modulator frequencies be denoted ω_1 and ω_2, where ω_1 is the frequency before switching, and ω_2 is the frequency after switching. Then from Fig. 3,

$$\omega_1 = \frac{\theta_1}{\tau_\epsilon}$$

$$\omega_2 = \frac{\theta_1 + \theta_\epsilon}{\tau_\epsilon}.$$

Thus

$$\tau_\epsilon = \frac{\theta_\epsilon}{\omega_2 - \omega_1}, \qquad \left| \theta_\epsilon \right| \leqq \frac{\pi}{2}. \tag{1}$$

For arbitrary θ_ϵ, this may be written

$$\tau_\epsilon = \min_n \frac{\theta_\epsilon - n\pi}{\omega_2 - \omega_1}, \qquad n \text{ an integer}, \tag{2}$$

where $\min_n f(n)$ means that $f(n)$ is calculated for that value of n which minimizes $f(n)$. The form (1) will usually be used with the understanding that (2) holds if

$$\left| \theta_\epsilon \right| > \frac{\pi}{2}.$$

Let $\theta_{\epsilon m}$ be the maximum possible phase error for a given system, and
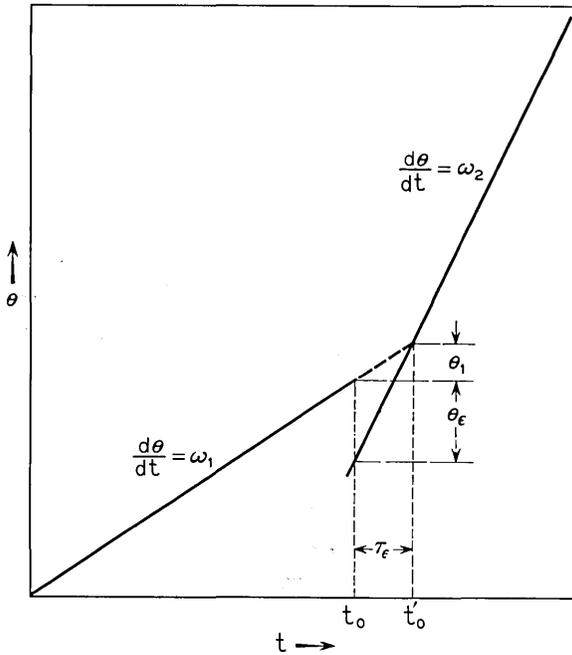
Fig. 3 — Relating phase error to time error.

let $\tau_{\epsilon m}$ be the resulting value of time error. Then (1) may be rewritten in a useful form as follows:

$$\tau_{\epsilon m} = \frac{\theta_{\epsilon m}}{(\omega_2 + \omega_1)\omega_2\left(1 - \dfrac{\omega_1}{\omega_2}\right)} \omega_2\left(1 + \frac{\omega_1}{\omega_2}\right),$$

or

$$\frac{\tau_{\epsilon m}}{T_0} = \frac{\theta_{\epsilon m}}{4\pi}\frac{1 + A}{1 - A}, \tag{3}$$

where $A = \omega_1/\omega_2$, and $T_o = 4\pi/(\omega_1 + \omega_2)$ is the period of the midfrequency (that frequency midway between ω_1 and ω_2). The value of (3) is thus a figure of merit for a system, giving the ratio of maximum jitter, $\tau_{\epsilon m}$, to the period of the midfrequency as a function of the frequency ratio A.

From reasoning such as that shown in Fig. 3, note that a positive phase error corresponds to a time advance for $A < 1$, but a time retarda-

Fig. 4 — Initial tank conditions.

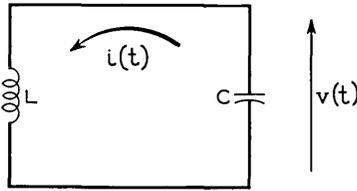tion for $A > 1$. From (3), then, positive $\tau_{\epsilon m}$ always corresponds to a time advance (an early transition) and negative $\tau_{\epsilon m}$ corresponds to a time retardation (a late transition).

IV. PRELIMINARY REMARKS

The analysis of the inherent time jitter associated with a particular modulator will proceed by first determining the maximum phase error that would occur under the worst conditions, and then relating that phase error to the time error by the use of (3). Before going further, it will be useful to point out certain miscellaneous facts. Several of these remarks pertain to ideal (lossless) tank circuits, since most of the oscillators studied are LC oscillators which are representable by lossless tank circuits.

First note that only one frequency may exist in an undriven lossless tank, namely the resonant frequency. Therefore, when the frequency of oscillation of a tank circuit is changed by suddenly changing the value of one or more of the tank reactances, the frequency also changes suddenly to the new resonant frequency. There are no transients except for the instantaneous transition; i.e., the tank instantaneously reaches its steady-state condition of amplitude and frequency. In particular, if the tank voltage and current are of magnitude v_o and i_o at $t = 0$, and are in the directions indicated in Fig. 4, then it is well known that the tank oscillation voltage and current will be given by

$$v(t) = V \cos (\omega t + \theta) \tag{4}$$

$$i(t) = I \sin (\omega t + \theta) \tag{5}$$

where*

$$V = \sqrt{v_o^2 + \frac{L}{C} i_o^2} \tag{6}$$

* These are easily derivable, particularly from energy relations.

$$I = \sqrt{\frac{C}{L} v_o^2 + i_o^2} = V \sqrt{\frac{C}{L}} \tag{7}$$

$$\theta = \tan^{-1} \sqrt{\frac{L}{C}} \frac{i_o}{v_o}. \tag{8}$$

The energy stored in this tank is

$$E = \tfrac{1}{2} Cv^2(t) + \tfrac{1}{2} Li^2(t) = \tfrac{1}{2} CV^2 = \tfrac{1}{2} LI^2, \tag{9}$$

and is always constant as long as the tank is undisturbed.

It is of interest to physically relate the phase error to the frequency-shift waveform. Fig. 5 shows two independent ways in which the phase error may manifest itself in the time varying waveform when the frequency of a wave is suddenly changed. Fig. 5(a) shows the obvious type of phase discontinuity which is associated with a discontinuity in a waveform of constant amplitude. Fig. 5(b) shows the less obvious case in which the instantaneous voltage and current in the tank are continuous, but in which the amplitude of oscillation for one frequency is not the same as that for the other frequency. The phase error is determined from the condition of waveform continuity. Referring to Fig. 5(b) and considering switching at $t = 0$, one obtains

$$V_1 \cos \theta_1 = V_2 \cos \theta_2,$$

or

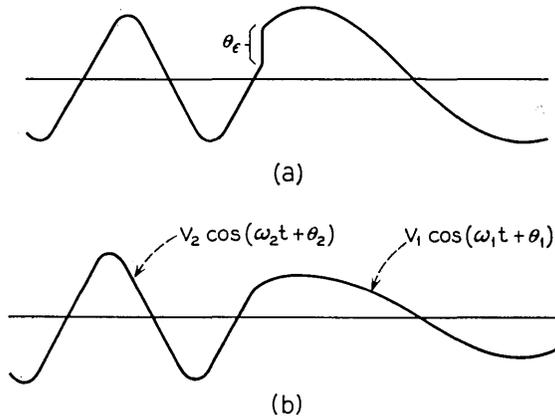$$\frac{\cos \theta_1}{\cos \theta_2} = \frac{V_2}{V_1}.$$

(a)

(b)

Fig. 5 — Relation of waveform to phase discontinuity: (a) phase discontinuity due to waveform discontinuity; (b) phase discontinuity due to amplitude change.

Thus the phase error will depend not only on the ratio of amplitudes, but also upon the phase angle at which the initial frequency is switched.

In the modulators to be described, either or both of these types of phase error may occur, depending upon the particular situation. In the case of amplitude variations, one might worry about the fact that a practical oscillator will try to maintain a constant amplitude. Thus, if the amplitude attempts to change as in Fig. 5(b), it will quickly recover to the initial value, either due to the drive of the active element in the case of an amplitude drop, or due to the limiting element in the case of an amplitude increase. However, it can be shown that this recovery is an exponential type of recovery; that is, it may be represented by

$$Ve^{\beta(t)t} \cos{(\omega t + \theta)}.$$

Since $e^{\beta(t)t} > 0$ (β is finite in value), the zero crossings of the wave are unchanged. Thus the phase error is unaffected by oscillator recovery, and we will therefore not consider this problem further.

One final point should be made. Some of the discontinuities are rather complicated, in that the voltage discontinuity and current discontinuity may be seemingly unrelated, and the voltage and current amplitude changes may be different. However, the phase discontinuity associated with either the voltage or current waveform will be identical, since the voltage and current must always maintain a $90°$ phase relationship. Thus, in the following analysis, the calculation of the phase discontinuity for only one of these quantities is derived.

V. THE REACTANCE TUBE MODULATOR AND VARIABLE REACTANCE OSCIL-
    LATOR

The jitter associated with the reactance tube modulator and variable reactance oscillator will be derived first. The reactance tube type of modulator is well known in the art.[2] It comprises an oscillator which has one of its reactances determined in part by a virtual reactance, which in turn is determined by the gain of another active stage with appropriate reactance feedback. By varying the gain of the active element (or by varying its feedback parameters), the magnitude of the virtual reactance may be changed, thus changing the resonant frequency of the oscillator. The variable reactance oscillator[1] is essentially the combination of the functions of oscillation and variable reactance into a single active element.

If the frequency of oscillation is shifted by suddenly changing the gain of the reactance-determining active element, then it can be shown

that there is no discontinuity in the voltage and current waveforms at the time of switching. These modulators may therefore be modeled by a simple LC tank, as in Fig. 4, in which one or both of the reactances are suddenly changed to produce a frequency shift, but in such a way that the current and voltage are maintained at the switching instant. In this case, phase error is caused solely by an amplitude change.

Let the subscript 1 refer to the waveform before switching, and the subscript 2 refer to the waveform after switching. Then, using (4), (5), and (7), and assuming switching at $t = 0$, the conditions of voltage and current continuity require that

$$V_1 \cos \theta_1 = V_2 \cos \theta_2 \qquad (10)$$

$$V_1 \sqrt{\frac{L_1}{C_1}} \sin \theta_1 = V_2 \sqrt{\frac{L_2}{C_2}} \sin \theta_2. \qquad (11)$$

Dividing (11) by (10) and rearranging yields

$$\tan \theta_2 = \sqrt{\frac{L_1}{C_1} \cdot \frac{C_2}{L_2}} \tan \theta_1. \qquad (12)$$

In most cases, only one of the reactances is changed. Let us assume that the value of the inductance is the shifted parameter, and further that $L_2 < L_1$ (that is, $\omega_2 > \omega_1$). All other cases (i.e., when $L_2 > L_1$, or when the capacitance is varied) are completely analogous and result in the same magnitude of jitter. Equation (12) may then be written as

$$\theta_2 = \tan^{-1} \frac{1}{A} \tan \theta_1,$$

where $A = \omega_1/\omega_2 < 1$ as previously defined in the discussion on zero-crossing detection.

The phase error as a function of the phase at shifting, θ_1, is then

$$\theta_\epsilon = \theta_2 - \theta_1 = \left(\tan^{-1} \frac{1}{A} \tan \theta_1 \right) - \theta_1. \qquad (13)$$

In order to determine $\theta_{\epsilon m}$, the maximum value of θ_ϵ, (13) is differentiated with respect to θ_1 and equated to zero (the value of θ_1 satisfying this condition will be denoted θ_{1m}):

$$\frac{1}{1 + \frac{1}{A^2} \tan^2 \theta_{1m}} \frac{1}{A} \sec^2 \theta_{1m} - 1 = 0.$$

Solving this for θ_{1m} yields

$$\theta_{1m} = \cos^{-1} \frac{\pm 1}{\sqrt{1 + A}} = \pm \tan^{-1} \sqrt{A} \, .$$

Thus

$$\theta_{\epsilon m} = \pm \left(\tan^{-1} \frac{1}{\sqrt{A}} - \tan^{-1} \sqrt{A} \right). \tag{14}$$

This is a monotonically decreasing function of A, and reaches a maximum for $A = 0$ (infinite frequency shift) of $\pi/2$ radians. For no frequency shift ($A = 1$), the phase error is zero as one would expect. This relation is shown plotted as the "∞" line in Fig. 6.
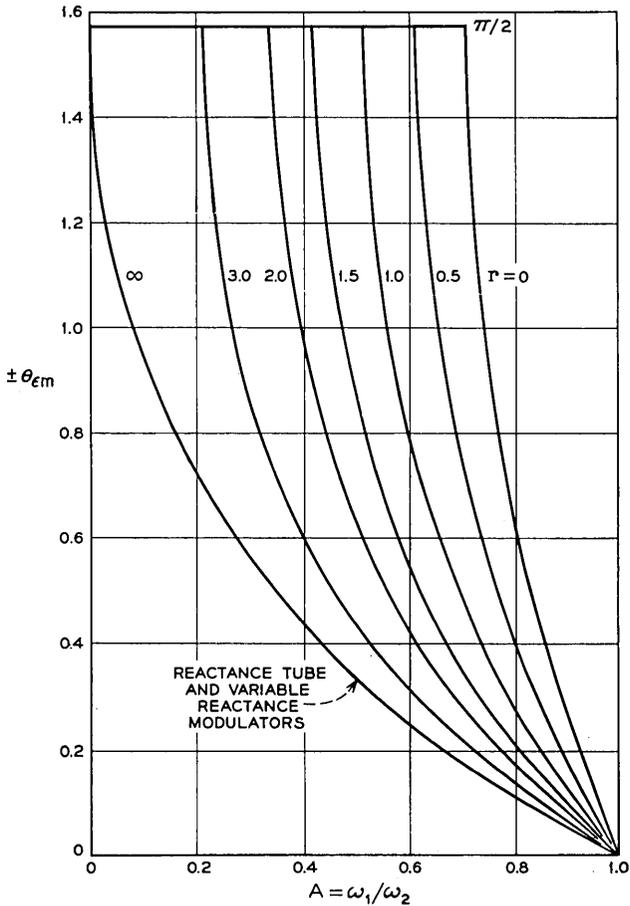

Fig. 6 — Peak phase error for the LC modulators; $r =$ (bit length)/ (dc time constant).

Noting that the phase error never exceeds $\pi/2$ radians, the associated time error, or jitter, is determined from (3):

$$\frac{\tau_{\epsilon m}}{T_o} = \pm \frac{1}{4\pi} \frac{1 + A}{1 - A} \left(\tan^{-1} \frac{1}{\sqrt{A}} - \tan^{-1} \sqrt{A} \right). \qquad (15)$$

For infinite frequency shift, this gives a jitter of one-eighth of a cycle of the midfrequency $(1/T_o)$. For zero frequency shift, the time jitter is, interestingly enough, not zero. Rather, (15) converges to a value of jitter equal to $1/4\pi$ of a cycle of the midfrequency. An insight into the reason for this may be obtained by referring to Fig. 2. Note that, as the two frequencies approach each other, the slopes of the phase loci also approach each other. Thus, for a fixed θ_ϵ, τ_ϵ increases as A approaches one. In the case just studied, θ_ϵ approaches zero as A approaches one, but evidently at about the same rate as τ_ϵ increases under the same condition.

Equation (15) is plotted as the lowest curve in Fig. 7(a). Note that the jitter measured in terms of the period of the midfrequency does not change appreciably with the magnitude of the frequency shift for these types of oscillators.

One final point is to be noted. From (15), it is seen that the time error has equal positive and negative excursions. Furthermore, (15) is symmetric in A; that is, replacing A by $1/A$ does not change the expression. Thus the opposite transition in which $\omega_2 < \omega_1$ has a time jitter function identical to (15).

VI. THE SWITCHED REACTANCE MODULATORS

A switched reactance modulator is one in which the resonant frequency of the tank is changed by physically switching an additional reactance in and out. Only those modulators consisting of a simple LC tank with a single additional switched reactance will be considered. There are four possible ways of doing this, leading to the four modulator models shown in Fig. 8. The modulators of Figs. 8 (a) and 8 (b) are clearly duals, and will be referred to as Type I modulators. The modulators of Figs. 8 (c) and 8 (d) are also duals, and will be referred to as Type II modulators. Because of the duality property, only one modulator of each type need be analyzed. It will be seen that all four types give rise to identical jitter expressions.

Let us first analyze the Type I modulator by considering the modulator of Fig. 8 (a). The case of switch closure is treated simply by noting that, since no current flows in the switched inductance prior to closure, the inductance value is changed (reduced) by the switch closure without
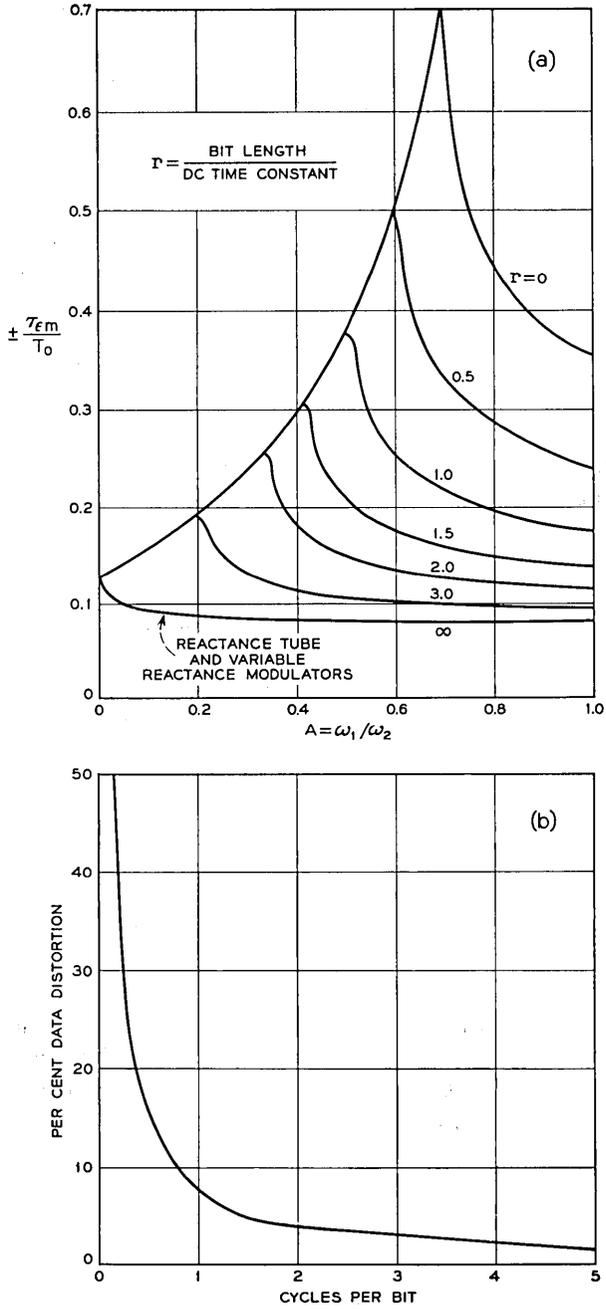
Fig. 7 — (a) Peak jitter for the LC modulators; (b) minimum peak jitter for the LC modulators.
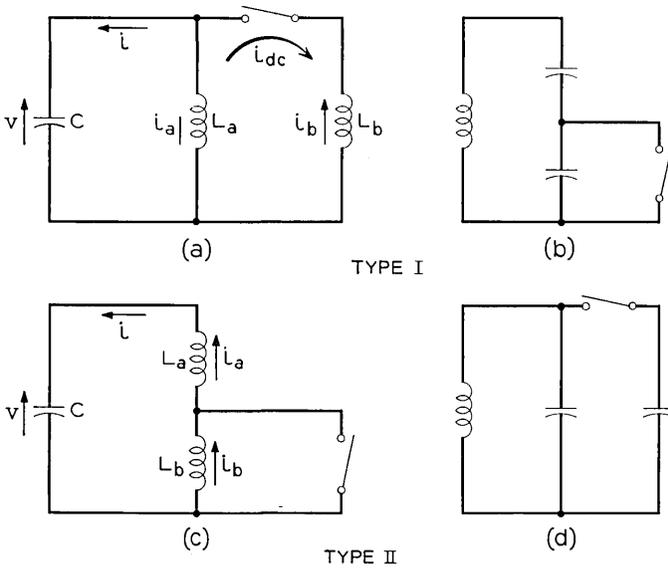
Fig. 8 — Switched reactance modulators.

disturbing the instantaneous voltage or current in the tank (the inductor looks like an open circuit at the time of switch closure). This is exactly the case considered in the previous section. Thus, (14) and (15) and the resulting curves of Figs. 6 and 7 describe the maximum phase and time errors, respectively, for this case.

In Fig. 8(b), the opening of the switch is the dual to the above case, since the switched capacitor initially looks like a short circuit. Thus the capacitance is changed without affecting the instantaneous values of the voltage and current.

In the case of switch opening in Fig. 8(a), current continuity in the capacitor is not preserved, since the current is suddenly reduced from the sum of the currents flowing in both inductors, $i_a + i_b$, to just that current flowing in the permanent tank·inductor, i_a. The case of switch opening is furthermore complicated by the fact that a dc current may be flowing around the inductor loop just prior to switch opening. This may be seen more clearly from Fig. 9, in which is plotted the current, i_b, through the switched inductor, L_b. Consider the case shown of switch closure at the instant that the tank voltage is going through zero. The inductor current i_b is the integral of the applied voltage, and is as shown. Note that this current contains a dc component. The case
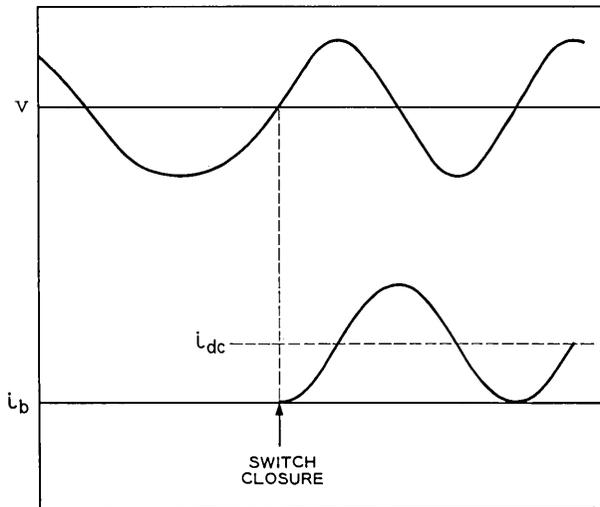
Fig. 9 — The dc component in a switched reactance modulator.

of Fig. 9 is the worst case; if the switch had been thrown at a voltage maximum, then the dc current component would have been zero.

This dc component will die exponentially with a time constant determined by the inductive loop. It does not affect the operation of the tank circuit as long as the switch is closed. However, whatever dc current remains is added to the current i [see Fig. 8(a)] at the time of switch opening. Thus the tank current i just before switch opening is given by $i_a + i_b$, and just after switch opening by $i_a + i_{dc}$. The dc current may be such as to actually reverse the tank current at the instant of switching. Thus large phase errors and hence large time errors may be expected.

Since the phase error will depend upon the magnitude of the dc component, which in turn involves the phase at which the switch was closed, then the phase error at switch opening depends on the phase at the time the switch is opened as well as the phase at the time the switch was previously closed. For purposes of the following analysis, let the following subscripts apply:

1 — just before switch closure.
2 — just after switch closure.
3 — just before switch opening.
4 — just after switch opening.

Then

$$L_1 = L_4 = L_a. \tag{16}$$

$$L_2 = L_3 = \frac{L_a L_b}{L_a + L_b}. \tag{17}$$

$$A^2 = \left(\frac{\omega_1}{\omega_2}\right)^2 = \frac{L_2}{L_1} = \frac{L_b}{L_a + L_b} < 1. \tag{18}$$

At the time of switch closure, voltage and current are maintained. Thus

$$v_1 = V_1 \cos \theta_1 = v_2. \tag{19}$$

$$i_1 = V_1 \sqrt{\frac{C}{L_1}} \sin \theta_1 = i_2. \tag{20}$$

The dc current which is initiated upon switch closure may be determined by a transient analysis or more simply from the energy conditions:

$$E_1 = \tfrac{1}{2} L_1 i_1^2 + \tfrac{1}{2} C v_1^2.$$

$$E_2 = \tfrac{1}{2} L_2 i_1^2 + \tfrac{1}{2} C v_1^2.$$

The difference in energy must be due to the circulating dc current, since the initial current in the switched inductor is zero. Denote this energy difference by E_{dc}. Then

$$E_{dc} = \tfrac{1}{2} (L_a + L_b) i_{dc}^2 = E_1 - E_2 = \tfrac{1}{2} (L_1 - L_2) i_1^2.$$

Making use of (16), (17), and (18), the resulting dc current may be written

$$i_{2dc} = (1 - A^2) i_1 = V_1 \sqrt{\frac{C}{L_1}} (1 - A^2) \sin \theta_1. \tag{21}$$

The tank voltage is continuous during both switch closure and switch opening. Since the current is also continuous during switch closure (assuming zero initial current in L_b), the amplitude of oscillation after switch closure is, from (6), (19), and (20),

$$V_2 = V_3 = \left(\frac{L_2}{C} i_1^2 + v_1^2\right)^{\frac{1}{2}} = V_1 (A^2 \sin^2 \theta_1 + \cos^2 \theta_1)^{\frac{1}{2}}. \tag{22}$$

The tank voltage at switch opening may then be expressed as

$$v_3 = v_4 = V_3 \cos \theta_3.$$

Then, from (22),

$$v_4 = V_1 (A^2 \sin^2 \theta_1 + \cos^2 \theta_1)^{\frac{1}{2}} \cos \theta_3. \tag{23}$$

From (5), (7), and (22), the tank current immediately before switch opening is

$$i_3 = V_3 \sqrt{\frac{C}{L_2}} \sin \theta_3.$$

At this instant the share of the tank current through the permanent tank inductor is

$$i_{3a} = \frac{L_b}{L_a + L_b} i_3 = V_1 \sqrt{\frac{C}{L_2}} A^2 (A^2 \sin^2 \theta_1 + \cos^2 \theta_1)^{\frac{1}{2}} \sin \theta_3, \tag{24}$$

where (22) was used.

If the sum of the resistances of the two inductors is R, and the minimum time between switch closing and switch opening is τ_b (normally the bit length), then the dc current just before switch opening is at most

$$i_{3dc} = \exp\left(-\frac{R\tau_b}{L_a + L_b}\right) i_{2dc} = D i_{2dc},$$

where $D = \exp [- (R\tau_b)/(L_a + L_b)]$ will be called the dissipation parameter.

The actual current through the permanent inductor is the sum of its share of the tank current and the dc current. Immediately after switch opening, this current must be maintained, so that

$$i_4 = i_{3a} + D i_{2dc}.$$

From (21) and (24),

$$i_4 = V_1$$
$$\sqrt{\frac{C}{L_1}} [A (A^2 \sin^2 \theta_1 + \cos^2 \theta_1)^{\frac{1}{2}} \sin \theta_3 + D(1 - A^2) \sin \theta_1]. \tag{25}$$

The current and voltage immediately after switch opening have now been determined in terms of the phase angles at which the switch was initially closed (θ_1) and the phase angle at which it was then reopened (θ_3). These expressions are given by (23) and (25). Using (8), the phase angle immediately after switch opening may now be determined by the relation

$$\theta_4 = \tan^{-1} \sqrt{\frac{L_1}{C}} \frac{i_4}{v_4}$$

$$= \tan^{-1} \frac{A(A^2 \sin^2 \theta_1 + \cos^2 \theta_1)^{\frac{1}{2}} \sin \theta_3 + D(1 - A^2) \sin \theta_1}{(A^2 \sin^2 \theta_1 + \cos \theta_1)^{\frac{1}{2}} \cos \theta_3}.$$

The phase error at switch opening is then

$$\theta_\epsilon = \theta_3 - \theta_4$$

$$= \theta_3 - \tan^{-1} \left[A \tan \theta_3 + \frac{D(1 - A^2) \sin \theta_1}{(A^2 \sin^2 \theta_1 + \cos^2 \theta_1)^{\frac{1}{2}} \cos \theta_3} \right]. \tag{26}$$

We desire to find those values of θ_1 and θ_3 which maximize this function. These values will yield the peak phase error and thus the peak time jitter. Denote these values by θ_{1m} and θ_{3m}, respectively. It is shown in Appendix A that for $A_p \leqq A \leqq 1$,

$$\theta_{1m} = \pm \frac{\pi}{2}$$

and

$$\theta_{3m} = \pm \sin^{-1} \frac{1}{2A} \left[D(2A - 1) \right.$$
$$\left. - \left(\frac{4(1 - D^2)A^2 + D^2(A + 5)}{A + 1} \right)^{\frac{1}{2}} \right]. \tag{27}$$

where A_p is the value of A for which $\theta_{3m} = \pm \pi/2$. It is further shown in Appendix A that, for $D = 0$, $A_p = 1/\sqrt{2}$; for $D = 1$, $A_p = 0$. For $0 \leq A \leq A_p$, the phase error may take on continuous values in excess of $\pi/2$ radians. Thus it can always take on the worst possible value, $\pi/2$. Hence

$$\theta_{\epsilon m} = \pm \theta_{3m} + \tan^{-1} \frac{A}{\cos \theta_{3m}} \left[\sin \theta_{3m} - D \left(\frac{1 - A^2}{A^2} \right) \right], \quad A_p \leqq A \leqq 1$$

$$\theta_{\epsilon m} = \pm \pi/2, \quad 0 \leq A \leq A_p,$$

where θ_{3m} is given by (27). Again, the peak phase error, and thus the peak jitter, is symmetric about the true value; that is, these functions may assume equal positive or negative value.

These phase error functions are plotted in Fig. 6, and the associated peak jitter functions as determined from (3) in Fig. 7(a), for various

values of the dissipation factor D. These curves were calculated with the aid of the IBM 7090 digital computer. The curve parameters in Figs. 6 and 7(a) are actually

$$r = -\ln D = \frac{R\tau_b}{L_a + L_b},$$

which is the ratio of the bit length, τ_b, to the time constant of the inductor loop. Note that the peak jitter is considerably greater for the case of small r (large dc currents), than for the case when the time constant is sufficiently short so that the dc current may die in one bit interval. For the case of zero dc current at switch opening ($D = 0$, or $r = \infty$) the quantity θ_{3m} becomes

$$\theta_{3m} = \pm \sin^{-1} \frac{1}{\sqrt{A+1}} = \pm \tan^{-1} \frac{1}{\sqrt{A}}.$$

Then the peak phase error is

$$\theta_{\epsilon m} = \pm \left(\tan^{-1} \frac{1}{\sqrt{A}} - \tan^{-1} \sqrt{A} \right).$$

But this is exactly the form of the peak phase error for the case of the variable reactance oscillator and reactance tube modulator. It may seem strange that the two classes of modulators should have the same peak jitter, since in one case a tank reactance is changed without affecting the instantaneous values of the currents and voltages, whereas in the other case a tank reactance is also changed, but a current discontinuity occurs (from i_3 to i_{3a} in the previous notation). However, a detailed examination of the equations will show that the phase error due to the current discontinuity is in such a direction as to partially compensate for the amplitude change, the result being a peak phase error equal to that resulting from the amplitude discontinuity alone.

As stated before, the modulator of Fig. 8(b) is the dual of the modulator just analyzed, and the same peak phase error and jitter equations therefore result. A switch opening in Fig. 8(b) is equivalent to a switch closure in Fig. 8(a). Analogous to the dc current in Fig. 8(a), a dc voltage may appear across the switched capacitor, and is balanced out by an equal and opposite voltage on the permanent tank capacitor. Then, upon reclosing the switch in Fig. 8(b), the tank voltage suddenly changes to the difference between the ac and dc voltages across the permanent tank capacitor, in complete analogy to the first modulator. Again, this troublesome dc voltage may be bled off by a resistor in parallel with each capacitor, leading again to the dissipation parameter.

It now remains to show that the modulators of Figs. 8(c) and 8(d) lead to the same phase error relationships as derived for the first two modulators. Consider the modulator of Fig. 8(c). The case of the switch closure is identical to the conditions for the variable reactance oscillator and reactance tube modulator; i.e., the value of the inductance is changed, but the instantaneous values of the tank current and voltage are unchanged. Hence the lowest curves for peak phase error and peak jitter in Figs. 6 and 7(a) hold for this case. However, the switched inductor, L_b, will have a current flowing through it just prior to switch closure, and will retain this current after the switch has closed. L_b may begin to discharge due to series resistance, but in general will have a nonzero current flowing through it at the time of switch opening. At switch opening, the flux in L_a and L_b will redistribute so that the currents through the two inductors are equalized, thus causing a current transient.

Using the same subscripts as before, define

$$L_1 = L_4 = L_a + L_b .$$

$$L_2 = L_3 = L_a .$$

$$A^2 = \left(\frac{\omega_1}{\omega_2}\right)^2 = \frac{L_2}{L_1} = \frac{L_a}{L_a + L_b} < 1.$$

Immediately after switch closure, the dc current flowing through L_b is

$$i_{2b} = i_{2dc} = i_1 = V_1 \sqrt{\frac{C}{L_1}} \sin \theta_1 .$$

Just before switch opening, the dc current flowing through L_b is

$$i_{3dc} = Di_{2dc} = V_1 D \sqrt{\frac{C}{L_1}} \sin \theta_1 ,$$

where the dissipation factor, D, is now given by

$$D = \exp\left(-\frac{R\tau_b}{L_b}\right),$$

where R is the loop resistance containing L_b and the closed switch. The value of the current through L_a just before switch opening is

$$i_{3a} = V_3 \sqrt{\frac{C}{L_2}} \sin \theta_3 = V_1 \sqrt{\frac{C}{L_2}} (A^2 \sin^2 \theta_1 + \cos^2 \theta_1)^{\frac{1}{2}} \sin \theta_3 ,$$

where V_3 is determined exactly as in the previous case.

At the instant of switch opening, one is faced with the problem of two

inductors with different initial currents being connected in series. The series current must instantly adjust to some common value. To determine this common value, note that the tank voltage v must be continuous. This is true because there is no process by which an impulse in the tank current may be caused; thus the voltage across the capacitor and hence the tank voltage cannot change instantaneously.

Since the voltage across the two inductors is the same immediately before as after the switch opening, then the total flux stored in the two inductors must be preserved. The instantaneous redistribution of flux between the two inductors will cause a voltage impulse to appear across each inductor, but these impulses will be of equal magnitude and opposite sign, thus canceling. The total stored flux immediately before the switch opening is

$$\varphi_3 = L_a i_{3a} + L_b i_{3dc}.$$

Immediately after the switch opening, the stored flux is

$$\varphi_4 = (L_a + L_b) i_4 .$$

Equating φ_3 and φ_4 , one obtains

$$i_4 = A^2 i_{3a} + (1 - A^2) i_{3dc}$$
$$= V_1 \sqrt{\frac{C}{L_1}} [A (A^2 \sin^2 \theta_1 + \cos^2 \theta_1)^{\frac{1}{2}} \sin \theta_3 + D(1 - A^2) \sin \theta_1]. \tag{28}$$

The voltage immediately after switch opening is again

$$v_4 = V_3 \cos \theta_3 = V_1 (A^2 \sin^2 \theta_1 + \cos^2 \theta_1) \cos \theta_3. \tag{29}$$

Equations (28) and (29) are identical to (25) and (23) respectively for the case of the Type I modulator. Thus the peak phase and jitter functions for the Type II modulator are identical to those for the Type I modulator [Figs. 6 and 7(a)], even though the waveform discontinuities are caused by an entirely different phenomenon.

The circuit of Fig. 8(d) is of course the dual to that of Fig. 8(c). Switch closure in one corresponds to switch opening in the other, and vice versa. In the circuit of Fig. 8(d), when the switch is opened, a voltage is left on the switched capacitor. It may decay through a leakage resistance, but upon switch closure the two different voltages on the two capacitors must instantly adjust to some common voltage according to the condition of charge conservation, in complete analogy to the circuits of Fig. 8(c).

Note that the jitter characteristic for all of the switched reactance mod-

ulators approaches that of the variable reactance-type modulators for low bit rates. This latter curve is almost a constant ($\tau_{\epsilon m}/T_o = 1/4\pi$) over the range of A which might be commonly used. This then is a useful rule of thumb: In a modulator whose frequency is shifted by changing one reactance in the tank of an oscillator, the minimum inherent peak jitter is roughly $1/4\pi$ of the period of the midfrequency. This rule is shown plotted in Fig. 7(b) in a somewhat different form. The abscissa is the number of cycles of the midfrequency per bit:

$$\text{cycles/bit} = \frac{\tau_b}{T_o}.$$

The ordinate is the per cent data distortion, defined by

$$\text{distortion} = \frac{\tau_{\epsilon m}}{\tau_b} = \frac{1}{4\pi}\frac{T_o}{\tau_b}.$$

Thus

$$(\text{distortion})(\text{cycles/bit}) = \frac{1}{4\pi}.$$

VII. THE MULTIVIBRATOR MODULATOR

A multivibrator type of modulator, using transistors as an example, is shown in Fig. 10(a). It consists of a standard symmetric multivibrator whose frequency may be controlled by varying the control voltage V_c. Often a low-pass filter follows the multivibrator. The function of this filter is to eliminate the harmonics of the multivibrator output, thus converting the square-wave output to a sine wave. This filter may add additional zero-crossing distortion, but this distortion will not be considered here. Only the zero-crossing distortion inherent in the multivibrator itself will be analyzed.

The analysis will proceed in the following manner. It will be assumed that the multivibrator is oscillating with some half-period η_1. At some time t_o, measured with respect to the last multivibrator transition [see Fig. 11(a)], the control voltage V_c is suddenly changed from its initial value V_{c1} to a new value V_{c2}. The multivibrator then oscillates with some new half-period η_2. The time between the two transitions on either side of t_o will be denoted η_o where η_o has a value between η_1 and η_2.

The resulting zero crossings will be compared to those of an ideal FM wave shown in Fig. 11(b) whose zero crossings correspond to those of the multivibrator before the switching instant, but are separated from those of the multivibrator by a time error of T_ϵ for times after the switch-
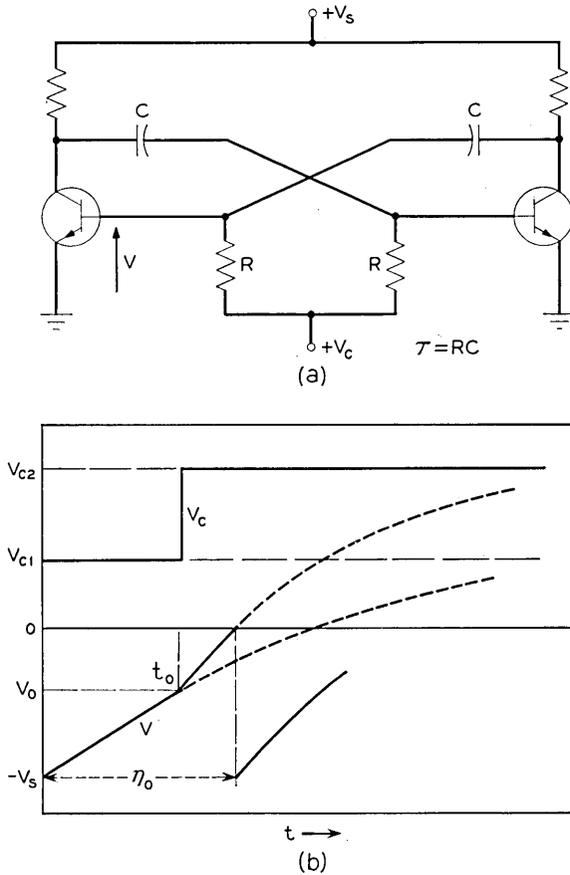
Fig. 10 — The multivibrator modulator: (a) multivibrator circuit; (b) base voltage waveform.

ing instant. This corresponds to a phase error of

$$\theta_\epsilon = 2\pi \frac{T_\epsilon}{2\eta_2}. \tag{30}$$

The worst value for the transition time will be determined, leading to a maximum value for θ_ϵ, denoted $\theta_{\epsilon m}$. From (3), the peak time error $\tau_{\epsilon m}$ in the data transition with respect to the period of the midfrequency T_o is

$$\frac{\tau_{\epsilon m}}{T_o} = \frac{1}{2} \frac{1 + A}{1 - A} \frac{T_{\epsilon m}}{2\eta_2}. \tag{31}$$
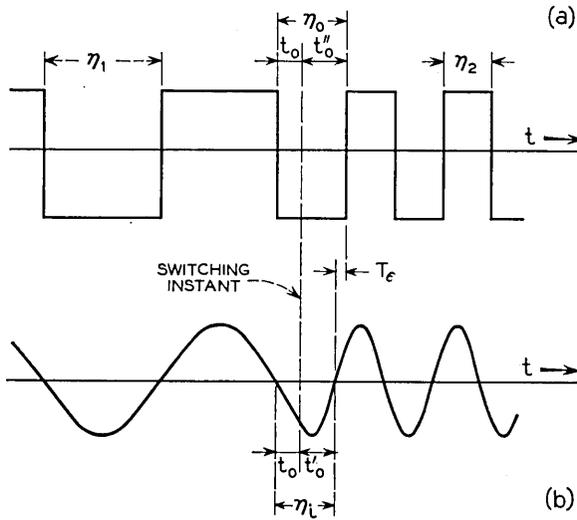
Fig. 11 — Comparing zero crossings of multivibrator modulator to those of ideal FM: (a) multivibrator outputs; (b) ideal FM.

Let us first derive the time between zero crossings on either side of the switching instant for an ideal FM wave. This time will be called η_i. From Fig. 11(b),

$$\eta_i = t_o + t_o'.$$

Because the amplitudes of the two sinusoids are the same, and the voltage is continuous at the transition, one may write

$$\sin \omega_1 t_o = \sin \omega_2 (\eta_2 - t_o').$$

Thus

$$t_o' = \eta_2 \left(1 - \frac{t_o}{\eta_1} \right),$$

and

$$\eta_i = \eta_2 + t_o \left(1 - \frac{\eta_2}{\eta_1} \right). \tag{32}$$

We now derive the analogous time, η_0, for the multivibrator. In Fig. 10(b) is shown the operation of the multivibrator in terms of the voltage at a base. Immediately after a transition, the transistor is reverse biased by a voltage equal to the supply voltage, V_s. The voltage at this point

will start rising exponentially to the control voltage V_c, with a time constant τ, and is given by

$$v = V_c - (V_s + V_c)e^{-t/\tau},$$

where τ is defined in Fig. 10 as $\tau = RC$. For a constant control voltage, the half-period of oscillation, η, is determined by that time required for the voltage waveform to reach zero voltage (ignoring the transistor threshold voltage). Thus

$$\eta = \tau \ln\left(1 + \frac{V_s}{V_c}\right).$$

Let us define the following parameters:

$$A = \frac{\omega_1}{\omega_2} = \frac{T_2}{T_1} = \frac{\eta_2}{\eta_1}.$$

$$\alpha = \frac{V_s}{V_{c1}}.$$

$$\beta = \frac{V_s}{V_{c2}}.$$

Then

$$\eta_1 = \tau \ln(1 + \alpha),$$

$$\eta_2 = \tau \ln(1 + \beta).$$

At a time t_o after the last transition, there will be a base voltage v_o of

$$v_o = V_{c1} - (V_s + V_{c1}) \exp(-t_o/\tau).$$

If at this time the multivibrator control voltage is suddenly switched from V_{c1} to V_{c2}, the time from t_o to the next transition will be

$$t_o'' = \tau \ln\left(1 - \frac{v_o}{V_{c2}}\right) = \tau \ln\left[1 - \frac{V_{c1}}{V_{c2}} + \frac{V_{c1}}{V_{c2}}\left(1 + \frac{V_s}{V_{c1}}\right) \exp\left(-t_o/\tau\right)\right].$$

Then

$$\eta_o = t_o + t_o'' = t_o + \tau \ln\left[1 - \frac{\beta}{\alpha} + \frac{\beta}{\alpha}(1 + \alpha \exp(-t_o/\tau)\right].$$

The difference between this and the like time, η_i for ideal FM is

$$T_\epsilon = \eta_o - \eta_i = \tau \ln\left[1 - \frac{\beta}{\alpha} + \frac{\beta}{\alpha}(1 + \alpha) \exp\left(-t_o/\tau\right)\right] \tag{33}$$

$$+ At_o - \eta_2.$$

From (30), θ_ϵ is maximized if T_ϵ is maximized. The value of t_o, denoted t_{om}, for which T_ϵ is a maximum is found by letting

$$\frac{\partial T_\epsilon}{\partial T_o} = \frac{\tau}{1 - \frac{\beta}{\alpha} + \frac{\beta}{\alpha}(1 + \alpha)\exp(-t_{om}/\tau)} \frac{\beta}{\alpha}(1 + \alpha)\left(-\frac{1}{\tau}\right)\exp(-t_{om}/\tau)$$

$$+ A = 0,$$

which results in

$$\exp(-t_{om}/\tau) = \frac{\left(1 - \frac{\beta}{\alpha}\right)}{\frac{\beta}{\alpha}(1 + \alpha)\left(\frac{1}{A} - 1\right)}$$

or

$$t_{om} = \tau \ln \frac{(1 + \alpha)(1 - A)}{A\left(\frac{\alpha}{\beta} - 1\right)}. \tag{34}$$

Substituting (34) into (33), one obtains

$$T_{\epsilon m} = \tau \ln \frac{1 - \frac{\beta}{\alpha}}{1 - A} + A\tau \ln \frac{(1 + \alpha)(1 - A)}{A\left(\frac{\alpha}{\beta} - 1\right)} - \eta_2,$$

which can be rewritten as

$$T_{\epsilon m} = \tau\left[(1 - A)\ln \frac{1 - \frac{\beta}{\alpha}}{1 - A} + A \ln \frac{\beta}{A\alpha} + A \ln(1 + \alpha) - \frac{\eta_2}{\tau}\right]. \tag{35}$$

But, since

$$\eta_2 = \tau \ln(1 + \beta)$$

and

$$A = \frac{\ln(1 + \beta)}{\ln(1 + \alpha)}, \tag{36}$$

then

$$\alpha = (1 + \beta)^{1/A} - 1,$$

$$\tau = \frac{\eta_2}{A \ln(1 + \alpha)}, \tag{37}$$

and

$$T_{\epsilon m} = \frac{\eta_2}{A \ln (1 + \alpha)} \left[(1 - A) \ln \frac{1 - \frac{\beta}{\alpha}}{1 - A} + A \ln \frac{\beta}{A\alpha} \right],$$

or

$$\theta_{\epsilon m} = 2\pi \frac{T_{\epsilon m}}{2\eta_2} = 2\pi \frac{\left(\frac{1 - A}{A}\right) \ln \frac{1 - \frac{\beta}{\alpha}}{1 - A} + \ln \frac{\beta}{A\alpha}}{2 \ln (1 + \alpha)}. \qquad (38)$$

The peak time jitter is then determined from (3):

$$\frac{\tau_{\epsilon m}}{T_o} = \frac{1}{4} \frac{(1 + A)}{(1 - A)} \frac{\left(\frac{1 - A}{A}\right) \ln \frac{1 - \frac{\beta}{\alpha}}{1 - A} + \ln \frac{\beta}{A\alpha}}{\ln (1 + \alpha)}. \qquad (39)$$

Equations (37) and (38) give the peak phase error for a transition in either direction (i.e., from the lower to the higher frequency, or vice versa) as a function of the two variables A and β. It is shown in Appendix B that the peak phase error for the transition in one direction is equal in magnitude but opposite in sign to the peak phase error for the opposite transition.

From the relation (3), it is then seen that the peak time error for the multivibrator is equal in magnitude and is always negative for either transition. Thus the multivibrator differs in its jitter characteristics from the LC modulators in that the jitter is one-sided, rather than symmetric, about the true transition time. The jitter is such that the actual transitions are delayed in time from the true transition ($-\tau_{\epsilon m}$ corresponds to a time retardation).

The parameter β is essentially a "linearity" parameter; i.e., as $\beta \to 0$, less and less of the exponential of Fig. 10 is used. For α and β sufficiently small, the base voltage is essentially linear. In this case, from (37),

$$\beta \approx \alpha A.$$

Under this condition, (39) goes to zero. Thus the multivibrator type of modulator may be designed to have as little jitter as desired by making the control voltage, V_c, very much greater than the supply voltage, V_s.

It is also of interest to study the other limiting condition, i.e., $\beta \to \infty$. From (37), for $\beta \gg 1$,

$$\alpha \approx \beta^{\frac{1}{2}}.$$

Substituting this into (38) for the peak phase error, and taking the limit as $\beta \rightarrow \infty$, one finds

$$\lim_{\beta \to \infty} \theta_{\epsilon m} = -(1 - A)\pi,$$

for $\frac{1}{2} \leqq A \leqq 1$, $| \theta_{\epsilon m} | \leqq \pi/2$; therefore, from (39),

$$\lim_{\beta \to \infty} \frac{\tau_{\epsilon m}}{T_o} = -\frac{1 + A}{4}, \quad \frac{1}{2} \leqq A \leqq 1. \tag{40}$$

However, for $0 \leqq A \leqq \frac{1}{2}$, θ_ϵ may take on values in excess of $\pi/2$. Thus

$$\lim_{\beta \to \infty} \theta_\epsilon = -\frac{\pi}{2}$$

$$0 \leqq A \leqq \frac{1}{2}.$$

$$\lim_{\beta \to \infty} \frac{\tau_{\epsilon m}}{T_o} = -\frac{1}{8}\frac{1 + A}{1 - A}$$

Plots of $\theta_{\epsilon m}$ and $\tau_{\epsilon m}/T_o$ for the multivibrator are given in Figs. 12 and 13 respectively. Fig. 13(b) shows peak jitter on an expanded scale for small values. For comparison, the corresponding curve for the peak jitter inherent in the reactance tube type of modulator is shown dotted in Figs. 13(a) and 13(b).

Note that a given time error for the multivibrator corresponds to only half the distortion caused by the same time error associated with one of the LC modulators because of the one-sided property of the multivibrator jitter.

VIII. EXPERIMENTAL VERIFICATION

The results of the theory just presented were checked by measuring the peak jitter in some existing systems. In Table I are shown some experimental and theoretical results for the modulators of the Bell System DATA-PHONE Data Sets 101A, 103A, and 202A.[3] In all cases, a dotting (alternate marking and spacing) signal was used to avoid the effects of intersymbol interference. The receiver used for the 100 series data sets was the 101A receiver. It contains a limiter followed by a standard discriminator and slicing amplifier. Because of the limiter, the zero-crossing information is all that is retained. The 202A receiver was used with its modulator. This receiver is indeed a zero-crossing detector. It generates a pulse for each zero crossing, integrates the resulting pulse train, and delivers this resulting signal to a slicing circuit.

The 100 series data sets are capable of operating in either of two bands. These bands are denoted the f_1 band and the f_2 band. In the case of the
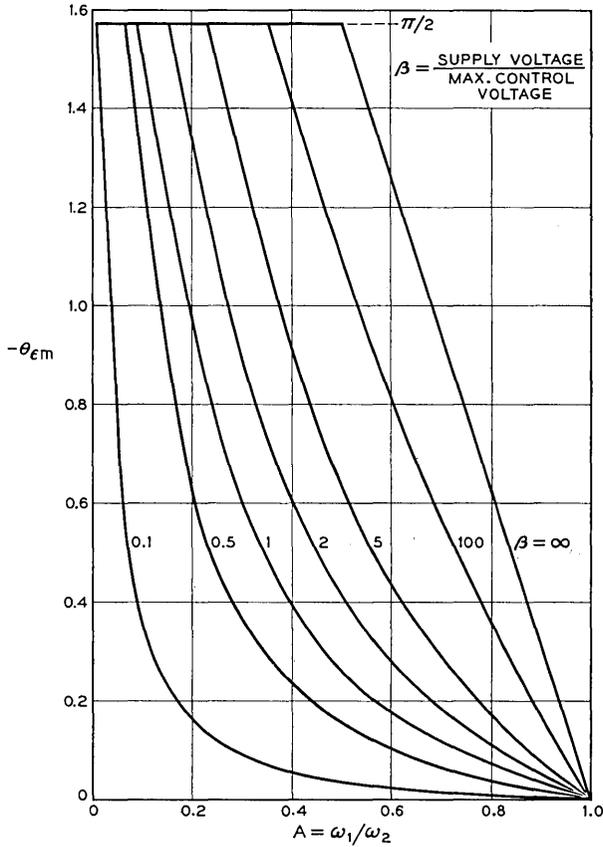
Fig. 12 — Peak phase error for the multivibrator modulator.

TABLE I — EXPERIMENTAL VERIFICATION

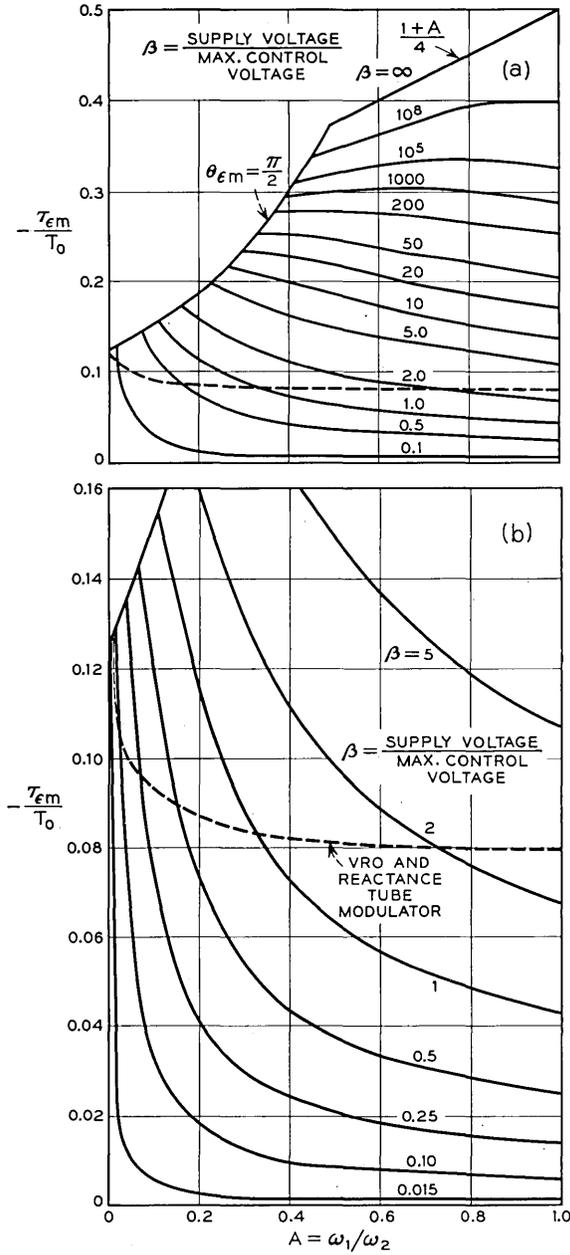| Modulator	Type	ω_1	ω_2	Bit Rate	Transition	Experimental Peak Jitter (μsec)	Theoretical Peak Jitter (μsec)
101	Switched Reactance	1070	1270	100	$\omega_1 \rightarrow \omega_2$	165	136
					$\omega_2 \rightarrow \omega_1$	280	280
		2025	2225	100	$\omega_1 \rightarrow \omega_2$	100	72
					$\omega_2 \rightarrow \omega_1$	130	112
103	Reactance Transistor	1070	1270	100	Either	165	136
				200	Either	165	136
202	Multivibrator	1200	2200	1200	Either	50	44.5

Fig. 13 — (a) Peak jitter for the multivibrator modulator; (b) peak jitter for the multivibrator modulator — expanded scale.

101A modulator, both the f_1 band and the f_2 band were used for the test. The marking and spacing frequencies in the f_1 band are 1070 and 1270 cycles, resulting in an A of 0.843. In the f_2 band, the corresponding frequencies are 2025 and 2225 cps, giving an A of 0.910. The modulator is a switched reactance modulator of the type shown in Fig. 8(a). For the f_1 band, the sum of the two inductances is 0.324 henry and the total series resistance is 44.5 ohms. For the f_2 band these parameters are 0.151 henry and 28.7 ohms. This modulator was tested at 100 bits per second, the corresponding values of r being 1.37 and 1.90 for the f_1 band and f_2 band respectively.

The 103A modulator was tested at 100 and 200 bits per second using the f_1 band and again the 101A demodulator. The 103A modulator is of the reactance transistor type (analogous to the reactance tube modulator). The results agree well with theory.

The 202A modulator was tested at 1200 bits per second, using 1200 cps and 2200 cps as the two frequencies. This corresponds to an A of 0.54. In this modulator, the value of β is 1.405 ($V_{c2} = 12.8$ v, $V_s = 18$ v). Again, the agreement with theory is quite good.

Because all of the above experiments yielded jitter comparable to that expected from the modulator alone, one is led to the conclusion that most of the back-to-back jitter in these data sets originates in the modulator, and that the demodulators approach fairly closely the ideal zero-crossing detector.

IX. DISTORTIONLESS, ASYNCHRONOUS, SINUSOIDAL FREQUENCY MODULATION

From (8), it is possible to obtain the conditions for distortionless modulation when the modulation is accomplished by changing the parameters of an LC tank. Let the subscript 1 refer to the instant before the transition, and the subscript 2 to the instant after. There will be no jitter if there is no phase error, that is, if

$$\theta_1 = \theta_2 .$$

From (8), this requires that

$$\sqrt{\frac{L_1}{C_1}} \frac{i_1}{v_1} = \sqrt{\frac{L_2}{C_2}} \frac{i_2}{v_2}.$$

One way of insuring that this condition holds is to maintain voltage and current continuity at the transition ($i_1 = i_2$, $v_1 = v_2$), and then to change both the inductance and capacitance by such an amount that

their ratio remains constant. That is, if the resonant frequency of a tank circuit is changed in such a way that the instantaneous tank voltage and current are continuous, and so that the characteristic tank imped-ance, $\sqrt{L/C}$, is maintained, then there will be no phase error.

Such a modulator may be implemented by using a balanced VRO[1] (Variable Reactance Oscillator) configuration as shown in Fig. 14, in which one active element displays a variable capacitance and negative resistance, and the other a variable inductance and negative resistance. The g_m's of each active element are switched in such a way that the quantity L/C remains constant. The modulator of Fig. 15 was con-structed and tested. To give an idea of its performance, typical frequency transitions between 1950 cps and 2250 cps are shown in the oscillogram of Fig. 16.

X. CONCLUSION

It has been shown that phase error at a transition in a frequency shift signal will cause a time error in the output of a zero-crossing detector. The maximum value of this time error may be calculated, leading to the determination of the peak jitter.

It has been further shown that the switched reactance modulators have the largest inherent peak jitter, and that this jitter is bit-rate dependent.
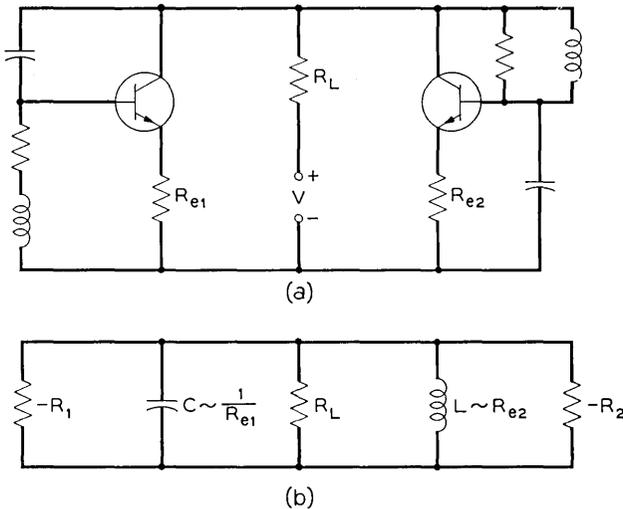

Fig. 14 — The balanced VRO configuration for distortionless frequency modu-lation: (a) basic balanced VRO; (b) equivalent circuit of basic balanced VRO.
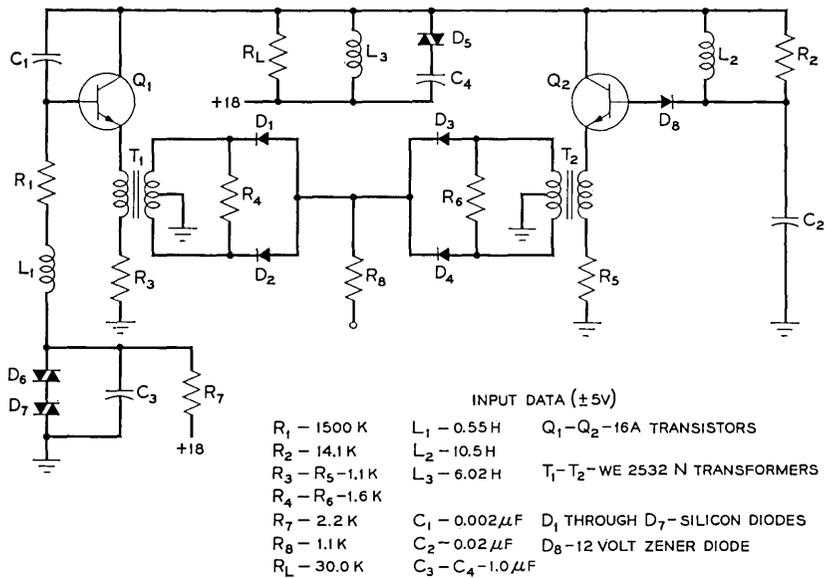
Fig. 15 — Balanced VRO modulator schematic diagram.

INPUT DATA (±5V)

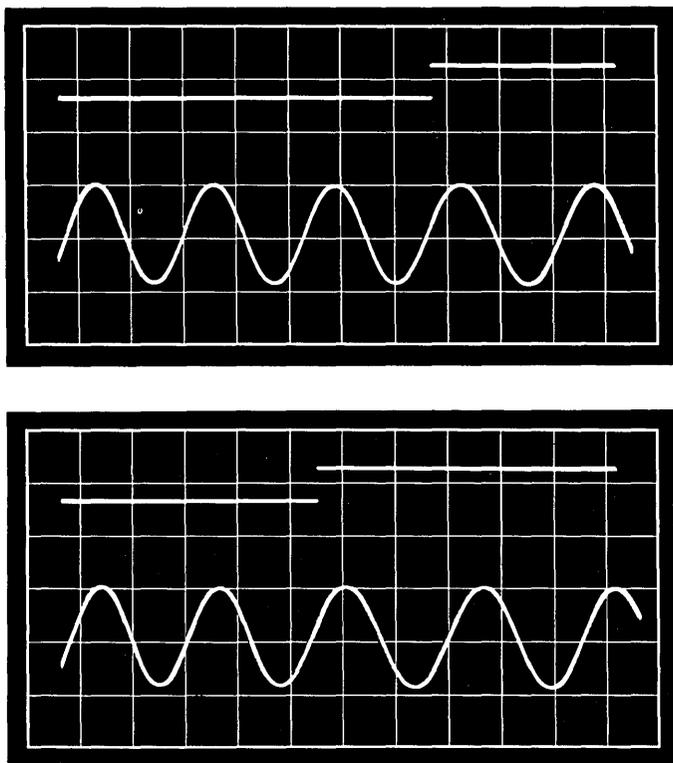|		
R_1 — 1500 K	L_1 — 0.55 H	Q_1–Q_2–16A TRANSISTORS
R_2 — 14.1 K	L_2 — 10.5 H	
R_3 – R_5–1.1 K	L_3 – 6.02 H	T_1–T_2– WE 2532 N TRANSFORMERS
R_4 – R_6–1.6 K		
R_7 – 2.2 K	C_1 – 0.002 μF	D_1 THROUGH D_7– SILICON DIODES
R_8 – 1.1 K	C_2 – 0.02 μF	D_8–12 VOLT ZENER DIODE
R_L – 30.0 K	C_3 – C_4–1.0 μF	

Fig. 16 — Examples of switching performance of balanced VRO: upper trace is data input; lower trace is modulator output; frequencies are 1950 and 2250 cps.

1730

The reactance tube type of modulator and variable reactance oscillator have less peak jitter. The multivibrator can be designed to have as low a value of peak jitter as desired. By using an LC type of modulator in which the tank impedance is held constant at switching, it is possible in principle to design a frequency shift modulator having zero peak jitter.

All of the main points of the theory have been experimentally verified.

XI. ACKNOWLEDGMENT

APPENDIX A

Maximum Phase Error for the Switched Reactance Modulator

The phase error associated with the more severe transition in the switched reactance modulator (e.g., switch opening in the parallel inductor case) is given by (26):

$$\theta_\epsilon = \theta_3 - \tan^{-1}\left[A \tan \theta_3 + \frac{D(1 - A^2) \sin \theta_1}{(A \sin^2 \theta_1 + \cos^2 \theta_1)^{\frac{1}{2}} \cos \theta_3}\right]. \quad (41)$$

It is desired to find those values of θ_1 and θ_3 which maximize this expression. These values will be denoted θ_{1m} and θ_{3m} respectively.

Consider θ_1 first. Differentiating (41) with respect to θ_1 yields

$$\frac{\partial \theta_\epsilon}{\partial \theta_1} = \frac{\gamma \cos \theta_1}{(1 + \beta^2) \cos \theta_3}\left[1 + \frac{(1 - A^2) \sin^2 \theta_1}{A^2 \sin^2 \theta_1 + \cos^2 \theta_1}\right], \quad (42)$$

where

$$\beta = A \tan \theta_3 + \frac{\gamma \sin \theta_1}{\cos \theta_3},$$

and

$$\gamma = \frac{D(1 - A^2)}{(A^2 \sin^2 \theta_1 + \cos^2 \theta_1)^{\frac{1}{2}}}.$$

We are interested in those values of θ for which $\partial \theta_\epsilon / \partial \theta_1 = 0$. Since $A \leqq 1$, all quantities enclosed within the brackets in (42) are always nonnegative; therefore, this term will never become zero. Furthermore,

θ_1 can never cause β to become infinite, nor γ to become zero. Therefore

$$\theta_{1m} = \pm \frac{\pi}{2}$$

is the only value of θ_1 which causes (42) to go to zero. It can be shown that this value of θ_1 corresponds to a maximum point for θ_ϵ. θ_{1m} represents switching at the instant corresponding to the creation of the maximum value for the undesired dc quantity.

Investigation of (42) will reveal that $\theta_3 = \pm\pi/2$ will also cause $d\theta_\epsilon/d\theta_1$ to be zero; however, it can be shown that this corresponds to a minimum point for θ_ϵ. No other combinations of θ_1 and θ_3 will cause (42) to go to zero.

Equation (42) may now be simplified by allowing θ_1 to be $\pm\pi/2$:

$$\theta_\epsilon = \theta_3 - \tan^{-1} \left[A \tan \theta_3 \pm D \frac{(1 - A^2)}{A} \frac{1}{\cos \theta_3} \right]. \qquad (43)$$

Then

$$\frac{\partial \theta_\epsilon}{\partial \theta_3} = 1 - \frac{1}{(1 + \beta^2) \cos^2 \theta_3} (A \pm \gamma \sin \theta_3), \qquad (44)$$

where β and γ are now given by the simplified expressions

$$\beta = A \tan \theta_3 \pm \frac{\gamma}{\cos \theta_3} \qquad (45)$$

$$\gamma = D \frac{(1 - A^2)}{A}. \qquad (46)$$

We are interested now in determining those values of θ_3 which cause $\partial \theta_\epsilon/\partial \theta_3$ to be zero. Setting (44) to zero, one obtains

$$A \pm \gamma \sin \theta_{3m} = (1 + \beta^2) \cos^2 \theta_{3m}.$$

Using the expression (45) for β, and making the substitution $\cos^2 \theta_{3m} = 1 - \sin^2 \theta_{3m}$, a quadratic in $\sin^2 \theta_{3m}$ is obtained:

$$(A^2 - 1) \sin^2 \theta_{3m} \pm \gamma (2A - 1) \sin \theta_{3m} + (\gamma^2 + 1 - A) = 0.$$

Replacing γ with (46) and rearranging, this quadratic becomes

$$\sin^2 \theta_{3m} \mp \frac{D(2A - 1)}{A} \sin \theta_{3m} - \left(\frac{D^2(1 - A^2)(1 + A) + A^2}{A^2(1 + A)} \right) = 0.$$

Thus

$$\sin \theta_{3m} = \pm \frac{D}{2A} (2A - 1) \pm \left[\frac{4A^2 \frac{(1 - D^2)}{D^2} + (A + 5)}{A + 1} \right]^{\frac{1}{2}}. \quad (47)$$

The range of interest for both A and D is from zero to one. Consider the contents of the square brackets in (47). This is minimum for $D = 1$, for which

$$\sin \theta_{3m} \mid_{D=1} = \pm \frac{1}{2A} \left[(2A - 1) \pm \left(\frac{A + 5}{A + 1} \right)^{\frac{1}{2}} \right].$$

If the plus sign in front of the term $[(A + 5)/A + 1]^{\frac{1}{2}}$ were to be used, then

$$\sin \theta_{3m} \mid_{D=1} > 1,$$

for all A. Since $\sin \theta_{3m}$ must be less than one, this is not possible. For $D < 1$, the magnitude of $\sin \theta_{3m}$ is even greater, since the term in the square brackets of (47) is now larger. Thus the minus sign must be used, and

$$\sin \theta_{3m} = \pm \frac{D}{2A} (2A - 1) - \left[\frac{4A^2 \frac{(1 - D^2)}{D^2} + (A + 5)}{A + 1} \right]^{\frac{1}{2}}. \quad (48)$$

Now, for any D, and $A = 1$, the magnitude of $(\sin \theta_{3m})$ is less than one. However, as A decreases, $\mid \sin \theta_{3m} \mid$ increases, and finally reaches unity for some $A = A_p$. For instance, for $D = 1$ (infinite dc time constant), $\sin \theta_{3m} = \pm 1$ for $A = A_p = 1/\sqrt{2}$; for $D = 0$ (zero dc time constant), $A_p = 0$. For other values of $0 < D < 1$, $0 < A_p < 1/\sqrt{2}$.

Thus for a given D and for $A_p < A \leqq 1$, the magnitude of θ_{3m} is less than $\pi/2$ and thus may be used to calculate the peak phase error by substitution into (43). For $A = A_p$, $\theta_{3m} = \pm \pi/2$, and it can be shown that at this point $\theta_{\epsilon m} = \pm \pi/2$. Furthermore, for $A < A_p$, a more detailed study of the expression for phase error (43) will reveal that the phase error may take on any value. Since it is assumed that $\pm \pi/2$ is the worst possible phase error, then we set $\theta_{\epsilon m} = \pm \pi/2$ for $A < A_p$

Summarizing these results, the peak phase error is given by

$$\theta_{\epsilon m} = \pm \theta_{3m} + \tan^{-1} \frac{A}{\cos \theta_{3m}} \left[\sin \theta_{3m} + D \left(\frac{1 - A^2}{A^2} \right) \right], \quad A_p \leqq A \leqq 1,$$

where

$$\sin \theta_{3m} = \frac{D}{2A} (2A - 1) - \left[\frac{4A^2 \frac{(1 - D^2)}{D^2} + (A + 5)}{A + 1} \right]^{-\frac{1}{2}},$$

and

$$\theta_{\epsilon m} = \pm \frac{\pi}{2} \quad \text{for} \quad 0 \leqq A \leqq A_p.$$

A_p is the value of A for which $| \sin \theta_{3m} | = 1$.

APPENDIX B

Jitter Symmetry in the Multivibrator Modulator

The expression for peak phase error in the multivibrator is given by (38):

$$\theta_{\epsilon m} = 2\pi \frac{\left(\frac{1 - A}{A} \right) \ln \frac{1 - \frac{\beta}{\alpha}}{1 - A} + \ln \frac{\beta}{A\alpha}}{2 \ln (1 + \alpha)}. \tag{49}$$

Unlike the LC modulators, this phase error is of only one sign for any one transition. In fact, from Fig. 12, it is seen that this phase error is always negative for $A < 1$ (i.e., $\omega_1 < \omega_2$, or switching from the lower to the higher frequency).

It is to be shown here that the phase error for the opposite transition is of the same magnitude but of opposite sign (thus $\theta_{\epsilon m} > 0$ for $A > 1$). This is accomplished by replacing in (49) A by $1/A$, α by β, and β by α. This replacement yields an expression which describes the peak phase error, $\theta_{\epsilon m}'$, for the opposite transition:

$$\theta_{\epsilon m}' = 2\pi \frac{(A - 1) \ln \frac{1 - \frac{\alpha}{\beta}}{1 - \frac{1}{A}} + \ln \frac{A\alpha}{\beta}}{2 \ln (1 + \beta)}.$$

β is related to α by (37):

$$\ln (1 + \beta) = A \ln (1 + \alpha). \tag{50}$$

Equation (49) may then be rewritten as

$$\theta_{\epsilon m}{}' = \frac{\dfrac{(A-1)}{A} \ln \dfrac{A\left(\dfrac{\alpha}{\beta} - 1\right)}{1 - A} + \dfrac{1}{A} \ln \dfrac{A\alpha}{\beta}}{2 \ln (1 + \alpha)}$$

$$= \frac{-\left(\dfrac{1-A}{A}\right) \ln \dfrac{\left(1 - \dfrac{\beta}{\alpha}\right) \cdot A\left(\dfrac{\alpha}{\beta} - 1\right)}{1 - A} + \dfrac{1}{A} \ln \dfrac{A\alpha}{\beta}}{2 \ln (1 + \alpha)}$$

$$= \frac{-\left(\dfrac{1-A}{A}\right) \ln \left(\dfrac{1 - \dfrac{\beta}{\alpha}}{1 - A}\right)}{2 \ln (1 + \alpha)}$$

$$\frac{+ \ln \dfrac{\beta}{A\alpha} + \left(\dfrac{1-A}{A}\right) \ln \dfrac{A\alpha}{\beta} - \left(\dfrac{1}{A} - 1\right) \ln \dfrac{A\alpha}{\beta}}{2 \ln (1 + \alpha)}$$

$$= -\frac{\left(\dfrac{1-A}{A}\right) \ln \left(\dfrac{1 - \dfrac{\beta}{\alpha}}{1 - A}\right) + \ln \dfrac{\beta}{A\alpha}}{2 \ln (1 + \alpha)}.$$

Thus

$$\theta_{\epsilon m}{}' = -\theta_{\epsilon m}. \tag{51}$$

Now consider the relation (3) between peak phase error and peak time error:

$$\frac{\tau_{\epsilon m}}{T_o} = \frac{\theta_{\epsilon m}}{4\pi} \frac{1 + A}{1 - A}. \tag{52}$$

Let us again study the reverse transition by replacing $\theta_{\epsilon m}$ with $\theta_{\epsilon m}{}'$, A by $1/A$, and $\tau_{\epsilon m}$ by $\tau_{\epsilon m}{}'$:

$$\tau_{\epsilon m}{}' = \frac{\theta_{\epsilon m}{}'}{4\pi} \frac{\left(1 + \dfrac{1}{A}\right)}{\left(1 - \dfrac{1}{A}\right)} = \frac{\theta_{\epsilon m}{}'}{4\pi} \frac{A + 1}{A - 1}.$$

Using (51),

$$\tau_{\epsilon m}{}' = \frac{\theta_{\epsilon m}}{4\pi} \frac{1 + A}{1 - A} = \tau_{\epsilon m},$$

and the peak time jitter is of the same sign and magnitude for each transition. Reference to Fig. 13 shows that the sign of the peak jitter is always negative. Physically, this means that the apparent transition occurs at a time later than the true transition would occur.

REFERENCES

1. Caputo, S., and Highleyman, W. H., An Analysis of a Class of Variable-Frequency Sinusoidal Oscillators Using a Single Active Element, Proc. I.R.E., **50,** February, 1962, pp. 162–170.
2. Crosby, M. G., Reactance-Tube Frequency Modulators, RCA Review, **5,** July, 1940, pp. 89–96.
3. Meyers, S. T., An FM Data Set for Serial Transmission up to 1600 Bits per Second, Conference Paper CP61-1166, presented at Fall General Meeting of the A.I.E.E., Detroit, Michigan, October, 1961.
4. Hysko, J. L., Rea, W. T., and Roberts, L. C., A Carrier Telegraph System for Short-Haul Applications, B.S.T.J., **31,** July, 1952, pp. 666–687.
5. Stumpers, F. L. H. M., Theory of Frequency-Modulation Noise, Proc. I.R.E., **36,** September, 1948, pp. 1081–1092.

Scheduling of Pole Line Inspections

By S. W. ROBERTS

This paper is concerned with the scheduling of pole line inspections. The schedules are based on the physical lifetime distribution of pressure-treated southern pine poles, which constitute some eighty per cent of the current telephone pole plant. Results of studies described herein indicate that for scheduling purposes the physical lifetime distribution of such poles is adequately described by the lognormal density function. Supporting evidence includes.the observation that sound older poles seem no more prone to failure than younger poles. As a consequence, there appears to be no need to decrease the intervals between inspections as poles age. Quality of treatment — particularly the amount of preservative retained — appears to be of primary importance in determining the physical lifetime of poles. The relative influences of environmental factors such as temperature, humidity, rainfall, soil conditions, length of growing season, etc., have not been adequately evaluated; however, for a given quality of treatment, poles tend to last longer in the North than in the South. Consequently, for pole lines in the South, inspections are scheduled earlier in the life of a pole and at shorter intervals thereafter than for similar pole lines in the North.

I. INTRODUCTION

In 1920 only ten per cent of the 14 million poles in line owned wholly or in part by the Bell System were treated full-length with preservatives. Of this ten per cent, most were creosoted southern pine poles. In 1960 about eighty per cent of the 23 million Bell System poles were pressure-treated southern pine poles; the majority of the others were Douglas fir and other western or Rocky Mountain species. Early pressure treatments used creosote; later, pentachlorophenol-petroleum solutions were also in common use. Today a creosote-penta mixture is specified for southern pine.

Early untreated poles, notably cedar and chestnut, had a much greater natural resistance to decay than untreated southern pine poles. They had relatively thin layers of sapwood surrounding the highly decay-

1737

resistant heartwood, whereas today's southern pine poles consist largely
of sapwood. Untreated southern pine poles might be expected to give
less than five years service in the deep South, and but little more in the
North. Treatment with preservatives toxic to decay fungi and insects
prolongs the lifetime of poles with thick sapwood for many decades.
The effectiveness of such treatment is reflected in the average physical
lifetime, which is taken to mean the average time from placement until
failure due to decay (or insect attack). *Physical life* is to be contrasted
with *service life*. Service life, which averages about 25 years, is defined
as the time from placement until replacement, regardless of whether
replacement is for reasons of decay or for obsolescence, line relocation,
fire, lightning, collisions, tornados, wind accompanying sleet, etc.

Periodic inspections serve to classify poles with respect to decay as:
(1) sound, (2) decayed but serviceable to the next inspection, or (3)
failed. With this classification there is for each pole a time interval t_d from
placement to the first appearance of decay, and a time interval t_f from
placement to failure. The difference, $t_f - t_d$, represents the time from
the first appearance of decay until the decay has progressed to such an
extent that the pole should be classed as failed. The time t_f represents
the physical lifetime of the pole.

For purposes of scheduling pole line inspections the distribution
functions of t_d, t_f, and $t_f - t_d$ would provide useful information. For
the type of schedule discussed in the present paper, information con-
cerning the general nature of distribution function of t_f is sufficient.

Based on experience and on experimental data presented in this
paper, the lognormal density function provides a useful model for the
distribution of t_d and of t_f. Experience indicates that adequately treated
poles remain relatively immune to decay even at advanced ages. Log-
normal density functions are shown to provide reasonably accurate
descriptions of the experimental data concerning the time to decay t_d.
Since some of the inspected poles were decayed but not failed, there is
relatively less information concerning t_f than t_d. One reason for not
presenting available data concerning t_f is that the definition of a failed
pole varies in accordance with the application — in particular, in the
test plot experiments a pole is classed as failed only when the decay
has advanced to such an extent that the pole is of no further value
in the experiment. However, based on available information it appears
that lognormal density functions are useful in describing the distribu-
tion of t_f as well as t_d.

Relatively little data are available concerning $t_f - t_d$, but consider-
able variability is evident. In some cases decay spreads rapidly, while

in others it makes very little progress between consecutive inspections. Such variations are not inconsistent with the concept that both t_d and t_f have lognormal distributions. As will become apparent, lack of specific information concerning the distribution of $t_f - t_d$ is of little consequence for the type of inspection plan considered here, nor is the fact that only very rough approximations to the distributions of t_d and t_f can be provided.

From 1945 through 1961 the American Telephone and Telegraph Company recommended that full-length treated southern pine poles be inspected at eighteen years from placement and at six-year intervals thereafter. These recommendations were revised in November, 1961, based partly on results reported in the present paper, which (1) supports the concept of constant intervals between inspections following an initial period of no inspections (due to indications of relatively constant failure rates), and (2) provides some information concerning the differences between the average physical lifetimes of poles in the North and the South.

The main shortcoming of the previous schedule was that it did not take into consideration the fact of earlier decay in the South than in the North. The revision has separate schedules for the North and the South.

As in the past, adherence to recommended schedules is expected to vary from Company to Company in response to their particular appraisals of the need for inspections, based on previous inspection results in their areas. The recommended inspection intervals are meant to serve as guides. If in particular applications consistently too many or too few failures, relative to a chosen economic level, are found, it might be well to adjust the frequency of inspection.

The primary purpose of this paper is to present background information concerning the physical lifetime of treated southern pine poles. This information may prove useful in adjusting the recommended schedules, should that be desirable. A model schedule, employing three-way classifications for geographical locations and for economic classes of poles, is presented in Table I of Section II. The use of three classes, rather than two, provides a buffer between extremes.

Section III discusses briefly the nature and causes of decay and of treatment to prevent decay. Section IV presents results of some of the pertinent field tests conducted as a part of a continuing program of the Outside Plant Laboratory of the Bell Telephone Laboratories for evaluating the effectiveness of various preservative treatments. An analysis of these results is contained in Section V. One conclusion is that the

lognormal density function describes the physical lifetime distribution of pressure-treated southern pine poles more realistically than the normal density function. The normal density function, which is used to advantage in many applications as a first approximation to lifetime distributions, fails to account for the many long-lived individual poles. For example, if, as has been assumed in some applications, the physical lifetime of a pole has a normal distribution with an average of 35 years and a standard deviation of 6-10 years, then a 60-year old pole would have a high probability of failing within the next six years, say. However, experience indicates that failure of such a pole in this 6-year interval is very unlikely — i.e., the 6-year failure rate at age 60 years is small. It is in this connection that the lognormal density function proves useful, for it is characterized by a failure rate function that increases to a maximum and then gradually decreases with age. This is to be contrasted with the ever-increasing failure rate function characterizing the normal density function.

One consequence of the assumption that the physical lifetime of pressure-treated southern pine poles has a lognormal, rather than normal, distribution function is that there is no need to increase the frequency of inspection of such poles as they age. Another consequence concerns estimates of the average physical lifetime. If early failures would indicate an average lifetime of 35 years, assuming a normal distribution function, these same failures might indicate an average lifetime of 100 years, assuming a lognormal distribution function. This sharp increase in estimated average lifetime reflects the fact that some of the individuals may be expected to have extremely long physical lifetimes. As noted in Section VI, estimates of average physical lifetime based on the assumption that a particular distribution function applies should be viewed with restraint appropriate to the application. It would be well to temper such estimates with supplementary information. For example, under certain conditions (i.e., when failed poles are soon replaced, and when there are an insignificant number of replacements for reasons other than decay) the inverse of the proportion of poles that fail annually provides a rough estimate of the average physical lifetime — e.g., an average physical lifetime of fifty years is indicated if over the period of several years an average of two per cent per year of poles in line fail due to decay.

Comparisons of average physical lifetimes can be misleading, for in most applications the distribution of early failures is of primary importance. Potential long-lived poles may be replaced early for reasons other than decay, since the average service life is about 25 years. The

proportion of poles expected to fail within 25 years, or some other selected value, might serve better than average physical lifetime as a measure of the effectiveness of treatment. Alternatively, the expected time until a selected proportion of poles can be expected to have failed might prove useful for comparisons. For example, the median might be used.

II. INSPECTION SCHEDULES FOR SOUTHERN PINE POLES

A model for inspection schedules for southern pine poles is shown in Table I. The zones referred to are delineated on the map that forms Fig. 1. The zones serve to separate the inspection results into three classes: Zone 3 represents areas where environmental conditions are relatively favorable to decay; Zone 1 represents areas of relatively little decay; and Zone 2 serves as a buffer between the two extremes. The zone boundaries are rather arbitrary. The area west of the eastern boundary of the Mountain States Telephone and Telegraph Company has not been included because southern pine poles, with which this paper is primarily concerned, are not generally used in the West, and therefore no inspection results were obtained. For a given quality of treatment, poles definitely have longer life expectancies in Zone 1 than in Zone 3. However, there is no sharp demarcation between adjacent zones. Quality of treatment, particularly the amount of preservative retained after treatment, appears to be of first importance in determining the lifetime of a pole. Poorly treated poles placed in the North may be expected to fail sooner than well treated poles placed in the South.

The classification of pole lines according to economic value is in recognition of the fact that the inspection of poles is largely an economic matter, though safety is also an important factor. The classification in Table I is primarily for illustrative purposes. It may prove helpful to

TABLE I

Economic Class of Line	Zone 1		Zone 2		Zone 3	
	x	y	x	y	x	y
1. (Toll)	8	18	7	15	6	12
2. (Exchange)	10	21	8	18	7	15
3. (Rural)	12	24	10	21	8	18

Inspect pole line every x years. On new line, first inspection should be made at age y years. For replacement poles, omit first regular inspection only.
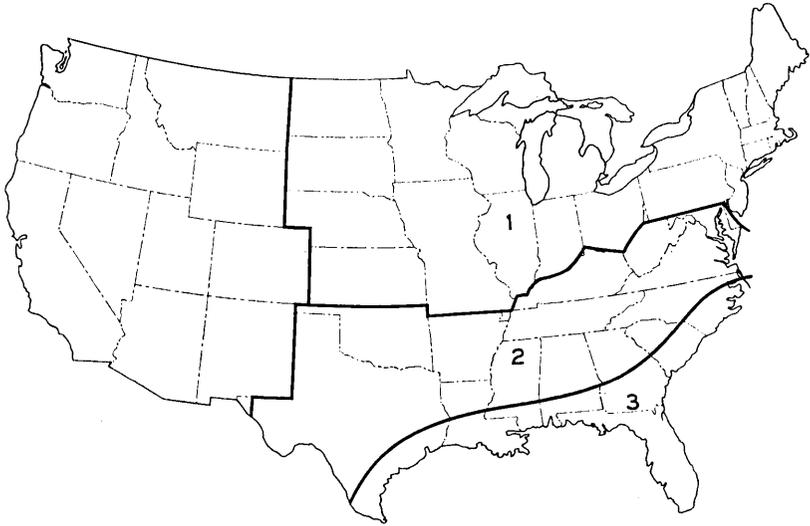
Fig. 1 — Zones used for study of decay in poles.

imagine that the inspection intervals of Table I were selected so that the per cent of failures expected in the three economic classes would be in the ratio of 6:7:8, as might be the case in Zone 3. It has been noted that as the interval between inspections is increased, so is the tendency of inspectors to classify serviceable decayed poles as failures.

Another feature of Table I is that it presumes that complete lines of poles are inspected, omitting young replacements. To illustrate the procedure that might be used, consider the typical pole record, an E-297 form, shown as Fig. 2. Poles on this particular line, which is a toll line in Zone 3, would first be inspected at age 12, in 1953. The replacement poles set in 1950 and 1951 would first be inspected in the inspection of 1959.

Presumably, 100 per cent of the eligible poles in a line will be inspected. Questions may arise as to the feasibility of employing a sampling plan so that inspections may be halted on a line when few failures are encountered in a random sample of poles. Under certain conditions, such as when a line is to be inspected for the first time, a sampling plan might prove useful. However, the appropriate conditions are not often encountered when routine inspections are made. Furthermore, the results of previous inspections in the same area may prove as useful in evaluating the conditions to be expected on a typical line as inspection results from a sample of poles from that line. If the proportion of failures

TOLL		POLE RECORD						
LINE *Shreveport -Lake Charles T.L.*			COUNTY		DATE *4-17-42*			
EXCHANGE OR C. O. DIST.		MUNICIPALITY *Calcasieu Parish*	TAX. DIST.		REWRITTEN			
					REPLACES			

POLE NUMBER	LOCATION DIAGRAM POLES, STUBS, BRACES, ANCHORS AND GUYS. (JOINT OWNERSHIP INDICATED BY CODE)	SPAN LENGTH (FEET)	POLE LENGTH	CLASS	TIMBER AND TREATMENT	JOINT OWNERSHIP FILE NUMBER	PERCENT EQUITY (TEL. CO.)	RIGHT OF WAY FILE NUMBER	YEAR SET
6883	o	136	307		CP				41
			307		CP				54
6882	o	136	307		CP				41
6881	o	136	307		CP				41
6880	o	136	307		CP				41
6879	o	136	307		CP				41
			305		CP				55
6878	o	136	307		CP				41
6877	o	136	307		CP				41
			307		CP				55
6876	o	136	307		CP				41
			305		CP				51
6875	o	136	307		CP				41
6874	o	136	307		CP				41
			305		CP				51
6873	o	136	307		CP				41
6872	o	136	307		CP				41
			309		CP				50
6871	o	136	307		CP				41
			309		CP				50
6870	o	136	307		CP				41
6869	o	136	307		CP				41
			307		CP				53
6868	o	136	307		CP				41
6867	o	136	307		CP				41
6866	o MB	136	307		CP				41
6865	o 728-B	136	307		CP				41
6864	o	136	307		CP				41
6863	o	136	307		CP				41

Location diagram center annotations: K.C.S. R.R. / STATE HIGHWAY No. 104

Fig. 2 — Typical pole record.

found on routine inspections in a general area over a long period of time is not consistent with a predetermined economic level, it may be well to adjust the interval between inspections in that general area.

Thoroughness of inspections may vary with the application. The procedures followed on routine inspections are somewhat different from those followed in this study on the experimental poles. In the latter case the instructions were:

(a) Record information found at the brand ten feet from the butt (species, preservative, supplier, class and length, and year treated) and pertinent comments.

(b) Visually examine above the ground line for mechanical damage, woodpecker holes, split tops, etc. Record findings.

(c) Remove earth from around the pole to a depth of about one foot (deeper in the drier areas of the country) to allow a visual examination and prodding in the critical sector just below the ground line.

(d) Sound the pole with a hand axe from below the ground line to eight feet above the ground line or as high as can be reached conveniently.

(e) In cases of suspicion of internal decay, as determined by sounding, take an increment boring and examine the wood thus removed. Make the boring at right angles to the vertical axis of the pole. Be sure to plug the hole with a locust heartwood or treated plug. Record findings.

(f) Rate the pole as (1) sound, (2) decayed but serviceable, or (3) failed.

At the test plot inspections, the sections are jacked from the ground for a thorough examination. In this way, too, disturbance of the soil is kept at a practicable minimum.

III. DECAY AND ITS PREVENTION

Decay of telephone poles is caused primarily by wood-destroying fungi. The survival and effectiveness of these plants are influenced by certain environmental conditions such as moisture content of the wood, an adequate oxygen supply, and a moderate (60–90°F) temperature. The wood of different species as well as the sapwood and heartwood of a given species varies in susceptibility to decay.

Southern pine is particularly susceptible. To deter or prevent decay, poles of this species are treated with preservatives, of which creosote and pentachlorophenol or mixtures of the two are most common. Generally the preservatives are toxic not only to fungi but also to insects, whose activity constitutes a secondary cause of pole failure.

Economic considerations play a prominent role in the specification

of the preservative treatment. The poles with which this paper is concerned were treated with creosote using the empty cell method of treatment. The specifications called for an average of eight pounds of creosote per cubic foot of wood (as measured by gauge). This is sufficient to penetrate most of the sapwood under the empty cell method, which replaced the full cell method in the early 1930's in Bell System specifications. The full cell method used more creosote — twelve pounds per cubic foot, on the average — but the penetration was not as deep or as uniform, in general. Poles treated under the 12-pound full cell method had more of a tendency to decay internally, and, in addition, were more subject to "bleeding" than poles treated under the 8-pound empty cell method. In fact, the problem of bleeding played an important role in specifying the amount of creosote to be used. More creosote would have resulted in longer-lasting poles, but bleeding would have been more prevalent.

Fig. 3 indicates how the actual amount of creosote absorbed varies from pole to pole within one treating lot.[1] Theoretically, decay is least likely and bleeding is most likely in those poles with the most creosote, though relative volume of sapwood, presence of defects, quality of treatment, and other factors enter the picture. Quality of treatment depends on such things as quality of creosote, conditioning of poles
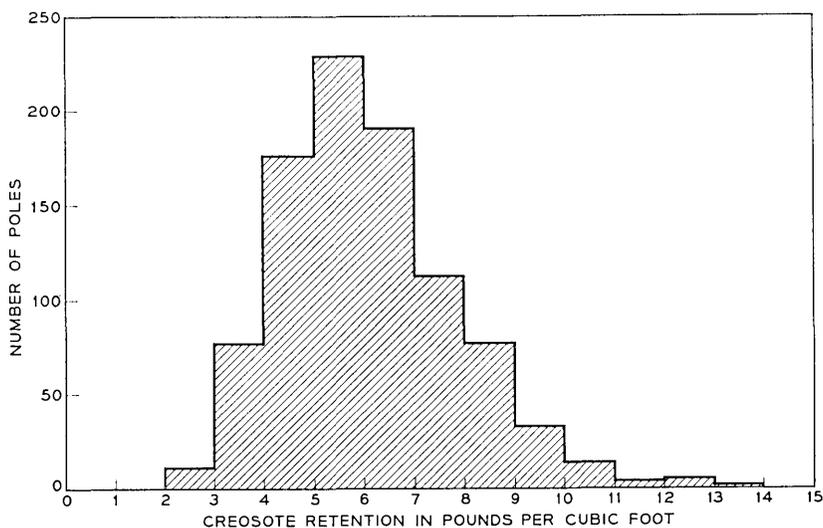
Fig. 3 — Creosote retention in individual poles as determined by gain in weight during treatment.

prior to creosoting, the treating cycle, the moisture content of the poles, and the uniformity and thoroughness of absorption.

IV. RESULTS OF FIELD TESTS

The description of lifetime distributions of items such as poles is often based on observations of lifetimes of a sample of similar items. The best description obtainable from the sample must await the failure of the longest-lived items in the sample. For example, the average cannot be estimated very well from only the early failures unless the nature of the distribution function is known. By the time the last failures occur, the then-current items may have properties that differ from the original items due to changes in design, production methods, or materials. Therefore a compromise between timeliness and accuracy is often necessary for practical reasons.

Commercial treatment for the Bell System of southern pine poles with preservatives using the empty cell method began in the early 1930's and continues today under essentially the same conditions, except that the preservative is now a fortified one containing both creosote and pentachlorophenol. In describing the lifetime distribution of these poles, we have the advantage of almost thirty years of experience. Foremost in usefulness are results of Laboratories field tests on sets of poles and ten-foot pole sections treated under controlled conditions in the 1930's and periodically inspected since that time.

4.1 *Test Plot Results*

Fig. 4 shows the results of inspections of groups of 10-foot pole sections that were treated in 1935 and 1936 and placed in 1936 and 1937 in test sites at Gulfport, Mississippi, and Chester, New Jersey. The sections were placed shortly after treatment. The sections represent either top, center, or bottom thirds of 30-foot poles.

There were 60 sections at each site in the 1935 series, and 55 in the 1936 series. Fig. 4 shows on lognormal probability paper the per cent of these poles classed as decayed (including those classed as failed) on the inspections, which were usually made biannually. Since there is no place on this lognormal paper to show zero per cent decayed, the early inspections at Chester are not represented. Because of the nature of the supporting data, the line through the Chester data was drawn parallel to the Gulfport line.

The advantage of using lognormal probability paper for Fig. 4 is

that if the lognormal distribution describes the time to decay, t_d, then the points will, with allowances for sampling variability, fall roughly along a straight line. Also, the fact that the points representing the Gulfport data do fall roughly along a straight line provides some evidence of the applicability of the lognormal distribution in this case, and, by inference, in similar cases. The line drawn through the Gulfport data may be used for estimates such as the time when 80 per cent of the sections can be expected to have decayed. This estimate would be 90 years. A different estimate would be obtained if a different line were selected to represent the Gulfport data. Such estimates are of limited accuracy.

As illustrated by Fig. 3, the creosote content varies widely among poles of a given charge. An important result of the test plot study was the high correlation between time to decay and creosote content — that is, in general decay appeared earliest in those pole sections with the least initial creosote content. This fact was emphasized in earlier papers.[2,3]
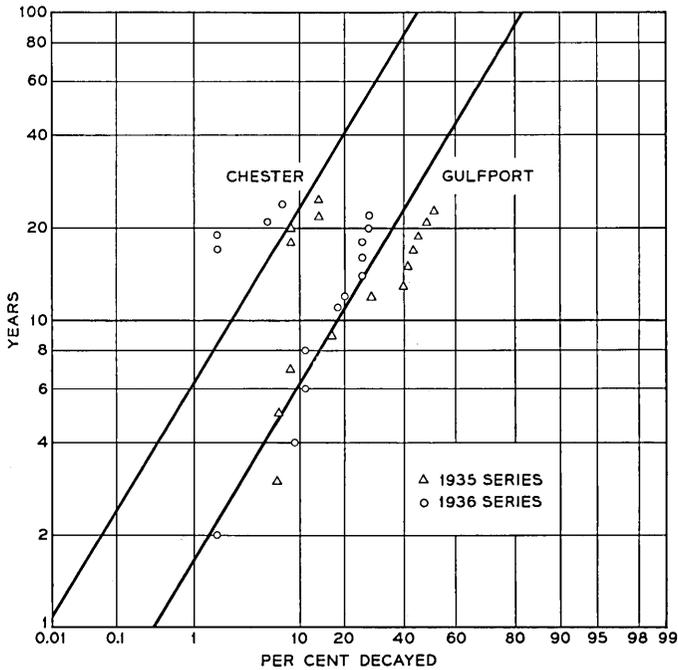
Fig. 4 — Distribution of time to decay, southern pine poles.

4.2 *Some Field Test Results*

Fig. 5 shows on lognormal probability paper the percentage of poles found decayed in several lines which were inspected three times. Most of these lines consist of poles treated under observation of Laboratories personnel in the early 1930's. In cases where the initial creosote content of the individual poles was measured, most of the early failures were poles that retained a relatively low amount of creosote.

4.3 *Other Results*

Because of (1) the limited sample sizes and environmental conditions, and (2) the possibility of bias due to close surveillance of the treatment in the tests whose results have been described thus far, it was decided to inspect representative lines throughout the country. Representative results of these inspections are shown in Figs. 6 through 8 for Zones 1 through 3 respectively. Most of the data for Figs. 6 and 8 were obtained in 1960; Fig. 7 is based on data collected in the early 1950's. The line drawn on Figs. 6–8 is for purposes of illustration. It is line 4 of Fig. 10, and it represents a lognormal distribution with a median of 80 years and a failure rate of roughly one per cent per year (more specifi-
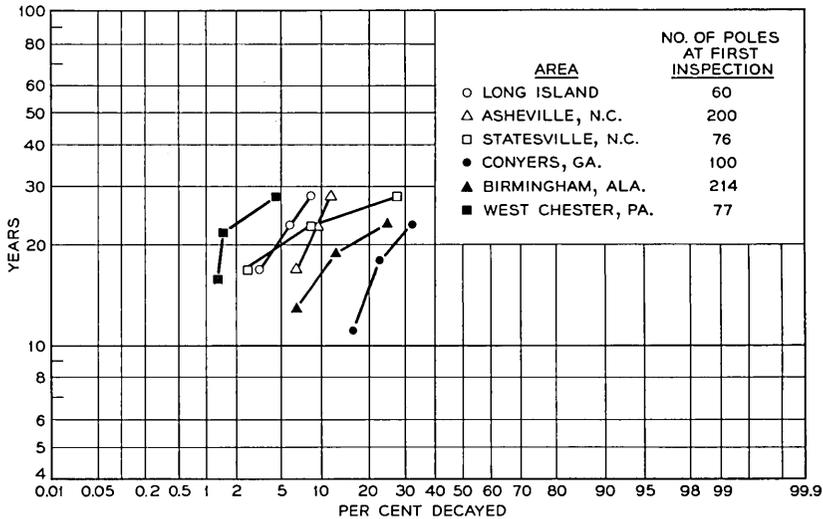
Fig. 5 — Distribution of time to decay, southern pine poles.
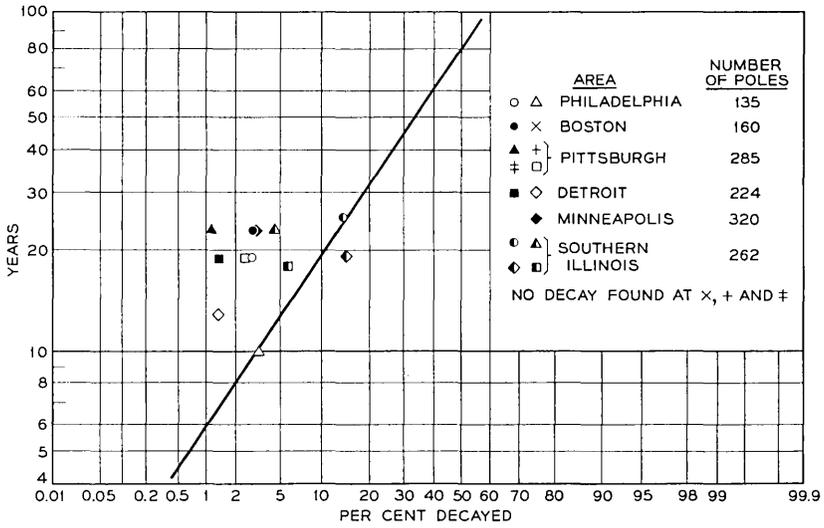
Fig. 6 — Inspection results, Zone 1.
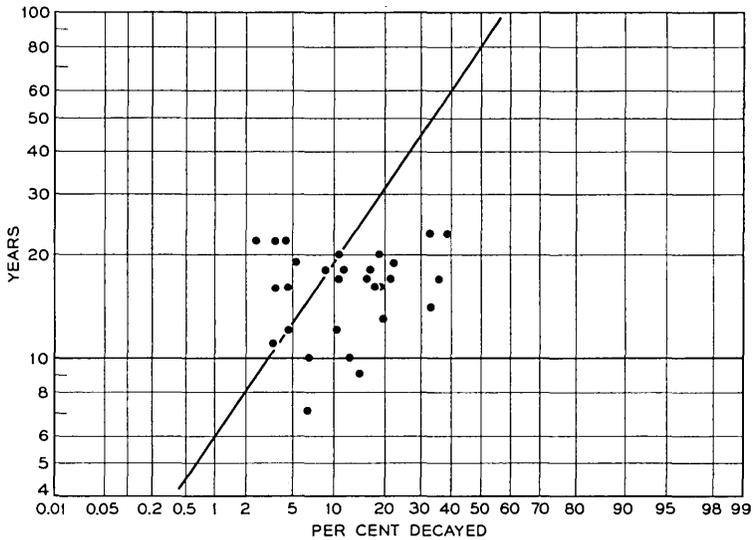
Fig. 7 — Inspection results, Zone 2.
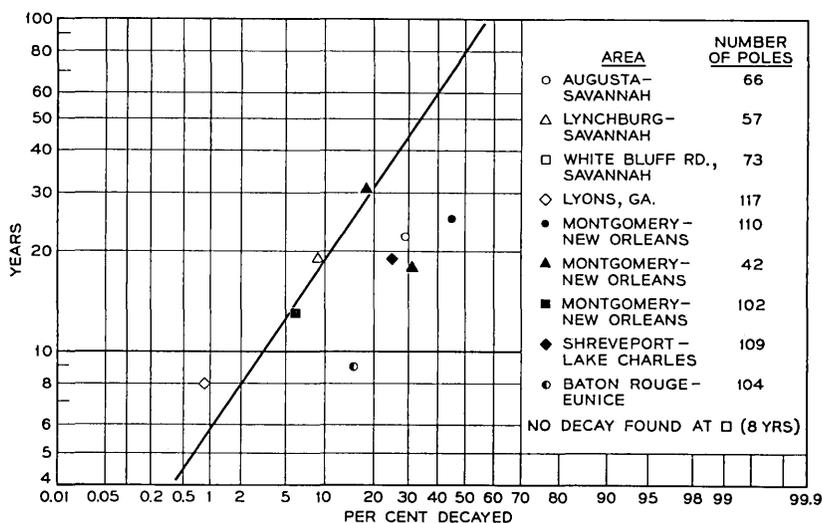
Fig. 8 — Inspection results, Zone 3.

cally, after fifteen years of age about one per cent of the poles that are sound at the beginning of a year will exhibit decay by the end of that year). Based on the data of Figs. 6–8, it appears that most of the pole lines in Zone 1 have failure rates of less than one per cent per year, and most of the pole lines in Zones 2 and 3 have failure rates greater than one per cent per year. Some of the discussion in Section V should prove helpful in interpreting the data.

4.4 Sources of Variability of Results

There are a number of sources of variability in the results presented. First of all, there are sampling errors. To illustrate the meaning of this term, consider a large number of poles treated under fixed conditions and subjected to the same environmental conditions. Let p_t be the probability that a pole selected at random will be decayed at time t. If N poles are inspected at time t, and x of these are classified as decayed, then x/N is an estimate of p_t, and $(x/N - p_t)$ is the sampling error. The absolute value of the sampling error may be expected to be reduced by increasing N. The abscissas of the points plotted on Figs. 4 through 8 are subject to sampling errors; the ordinates are also subject to error, because the age of the poles is given only to the nearest year.

Incidentally, the age shown is measured from time of placement until inspection; the time from treatment until placement is also of importance, but is seldom known.

There are also inspection errors. No two inspectors will consistently agree in their classification of the poles they inspect. As noted in Section II, our inspectors classified poles as (1) sound, (2) decayed but serviceable, or (3) failed. Cases of internal decay and incipient external decay may be noted by one inspector but not by another. It is also difficult to differentiate sharply between a badly decayed pole and a failed pole. How advanced should decay be before the pole is classed as failed? One can specify a proportion of the cross section that must be decayed before a pole is classed as failed, but measurements, particularly of internal decay, are crude. Errors due to differences between inspectors were minimized because most of inspections were by two Laboratories employees following the same general procedure.

In obtaining an estimate of the per cent p_t of poles decayed at age t, it is not adequate to select for inspection a set of N poles of age t at random from the field. The difficulty is that those poles of age t that had been previously removed because of decay would be missing from the sample. For example, suppose 50 per cent of poles of age 40 years have been removed for failure due to decay, and suppose we select at random 100 of the remaining poles for inspection and find ten of them decayed — the proper estimate of per cent decayed at age 40 years is not $\frac{10}{100} = 10$ per cent, but rather $\frac{110}{200} = 55$ per cent. Of course, in practice the per cent of poles of the selected age that have already been removed for decay is generally unknown. To minimize this difficulty, the poles inspected in 1960 in representative parts of the country were in lines of 100 or more poles that were treated and placed in a selected year. Every remaining original pole was inspected, and the estimated per cent of nonsound poles is taken as $(N_d + R_d)/(N_i + R_d)$ where R_d is the number of replacements due to decay in the section of line inspected, N_i is the total number of poles inspected, and N_d is the number of inspected poles classed as either decayed or failed. Because the number R_d had to be obtained (estimated in some cases) from pole records, the choice of lines was restricted to those where reasonably complete histories were available.

In some of the nonexperimental lines inspected prior to 1960 it was impossible to ascertain the number of poles in the inspection lot that had previously been removed for decay. For this reason, some of the estimates of per cent decayed shown in Fig. 7 may be too low.

V. DISTRIBUTION OF PHYSICAL LIFETIME OF CREOSOTED SOUTHERN PINE POLES

5.1 *Selection of Lognormal Distribution Function*

Section IV described results of inspections of selected groups of creosoted southern pine poles. From these results and other experience we would like to establish the nature of an appropriate lifetime distribution function. Then we can estimate parameters — generally average and standard deviation — that determine the particular equation to be used for a specific application. The parameters must reflect the influences of the factors, such as climate, that affect the physical lifetime distribution of the poles under consideration.

Three common types of distribution functions that may prove of practical value in describing the physical lifetime distribution of creosoted southern pine poles within the broad ranges of accuracy needed for setting up inspection schedules are: (1) normal, (2) lognormal, and (3) gamma (the exponential distribution is a special case of the gamma distribution). Fig. 9 illustrates the nature of these types of distribution functions, assuming an average lifetime of 40 years in each case. The top row of figures shows the density functions, which are

$$f(x) = \left\{ \exp -\frac{(x-\mu)^2}{2\sigma^2} \right\} \Big/ \sqrt{2\pi}\ \sigma,$$

$$= \left\{ \exp -\frac{(\log x - \mu)^2}{2\sigma} \right\} \Big/ \sqrt{2\pi}\ x\sigma, \quad \text{and}$$

$$= \{ \exp - \lambda x \}\ \lambda^{k+1}\ x^k / k!,$$

respectively, for normal, lognormal, and gamma; μ, σ, λ and k are parameters that are to be chosen to suit the application. The normal curve is symmetrical about its average value, μ. The probability that a pole will fail within x years is represented by the fraction of the total area under the curve that falls to the left of abscissa x. The second row of curves shows the fraction surviving,

$$S(x) = \int_x^\infty f(x)\ dx.$$

That is, it shows at abscissa x the probability that a pole will survive beyond x years. The third row of curves shows the instantaneous failure rate, $f(x)/S(x)$. This is the limit, as Δx approaches zero, of the probability that a pole that has survived to x years will fail within the
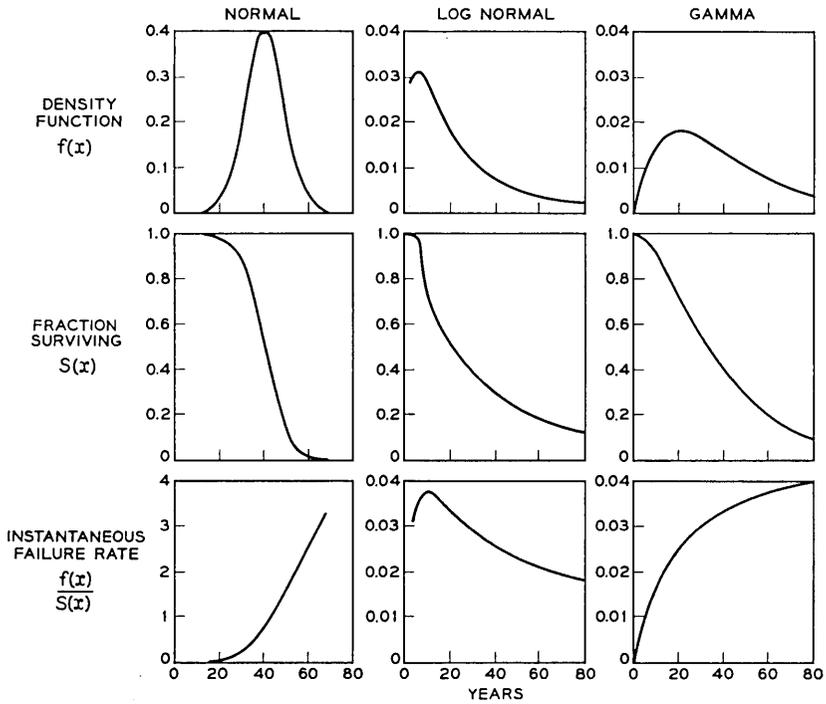
Fig. 9— Comparison of normal, lognormal, and gamma density functions.

interval between x and $x + \Delta x$. Later we shall be concerned with the six-year failure rate, which involves Δx of six years. The three types of distribution functions have different types of failure rate functions. The failure rate for the normal distribution increases monotonically and that for the gamma distribution approaches a constant, while the failure rate for the lognormal distribution increases to a maximum and then gradually decreases. Experience indicates that the failure rate functions of the gamma and lognormal distributions are considerably more realistic than that of the normal distribution. The normal distribution fails to account for the many long-lived poles observed in the field. If the failure rate of poles increased with age as indicated by the normal distribution, special attention should be given to poles as their ages passed beyond their expected values.

While for purposes of choosing inspection intervals, either the lognormal or gamma distribution would prove suitable, there are reasons to believe the lognormal distribution provides a more realistic descrip-

tion of failure rates of older poles. To explain why failure rates may decrease with age, we shall describe briefly some of the present thinking on the effectiveness of preservatives.

When poles are treated, there is variation in effectiveness of treatment even among poles in a single treatment charge. As illustrated by Fig. 3, some poles absorb and retain more than others; also, the uniformity of absorption may vary significantly around the circumference and along the length of a given pole. Let us assume for purposes of illustration that the amount of preservative retained in a selected cubic section near the surface of a pole is a good measure of the effectiveness of the treatment in deterring decay. Previous studies of the effectiveness of preservatives indicate that the expected life of a pole under fixed environmental conditions increases with increasing preservative content. Of course, there is an upper limit to the amount of preservative that wood can absorb. Further, depending on type of (1) wood, (2) preservative, (3) fungus, and (4) environment, there is a critical value of preservative content above which the wood is protected from that fungus. If, after the evaporation and migration that occurs with aging, the preservative content remains above the highest critical value (often referred to as the "threshold retention") for any fungus likely to be encountered, presumably the wood will never decay. Thus there is the possibility of a pole lasting indefinitely unless some new decay organism appears. It is primarily due to the existence of such poles that the lognormal distribution function appears to present a better description of pole lifetimes than either the normal or the gamma functions. Future results may indicate improvements over the lognormal distribution function in accounting for such poles. A recent book[4] discusses the lognormal distribution and the nature of many of its applications.

5.2 *Family of Lognormal Distribution Functions*

Once the lognormal distribution has been chosen to represent physical lifetime distributions, there remains the problem of selecting the appropriate parameters to use for a particular pole line. Two parameters are to be selected, and these may be thought of as determining the slope and an intercept of a straight line on lognormal probability paper. When two or more points are plotted on such paper to represent the per cent of failed poles found on two separate inspections of a given lot of poles, a straight line can be drawn through or near such points to represent the physical lifetime distribution. A single point will not suffice, and little confidence can be placed on a line drawn through a pair of points. Considerably more confidence could be placed in the

straight line if we knew its approximate slope, for example, or if ex-
perience indicated that it was likely to belong to a particular family
of straight lines. In these cases a single point would be of use.

Fig. 10 shows on lognormal probability paper a family of parallel
straight lines having slopes roughly the same as that of the line of Fig. 4
through the Gulfport test plot data. These lines, which will be called
Curves 1 through 6, are for purposes of illustration. If they represented
physical lifetime distributions of poles in six different poles lines, they
would indicate that these poles had median lifetimes of 10, 20, 40, 80,
160, and 320 years, respectively. The averages are 1.87 times the median
in each case.

Fig. 11 shows the 6-year failure rate functions for the Curves 1 through
6 of Fig. 10. Notice that the failures rates are slow to change.

To illustrate the application of Figs. 10 and 11, consider the pole
line from Asheville, N.C., represented on Fig. 5. Assume that the dis-
tribution of t_f rather than t_d is represented in Fig. 5. This pole line would
have characteristics somewhere between those represented by Curves
4 and 5. Looking at Fig. 11, we would be led to expect about 4 or 5
per cent of the poles surviving at 30 years to fail within the next six
years. The median lifetime of these poles might be expected to be
roughly 100 years, and, correspondingly, an average lifetime of 187
years is indicated, based on the assumptions used.

Considering the existence of sampling errors, the results shown on
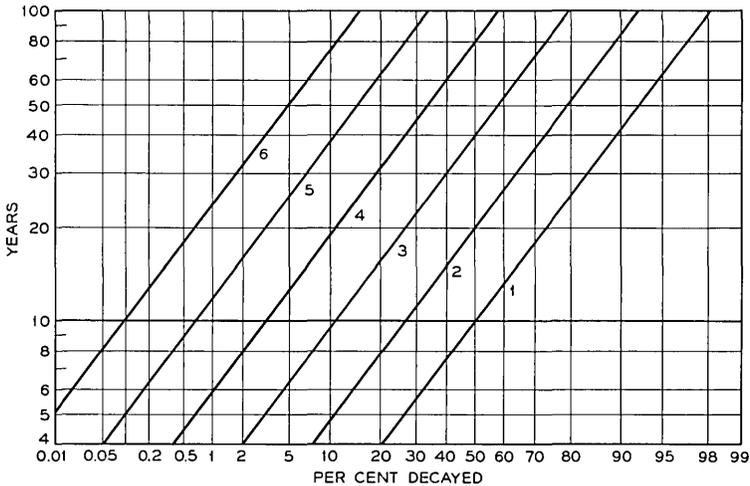
Fig. 10 — A family of lognormal density functions.
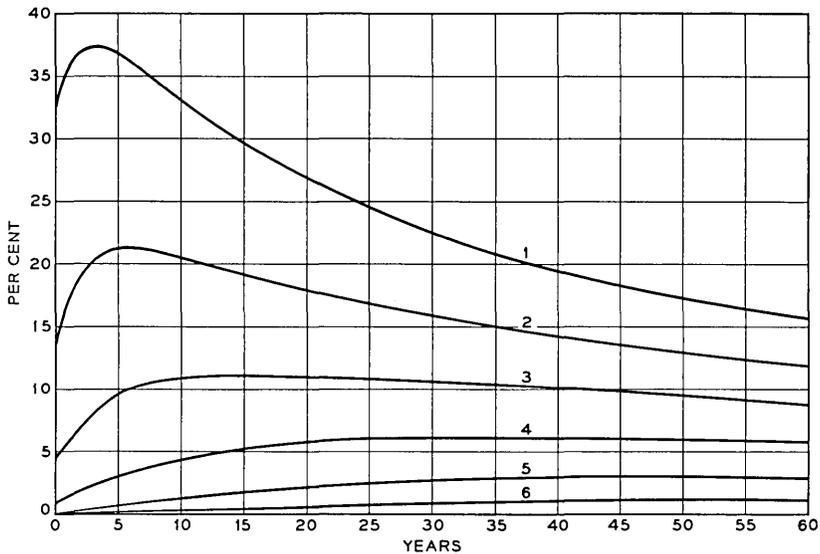
Fig. 11 — Six-year failure rates for curves of Fig. 10.

Fig. 5 are remarkably consistent among themselves, and they provide some support for the use of a family of distributions such as represented in Figs. 10 and 11. Of course, allowances must be made for the differences between time t_d to the first appearance of decay and the time t_f of failure. As a first approximation we might estimate that $t_f - t_d$ averages 6 years in the South and 10 years in the North. A comparison of the results shown in Figs. 5 through 8 with Figs. 10 and 11 leads to the conclusion that median pole lines (half of the pole lines will be better, half worse) in Zones 1, 2, and 3, respectively, will have failure rates in the order of 0.5, 1.3, and 1.5, per cent per year, respectively. This conclusion played a prominent role in the design of the inspection schedule of Table I.

VI. SUMMARY

An analysis of results of inspections of creosoted southern pine poles in test plots and in selected lines in the field indicates that their physical lifetime distribution appears to be adequately described by the lognormal distribution function. There is no evidence that the failure rate of these poles increases as they survive beyond their life expectancy;

indeed, there is reason to suspect that the failure rate may decrease, thereby supporting the contention that the lognormal distribution is suitable.

If the lognormal distribution is appropriate, the average physical lifetime of these poles is considerably greater than commonly believed. One explanation of this is that some of the poles may "never fail." Because of lack of evidence concerning these poles as they reach an advanced age, extrapolation of results from the first thirty years of pole life must necessarily be made with restraint. For this reason, estimates of average physical life should allow considerable latitude for accuracy. Under this circumstance, a rule-of-thumb for such estimates that may prove useful is as follows: (1) Estimate the average annual failure rate of poles in the 30–50 year age bracket. (2) The reciprocal is an estimate of the life expectancy of these poles. For example, suppose in a given area 10,000 poles in this age bracket were inspected and declared serviceable in 1950, and of these, 600 were declared to have failed by 1956. Then the failure rate is roughly one per cent per year, and an estimate of the life expectancy of these poles is $(0.01)^{-1} = 100$ years. This rule-of-thumb will indicate in general that the life expectancy is well over 35 years.

The results also support the observation that poles last longer in the North than in the South. Evidently this is due to a better environment for growth (length of growing season, annual rainfall, and average temperature and humidity are considered to be of primary importance) of wood-destroying fungi in the South. This fact leads to the requirement of more frequent inspections in the South to maintain a given level of pole line quality.

REFERENCES

1. Lumsden, G. Q., Fortified Wood Preservatives, Forest Products Jour., **10,** 1960, pp. 456–462. Bell System Monograph 3718.
2. Colley, R. H., The Evaluation of Wood Preservatives, B.S.T.J., **32,** January and March, 1953, pp. 120–169, 425–505.
3. Lumsden, G. Q., A Quarter Century of Evaluating Pole Preservatives, Proc. of the Amer. Wood-Preservers' Association, **48,** 1952, pp. 27–47.
4. Aitchison, J., and Brown, J. A. C., *The Lognormal Distribution*, Cambridge University Press, 1957.

Minimum-State Sequential Circuits for a Restricted Class of Incompletely Specified Flow Tables*

By E. J. Mc CLUSKEY, JR.†

(Manuscript received June 22, 1962)

This paper is concerned with the problem of obtaining minimum-state sequential circuits for incompletely specified flow tables. Attention is directed to relay-type flow tables in which the only unspecified entries are those which occur because of restrictions on the allowed input-variable changes. For this type of flow table it is shown that a simplified version of the Unger-Paull procedure is sufficient. In particular, only maximum compatibles need be considered in forming the minimum-state sequential circuit.

I. INTRODUCTION

One of the classical problems of sequential circuit theory is that of obtaining a minimum-state sequential circuit satisfying the requirements of a given flow table. When the flow table is incompletely specified, the procedures for obtaining the minimum-state sequential circuit are lengthy and require such extensive enumeration that they are impractical for computer implementation. This paper discusses a restricted type of incompletely specified flow table for which more efficient procedures can be devised. In particular, relay-type flow tables in which the unspecified entries all are present because of a restriction of the manner in which the inputs can change are considered. It is shown that for this type of flow table only the maximal compatibles or compatibility classes need be considered in forming a minimum-state circuit.

II. BACKGROUND

The problem of finding a minimum-state sequential circuit for an incompletely specified flow table has been discussed extensively in

previous papers. The results presented in these papers, particularly that of Paull and Unger,[1] are necessary for the results to be presented here. A brief summary of previous results assumed in this paper will be presented first.

The usual approach to the study of minimum-state sequential circuits involves consideration of which flow tables specify the same external behavior as a given flow table Q. Any flow table which does specify the same external behavior as Q is said to *cover* Q. The usual objective is to formulate a procedure for finding, for any flow table Q, a minimum-state flow table which covers Q. A formal definition of the covering relation among flow tables is:

Definition. A flow table P is said to cover a flow table Q (written $P \supset Q$) if and only if, for each internal state q_i of Q there is an internal state p_j of P such that for any input sequence applied to both tables initially in states q_i and p_j respectively, the output sequences are identical *whenever the output of Q is specified.*

The definition is suitable for flow tables in which each next-state entry is specified but some of the output entries may be unspecified. There is no loss of generality in considering this class of circuits since it has been shown by Narasimhan[2] that all flow tables can be placed in this form. This definition of a flow table covering another flow table induces a corresponding relation between the internal states of the two tables.

Definition. An internal state p_i of a flow table P is said to cover an internal state q_j of a flow table Q (written $p_i \supset q_j$) if and only if, for any input sequence applied to P and Q initially in states p_i and q_j, respectively, the outputs are identical whenever the output of Q is specified.

If flow table P covers flow table Q and P has fewer states than Q, then one state of P must cover more than one state of Q. Whenever two states of a flow table can be covered by a single state of another flow table, the two states must have the following relation:

Definition. Two internal states, q_i and q_j of Q, are *compatible* if and only if, for all input sequences, the output sequence which results when Q is initially in q_i is the same as the output sequence which results when Q is initially in q_j *whenever both outputs are specified.*

Theorem 1. If internal state p_i of P covers both internal states q_j and q_k of Q, then states q_j and q_k must be compatible.

Lemma. If internal state p_i of P covers internal states q_{j_1}, q_{j_2}, $\cdots$ q_{j_k} of Q then states q_{j_1}, q_{j_2}, $\cdots$ q_{j_k} must form a compatibility class; that is, each pair of the q_{j_1} must be compatible.

It follows from this that if $P \supset Q$, then each state p_i of P must cover a compatibility class of the states of Q. In addition, the compatibility classes covered by states of P must have the closure property, to be described next.

Definition. The input states of a sequential circuit will be represented by the symbols $\mathbf{x}^0$, $\mathbf{x}^1$, $\cdots$ $\mathbf{x}^v$. The internal states of a sequential circuit will be represented by the symbols s_1, s_2, $\cdots$ s_r.

Definition. The next-state entry specified by a flow table for input state $\mathbf{x}^\alpha$ and internal state s_i will be represented by the symbol $S(\mathbf{x}^\alpha, s_1)$.

Definition. A collection of compatibility classes is said to be *closed* if and only if for each compatibility class $\{s_1,\ s_2,\ \cdots\ s_m\}$, all of the states $S(\mathbf{x}^\alpha, s_1)$, $S(\mathbf{x}^\alpha, s_2)$ $\cdots$ $S(\mathbf{x}^\alpha, s_m)$ are included in a single compatibility class in the collection. This must be true for all choices of α.

Theorem 2. A flow table P covers a flow table Q if and only if:

(A) *each internal state of Q is included in at least one compatibility class of Q that is covered by an internal state of P, and*

(B) *the compatibility classes of Q which are covered by internal states of P form a closed collection.*

There is a procedure whereby for each closed collection of compatibility classes of a flow table Q (with every internal state of Q included in at least one compatibility class) it is possible to obtain a flow table P which covers Q and which contains the same number of internal states as there are compatibility classes in the collection. Thus, a minimum-state flow table which covers a given flow table Q can be formed from a closed collection of compatibility classes of Q containing a minimum number of such classes.

Satisfactory techniques for determining the compatibility classes for a given flow table are known.[1] Actually the maximal compatibility classes can be determined, and all other compatibility classes must be subclasses of these. Presently known techniques for obtaining minimum-state flow tables are inadequate because of the necessity for considering the inclusion of nonmaximal compatibility classes in the closed collection used in forming the covering flow table P.[1] Each subclass of the maximal compatibility classes must be considered, and this number of subclasses can be prohibitively large. The necessity for considering non-maximal compatibility classes results directly from the closure requirement. The object of this paper is to show that for a certain type of incompletely specified flow table it is always possible to use the maximal compatibility classes in forming a minimum-state flow table. For this type of flow table, the procedure for obtaining a minimum-state flow is very much simpler than in the general case. Moreover, the type of

flow table for which this result holds is the type most often encountered in actual design problems.

III. TYPE A FLOW TABLES

The following discussion applies specifically to flow tables for fundamental mode operation.[3] For the purposes of this paper, a circuit will be said to be operating in fundamental mode if no input is changed until after the circuit has "settled down," that is, until after all internal signal changes have stopped. This type of circuit operation is often referred to as "relay type" or "asynchronous."[4]

It is customary to begin the design of a fundamental mode sequential circuit by writing down a primitive flow table — a flow table in which there is exactly one stable state in each row. For such a table it is possible to associate one of the input states (columns of the flow table) with each internal state, since each internal state is stable for exactly one input state.

Definition. Let P be a primitive, fundamental-mode flow table. Let $s_1{}^\alpha, s_2{}^\alpha, \cdots s_\sigma{}^\alpha$ be the internal states of P which are stable for the input state $\mathbf{x}^\alpha$; $s_1{}^\beta, s_2{}^\beta, \cdots s_\tau{}^\beta$ be the internal states of P which are stable for input state $\mathbf{x}^\beta$, etc.

It will be assumed that in a flow table each unstable next-state entry is followed directly by a stable next-state entry — no multiple changes of internal state are allowed. Whether a flow table is of the type considered here, to be called Type A, depends on the mechanism whereby unspecified entries occur in the table. Specifically, a flow table is of Type A if the only unspecified entries are those which arise because of a restriction on which input states can directly follow each given input state.

Definition. A flow table is of Type A if and only if: (a) it is a flow table for fundamental mode operation; (b) it is a primitive flow table; (c) each unstable next-state entry refers to an internal state which is stable for the corresponding input state; and (d) the only unspecified entries are those which occur because of a restriction on the input states which can directly follow each possible input state.

For fundamental-mode flow tables it is common practice to assume that only single changes of input variables are possible. Thus, the input state for which $x_1 = 0$, $x_2 = 0$, cannot be followed by the input state with $x_1 = 1$, $x_2 = 1$. If this restriction is the only source of unspecified entries in the table, then the table is of Type A.

Part (d) of the above definition of Type A flow tables can be restated directly in terms of the pattern of unspecified entries in the table (rather than the mechanism by which they arise). In order to describe

this, it is convenient to assume that the rows in the table are partitioned so that all of the rows which are in the same partition are stable for the same input state and there is one partition for each input state. Actually, if the outputs associated with the stable states are all specified, each partition need only include rows which are all stable for the same input state *and* have the same outputs associated with the stable next-state entry. Part (d) of the definition of Type A flow tables can be considered satisfied if, whenever any row has an unspecified entry for an input state $\mathbf{x}^\alpha$, all other rows in the same partition also have unspecified entries for input state $\mathbf{x}^\alpha$. This condition is actually somewhat more general than the condition (d) given originally, but the theorems are all valid for this more general condition.

For Type A flow tables, the compatibility relation has certain properties which are not generally satisfied for arbitrary flow tables. It is these special properties which form the basis for the simplified procedure to be derived here.

Theorem 3. Let $s_i{}^\alpha$, $s_j{}^\alpha$, $s_k{}^\alpha$, be three internal states of a Type A flow table P which are all stable for input state $\mathbf{x}^\alpha$. If $s_i{}^\alpha$ and $s_j{}^\alpha$ are compatible, and $s_i{}^\alpha$ and $s_k{}^\alpha$ are compatible, then $s_j{}^\alpha$ and $s_k{}^\alpha$ are compatible.

Proof. By the definition of compatibility, when any input sequence is applied to P the output sequence with P initially in $s_j{}^\alpha$ will be the same as the output sequence with P initially in $s_i{}^\alpha$ whenever both outputs are specified. However, because P is a Type A flow table, whenever the output is specified for P initially in $s_i{}^\alpha$, the output for P initially in $s_j{}^\alpha$ will be specified and vice versa. Similar remarks apply to states $s_i{}^\alpha$ and $s_k{}^\alpha$. Thus the output for P initially in $s_j{}^\alpha$ must always agree with the output for P initially in $s_i{}^\alpha$, and the output for P initially in $s_k{}^\alpha$ must always agree with the output for P initially in $s_i{}^\alpha$. Whenever any one of these outputs is specified, all three must be specified; therefore the outputs for P initially in $s_j{}^\alpha$ and P initially in $s_k{}^\alpha$ must always agree. This shows that states $s_j{}^\alpha$ and $s_k{}^\alpha$ must be compatible. See also Ref. 4, pp. 183–185.

Let the fact that two states p and q are compatible be written symbolically as $p \bigcirc q$. Then for states satisfying the conditions of Theorem 3, the following properties must hold:

(P1) $s_i{}^\alpha \bigcirc s_i{}^\alpha$ (reflexive)

(P2) If $s_i{}^\alpha \bigcirc s_j{}^\alpha$ then $s_j{}^\alpha \bigcirc s_i{}^\alpha$ (symmetric)

(P3) If $s_i{}^\alpha \bigcirc s_j{}^\alpha$ and $s_i{}^\alpha \bigcirc s_k{}^\alpha$, then $s_j{}^\alpha \bigcirc s_k{}^\alpha$ (transitive).

A binary relation which satisfies these three properties is an equivalence relation.[5] The important characteristic of an equivalence relation is that it divides the set of objects on which it is defined into disjoint (nonoverlapping) equivalence classes.

Theorem 4. Let P be a Type A flow table. Let s_i^α and s_j^α be two internal states of P which are both stable for input state $\mathbf{x}^\alpha$, and let s_k^β be an internal state of P which is stable for input state $\mathbf{x}^\beta$. If s_i^α and s_j^α are compatible, and s_i^α and s_k^β are compatible then s_j^α and s_k^β are compatible.

Proof. For any input sequence, the outputs for P initially in s_i^α and for P initially in s_k^β must be identical whenever both are specified. However, the output for P initially in s_j^α is specified whenever the output for P initially in s_i^α is specified, and these outputs must always be the same. Thus, all specified outputs for P initially in s_j^α are the same as the corresponding outputs for P initially in s_i^α, and the s_i^α outputs are the same as the outputs for P initially in s_k^β whenever both outputs are specified. It follows from this that the outputs for P initially in s_j^α and for P initially in s_k^β must be the same when both are specified and hence that s_j^α and s_k^β are compatible.

Definition. A set of internal states of a flow table P is a maximum compatibility class if and only if (i) every pair of states which are both in the set are compatible, and (ii) there is no other state of P not in the set which is compatible with all of the states in the set.

Theorem 5. Let P be a Type A flow table. Let s_i^α and s_j^α be two internal states of P which are both stable for input state $\mathbf{x}^\alpha$ and which are compatible. Then any maximum compatibility set which includes s_i^α must also include s_j^α and vice versa.

Proof. Suppose that C is a maximum compatibility class which includes s_i^α. If there is any other state in C which is stable for input state $\mathbf{x}^\alpha$, say s_k^α, then s_i^α and s_k^α are compatible and s_i^α and s_j^α are compatible. By Theorem 3, states s_k^α and s_j^α must then be compatible. Thus s_j^α is compatible with all states in C which are stable for input $\mathbf{x}^\alpha$. Suppose that there is some state s_h^β in C which is stable for some input state β different from α. Then states s_i^α and s_h^β are compatible and states s_i^α and s_j^α are compatible. By Theorem 4, states s_h^β and s_j^α must then be compatible. Thus state s_j^α is compatible with all states in C and therefore must be included in C.

Theorem 6. Let P be a Type A flow table. Then any collection of maximum compatibility classes of P for which each internal state of P is included in at least one of the maximum compatibility classes is closed.

Proof. Let $\{s_1, s_2, \cdots s_m\}$ be one of the maximum compatibility classes. Then if the collection of maximum compatibility classes is closed, all of the states $S(\mathbf{x}^\alpha, s_1)$, $S(\mathbf{x}^\alpha, s_2) \cdots S(\mathbf{x}^\alpha, s_m)$ must be included in one of the maximum compatibility classes of the collection. Since P is a Type A flow table, all of the states $S(\mathbf{x}^\alpha, s_1)$, $S(\mathbf{x}^\alpha, s_2)$, $\cdots S(\mathbf{x}^\alpha, s_m)$ must be stable for input state $\mathbf{x}^\alpha$. It has been shown that all pairs of these states must be compatible since $\{s_1, s_2, \cdots s_m\}$ is a compatibility

class.[1] By Theorem 5 any maximum compatibility class which includes the internal state $S(\mathbf{x}^\alpha, s_1)$ must also include $S(\mathbf{x}^\alpha, s_2) \cdots S(\mathbf{x}^\alpha, s_m)$. The conditions of Theorem 6 assume that there is at least one maximum compatibility class in the collection which includes state $S(\mathbf{x}^\alpha, s_1)$. Therefore there must be at least one class in the collection which includes all of the states $S(\mathbf{x}^\alpha, s_1)$, $S(\mathbf{x}^\alpha, s_2)$, $\cdots S(\mathbf{x}^\alpha, s_m)$. From this it follows that the collection is closed.

Theorem 7. Let P be a type A flow table. Then there is at least one minimum-state flow table Q which (a) covers P, (b) contains the minimum number of internal states for any flow table covering P, and (c) for which each internal state of Q covers a maximum *compatibility class of P.*

Proof. There is at least one flow table — P itself — which covers P, and there must be at least one such table containing a minimum number of states. Suppose that R is a flow table containing a minimum number of states and covering P. If each state of R covers a maximum compatibility class of P, the theorem is satisfied. Therefore suppose that each state r_i of R covers a compatibility class C_i of P and that at least one of these compatibility classes is not maximal. Now form a new collection of compatibility classes by replacing each C_i by one of the *maximal* compatibility classes in which it is included. The maximal compatibility class which replaces C_i will be denoted as M_i. The collection of the M_i will (a) contain the same number of classes as the collection of the C_i, (b) include each state of P in at least one M_i, and (c) be closed because of Theorem 6. It is thus possible to form from the M_i a new flow table Q which satisfies all of the conditions of the theorem.

IV. EXAMPLE

In order to illustrate the significance of the theorems, an example of a Type A flow table will be discussed. Table I shows a Type A flow table and the corresponding maximal compatibility classes. States 5 and 10 are the only pair of compatible states which are both stable for the same input state. By Theorem 5, any maximal compatibility class which includes either of these two states (5 or 10) must include both of them. Inspection of Table I(c) shows this to be true. It follows from Theorem 6 that any closure requirements must involve only these two states, and Table I(b) shows this to be true. The formation of a minimum-row flow table which covers Table I(b) requires only that a sufficient number of maximum compatibility classes be chosen so that each internal state of Table I(a) is included in at least one maximal compatibility class. This problem is formally identical to the problem of choosing which prime implicants should be included in a minimal sum

TABLE I — A TYPE A FLOW TABLE

(a) Flow Table

S	x^0	x^1	x^2	x^3	x^4
1	①,0	2 ,0	—	5 ,0	—
2	4 ,1	②,0	3 ,0	—	—
3	—	2 ,0	③,0	5 ,0	6 ,0
4	④,1	8 ,1	—	10 ,0	—
5	—	—	3 ,0	⑤,0	7 ,1
6	1 ,0	—	3 ,0	5 ,0	⑥,0
7	4 ,1	—	9 ,0	10 ,0	⑦,1
8	4 ,1	⑧,1	9 ,0	—	—
9	—	8 ,1	⑨,0	10 ,0	6 ,0
10	—	—	3 ,0	⑩ ,0	7 ,1

S, Z

(b) Implication Table for Determining Compatibity

	1	2	3	4	5	6	7	8	9
2	x								
3	√	√							
4	x	x	x						
5	√	√	x	√					
6	√	x	√	x	x				
7	x	x	x	√	x	x			
8	x	x	x	√	x	x	√		
9	x	x	x	√	x	x	x	√	
10	5, 10	√	x	√	√	x	x	x	x

(c) Maximal Compatibility Classes

A: 4, 8, 9	E: 2, 3
B: 4, 7, 8	F: 2, 5, 10
C: 4, 5, 10	G: 1, 5, 10
D: 1, 3, 6	

for a Boolean function.[6] Therefore, the same techniques can be used. Table II shows a "prime implicant table" for the maximal compatibility classes of Table I. Each row of Table II corresponds to one of the maximal compatibility classes. Each column of Table II represents one of the internal states of Table I. An X is placed in a cell of Table II if the maximal compatibility class corresponding to the row includes

TABLE II — PRIME IMPLICANT TABLE FOR THE MAXIMAL
COMPATIBILITY CLASSES OF TABLE I

		Internal States									
		1	2	3	4	5	6	7	8	9	10
Maximal Compatibility Classes	*A				X				X	$\circledX$	
	*B				X			$\circledX$	X		
	C				X	X					X
	*D	X		X			$\circledX$				
	E		X	X							
	F		X			X					X
	G	X				X					X

the internal state corresponding to the column. A sufficient number of rows must be chosen so that each column has an X in at least one of the chosen rows. It follows from this that rows A, B, and D must be chosen, since columns 9, 7, and 6 each contain only a single X. After A, B, and D have been chosen, only columns 2 and 5 do not contain an X in any of the chosen rows. This may be remedied by also choosing row F. Thus the collection of maximal compatibility classes A, B, D and F corresponds to a minimum-row flow table which covers Table I(a). Such a table is shown in Table III.

Inspection of Table II shows that columns 5 and 10 are identical. Any states which are compatible and are stable for the same input state will always have identical columns in the ' prime implicant table" for maximal compatibility classes. It is therefore unnecessary to carry these states along explicitly. Each set of such states can immediately be replaced by a single state (this corresponds to Huffman's merging).[4] The sets of states which are "merged" in this step are exactly the sets of states which must be covered by single states of the new table in order

TABLE III — A MINIMUM ROW FLOW TABLE WHICH
COVERS TABLE I(a)

S		x^0	x^1	x^2	x^3	x^4
(4, 8, 9)	A	$\circledA$, 1	$\circledA$, 1	$\circledA$, 0	F , 0	D , 0
(4, 7, 8)	B	$\circledB$, 1	$\circledB$, 1	A , 0	F , 0	$\circledB$, 1
(1, 3, 6)	D	$\circledD$, 0	F , 0	$\circledD$, 0	F , 0	$\circledD$, 0
(2, 5, 10)	F	B , 1	$\circledF$, 0	D , 0	$\circledF$, 0	B , 1

S, Z

to insure that closure is satisfied. Thus, closure will always be satisfied
as long as these sets of states are identified; i.e., either all members of
the set are included in a compatibility class or all members are excluded.

After the collection of maximal compatibility classes which correspond
to a minimum-row flow table has been determined, states can some-
times be removed from some of the classes. The advantage of removing
states and thereby obtaining nonmaximal compatibility classes is the
corresponding introduction of unspecified entries in the minimum-row
flow table. Closure will still be satisfied as long as (i) only sets of states
which were identified previously, or single states which cannot be
identified with any other state, are removed; and (ii) each state is
still contained in one of the remaining compatibility classes. This pro-
cedure can be carried out until each state is included in only one of the
compatibility classes. In Table III, this could mean the removal of
states 4 and 8 from class B.

CONCLUSIONS

It has been shown that for incompletely specified flow tables which
satisfy certain very common conditions, greatly simplified procedures
for obtaining minimum-state flow tables exist. For this class of tables
it should now be possible to develop computer programs which are
guaranteed to work for tables with sufficiently large numbers of internal
states so that hand techniques are not feasible.

ACKNOWLEDGMENTS

REFERENCES

1. Paull, M. C., and Unger, S. H., Minimizing the Number of States in Incom-
    pletely Specified Sequential Switching Functions, I.R.E. Trans. on Electronic
    Computers, EC-8, No. 3, September, 1959, pp. 356–367.
2. Narasimhan, R., Minimizing Incompletely Specified Sequential Switching
    Functions, I.R.E. Trans. on Electronic Computers, EC-10, No. 3, Septem-
    ber, 1961, pp. 531–532.
3. McCluskey, E. J., Jr., Fundamental Mode and Pulse Mode Sequential Circuits,
    International Federation for Information Processing Congress, Munich,
    Germany, Aug. 27 to Sept. 1, 1962. Also Technical Report No. 29, Digital
    Systems Laboratory, Electrical Engineering Department, Princeton Uni-
    versity.
4. Huffman, D. A., The Synthesis of Sequential Switching Circuits, Journal of
    the Franklin Institute, 257, No. 3, March, 1954, pp. 161–190; No. 4, April,
    1954, pp. 275–303.
5. Birkhoff, G., and MacLane, S., A Survey of Modern Algebra, The Macmillan
    Company, New York, N.Y., 1941.
6. McCluskey, E. J., Jr., Minimization of Boolean Functions, B.S.T.J., 35, No-
    vember, 1956, pp. 1417–1444.

Timing Errors in a Chain of Regenerative Repeaters, I

By B. K. KINARIWALA

The pulse displacements produced by timing errors in a chain of regenerative repeaters (using tuned-circuit timing filters) are represented by a linear transformation of the pulse displacements at the output of the first repeater. To facilitate the discussion of the general problem, the simpler case of periodic pulse trains is considered first. For this case it is shown that while the mean value tends to infinity, the central moments of the pulse displacements remain bounded as the number of repeaters approaches infinity. Further results are obtained which show that all the moments of the spacing jitter remain bounded for an indefinitely long string of repeaters. Finally, the misalignment in the jitter at any given repeater is represented by a simple expression which shows that the essential component in the misalignment is flat delay.

The general problem of random pulse trains, infinite in length, is discussed in Part II in this issue. The results obtained for the general case are quite different from those obtained for the periodic case. The variance is unbounded in this case except for pulse trains with certain special restrictions. The computational aspects for the evaluation of jitter accumulation will be discussed in a subsequent paper.

I. INTRODUCTION

In regenerative digital transmission systems, one of the important problems is that of maintaining the proper distance between the signal pulses. The problem becomes much more serious when the system contains a rather long chain of regenerative repeaters. Several aspects of a theoretical nature in connection with this problem have been discussed by Sunde,[1] Bennett,[2] Rowe[3] and Rice.[4]

We study here the pulse displacements produced by tuning errors in a chain of repeaters using tuned-circuit timing filters. For simplicity, we shall consider the system free of noise, distortion, etc.

An idealized version of the physical system is a chain of repeaters with the input supposed to be a train of unit impulses. Each repeater is a device containing a resonant circuit which is excited by the incoming train of pulses. The response of the resonant circuit to the incoming signal will ideally consist of a sum of sinusoids and will pass upwards through zero at an instant determined by the resonant frequency of the circuit. This instant will coincide with the instant of occurrence of the pulse, if it occurs at all, when the resonant frequency is identical with the pulse repetition frequency. The repeater does its "repeating" by sending out a unit impulse, at the instant the response of the tuned-circuit passes upwards through zero, provided the input signal has a pulse at or near the same instant. If there is no pulse in the input, no pulse is sent out.

Due to tuning error, the tuned circuit in a practical repeater would resonate at a frequency somewhat different from the pulse repetition frequency. Further, the impulse response of the circuit is more truly a damped sinusoid. These considerations show that the positions of the pulses sent out by a practical repeater are somewhat displaced from the true positions of the pulses in the original pulse train.

Actually the system consists of a chain of repeaters. We are thus led to a consideration of the statistical properties of the pulse displacements produced in a random pulse train by the combined effect of mistuning in each successive repeater. Of particular concern is the behavior of the pulse displacements as the number of repeaters gets larger and larger. It is to this question that we attend.

We begin our discussion by a mathematical statement of the problem. We show that the pulse displacements at the output of a chain of repeaters may be represented by a linear transformation, in a Banach space, of the pulse displacements at the output of the first repeater.

The linear operator (or, the linear transformation) becomes unbounded, in the limit, as the number of repeaters gets indefinitely large. From this follows the result that the average value* of the pulse displacements increases indefinitely as the number of repeaters approaches infinity.

The behavior of the variance, as well as the other central moments, of the pulse displacements is investigated by considering a suitable projection, when it exists, in the Banach space. When the domain of the above linear transformation is a linear manifold obtained by the desired projection, we find that the linear operator is bounded. Conse-

---

* All averages are taken over the values of the pulse displacements. No averages over the mistunings should be compared with the results obtained here.

quently, all the central moments of the pulse displacements are shown to remain bounded as the number of repeaters approaches infinity. When the above-mentioned projection does not exist, the central moments are shown to be unbounded.

Practical situations call for a determination of the bounds on the central moments when the number of repeaters is finite. In such cases, the input pulse trains may be assumed to be periodic pulse trains with the period much larger than the time constants of the timing filters. The problem reduces to a linear transformation in a finite dimensional vector space. The central moments are bounded and they can be precisely evaluated. A simple procedure to determine these bounds is developed.

The same analysis can be directly applied to an investigation of the so-called "spacing jitter," or variations in the spacings between virtual pulse positions. Similar results are obtained for both a finite and an infinite number of repeaters in the chain.

We shall also have occasion to remark upon the "misalignment noise" which is the jitter introduced, by the nth repeater, in an already jittered pulse train coming into the same repeater.

Finally, in a subsequent paper we shall discuss the computational aspects for the evaluation of jitter accumulation in a long string of repeaters.

Organization of the paper is as follows. We start with the statement of the problem in completely general terms and express it as a linear transformation. Next, to facilitate the discussion of the general problem, we consider the simpler case of a periodic pulse train. In Part II of the paper,* we consider the general case of a completely random pulse train.

II. STATEMENT OF PROBLEM

The input to the chain of repeaters is supposed to be a train of unit impulses which occur, if they occur at all, at the instants

$$\{ \cdots, -2\tau, -\tau, 0, \tau, 2\tau, \cdots \}.$$

The occurrence or nonoccurrence of a pulse at time $t = -n\tau$ is determined by the value of the random variable α_n. If $\alpha_n = 1$, which happens with a given probability, a pulse is present. If $\alpha_n = 0$, no pulse is present.

The resonant circuit in the repeater is excited by the incoming train

---

* Part II of the paper appears in this issue, p. 1781.

of pulses. The response of the circuit to a unit impulse at time $t = 0$ is assumed to be

$$e^{-\sigma t} \sin \omega_0 t, \qquad t > 0 \tag{1}$$

where $\omega_0 \tau$ is almost 2π but, due to tuning error, misses its desired value by

$$\epsilon = 2\pi - \omega_0 \tau = 2\pi (f_r - f_0)/f_r . \tag{2}$$

Here $f_r = 1/\tau$ is the pulse repetition frequency. The decrement σ is related to the Q of the circuit by $\sigma \tau = \pi/Q$.

The response of the resonant circuit to the incoming pulse train will consist of a sum of terms of the form (1) and will pass upwards through zero at an instant near $t = (-n\tau)$, say at $t = (-n\tau + t_n)$. The repeater sends out a unit impulse at the instant $(-n\tau + t_n)$ if the input signal has a pulse near $(-n\tau)$. If there is no pulse in the input, no pulse is sent out. The response of the resonant circuit still goes through zero, and we can say that there is a "virtual" pulse displacement of amount t_n seconds (or of $2\pi t_n/\tau$ radians).

For a chain of repeaters, we assume that all of the resonant circuits have the same Q but that their mistunings ϵ_1, ϵ_2, $\cdots$ are distributed independently and at random. Let ξ_k^l be the displacement of the kth pulse (originally entering the first repeater at $t = -k\tau$) as it comes out of the lth repeater where $l = 1, 2, \cdots$. The displacement ξ_k^l is measured in radians, where 2π radians corresponds to the pulse interval τ. The superscript l signifies the output of the lth repeater. The mistuning in the resonant circuit in the lth repeater is represented by ϵ_l. When we assume that Q is very large and the mistunings ϵ_l are much smaller than $\sigma \tau = \pi/Q$ radians, we are led to a set of equations which relate the pulse displacements out of the lth repeater to those out of the $(l - 1)$th repeater. These equations are

$$\xi_k^l = \frac{\sum_{n=0}^{\infty} \alpha_{n+k} \beta^n (\xi_{n+k}^{l-1} + n\epsilon_l)}{\sum_{n=0}^{\infty} \alpha_{n+k} \beta^n}, \tag{3}$$

$$(l = 1, 2, 3, \cdots; k = 0, 1, 2, \cdots),$$

where $\beta = \exp(-\sigma \tau) \approx 1 - (\pi/Q)$ is a number slightly less than unity. The initial conditions are that the pulses entering the first repeater have zero displacement, i.e.,

$$\xi_k^0 = 0, \qquad k = 0, 1, 2, \cdots. \tag{4}$$

These equations are given by Rowe[3] and also by Rice.[4] Here we have followed their terminology very closely.

The physical problem dealing with a chain of repeaters is now replaced by the mathematical problem of studying the behavior of the variables $\xi_k{}^l$ defined by the above equations. The α_n's and ϵ_l's are either given explicitly or are random variables whose distributions are known.

III. LINEAR TRANSFORMATIONS

We note that the set of equations in (3) is a linear set, and we can express it as a linear transformation of the set of variables $\{\xi_k{}^{l-1}\}$ into the set $\{\xi_k{}^l\}$. We are, however, primarily interested in the behavior of $\{\xi_k{}^l\}$ when l is large and when no knowledge of $\{\xi_k{}^{l-1}\}$ is available. A more useful expression is obtained by rewriting (3) as

$$\xi_k{}^l = \frac{\sum_{n=0}^{\infty} \alpha_{n+k}\beta^n \xi_{n+k}{}^{l-1}}{\sum_{n=0}^{\infty} \alpha_{n+k}\beta^n} + \frac{\epsilon_l}{\epsilon_1}\xi_k{}^1, \tag{5}$$

where

$$\xi_k{}^1 = \frac{\sum_{n=0}^{\infty} \alpha_{n+k}\beta^n n\epsilon_1}{\sum_{n=0}^{\infty} \alpha_{n+k}\beta^n}. \tag{6}$$

In our formulation, zero mistuning does not introduce any jitter in a jitter-free pulse train. We will therefore understand the chain to start with a repeater having non-zero mistuning.

Equation (5) can be used to express $\{\xi_k{}^l\}$ as a linear transformation of $\{\xi_k{}^1\}$. To do this, define a matrix (infinite)

$$T = \begin{bmatrix} \dfrac{\alpha_0}{s_0} & \dfrac{\alpha_1\beta}{s_0} & \dfrac{\alpha_2\beta^2}{s_0} & \cdots & \\ 0 & \dfrac{\alpha_1}{s_1} & \dfrac{\alpha_2\beta}{s_1} & \dfrac{\alpha_3\beta^2}{s_1} & \cdots \\ 0 & 0 & \dfrac{\alpha_2}{s_2} & \dfrac{\alpha_3\beta}{s_2} & \cdots \\ \vdots & \vdots & \vdots & \vdots & \end{bmatrix}, \tag{7}$$

where

$$s_i = \sum_{n=0}^{\infty} \mathfrak{a}_{n+i}\beta^n; \tag{8}$$

and define a vector

$$X_l = [\xi_0{}^l, \xi_1{}^l, \xi_2{}^l, \cdots]. \tag{9}$$

Then (5) becomes

$$X_l = TX_{l-1} + \frac{\epsilon_l}{\epsilon_1} X_1; \qquad (X_0 = 0), \quad (l = 1, 2, 3, \cdots). \tag{10}$$

From (10) it follows that

$$X_l = \left[\frac{1}{\epsilon_1} \sum_{\nu=0}^{l-1} \epsilon_{l-\nu} T^\nu \right] X_1, \quad (T^0 = I). \tag{11}$$

One can, if need be, discuss the behavior of (11) in the above form. However, the ϵ's are usually of the same order of magnitude, and the equation is considerably simplified by assuming that the ϵ's are identical.* Then

$$X_{l+1} = \left[\sum_{\nu=0}^{l} T^\nu \right] X_1. \tag{12}$$

We are interested in the problem when l becomes indefinitely large, or, dropping superfluous subscripts,

$$Y = \lim_{l \to \infty} \left[\sum_{\nu=0}^{l} T^\nu \right] X. \tag{13}$$

Here X and Y represent the pulse deviations out of the first repeater and out of the $(l + 1)$th repeater, respectively.

The original problem is now represented as a linear transformation of X into Y. The linear transformation, when it exists, is a function of another linear transformation T. The domain, as well as the range, of the transformation T is a Banach space, as will be shown in Part II. Here, we pursue the simpler case of a periodic pattern.

Whether the variance is bounded or not is not a particularly important question for the periodic case. Such a question can be answered by a very simple argument. However, we give here instead a complete analysis of the periodic case. Our purpose in doing so is twofold. First, the analysis shows how certain basic properties of the operator T influence the questions of boundedness of the jitter; it also gives a simple

---

* We shall discuss elsewhere the difference, if any, in the results when we do not make this assumption.

computational procedure for evaluating the accumulated jitter. Second, the analysis serves as a simple introduction to the more complex argument pursued in Part II.

IV. PERIODIC PULSE TRAINS

We assume here that the α_n's form a pattern which repeats itself with a period m. The pattern is otherwise arbitrary. In such cases, the pulse displacements are also periodic with the same period m. Then,

$$\alpha_{n+m} = \alpha_n$$
$$\xi_{k+m}{}^l = \xi_k{}^l \tag{14}$$

for all values of indices n and k.

The domain of the operator T is thus an m-dimensional space. Since $\alpha_{n+m} = \alpha_n$, the range of T is also of dimension m. The problem reduces to the study of a linear transformation in a finite dimensional space. The operator T is now represented by a finite matrix A.

$$
A = \begin{bmatrix} \left(\dfrac{\alpha_0 + \alpha_m\beta^m + \alpha_{2m}\beta^{2m} + \cdots}{s_0} \right) & \left(\dfrac{\alpha_1\beta + \alpha_{m+1}\beta^{m+1} + \cdots}{s_0} \right) & \cdots \\[2ex] \left(\dfrac{\alpha_m\beta^{m-1} + \alpha_{2m}\beta^{2m-1} + \cdots}{s_1} \right) & \left(\dfrac{\alpha_1 + \alpha_{m+1}\beta^m + \cdots}{s_1} \right) & \cdots \\[2ex] \cdots & \cdots & \cdots \end{bmatrix}
$$

$$
= \begin{bmatrix} \dfrac{\alpha_0}{s_0{}'} & \dfrac{\alpha_1\beta}{s_0{}'} & \cdots & \dfrac{\alpha_{m-1}\beta^{m-1}}{s_0{}'} \\[2ex] \dfrac{\alpha_0\beta^{m-1}}{s_1{}'} & \dfrac{\alpha_1}{s_1{}'} & \cdots & \dfrac{\alpha_{m-1}\beta^{m-2}}{s_1{}'} \\[2ex] \vdots & & & \vdots \\[2ex] \dfrac{\alpha_0\beta}{s_{m-1}{}'} & & & \dfrac{\alpha_{m-1}}{s_{m-1}{}'} \end{bmatrix}, \tag{15}
$$

where

$$s_k{}' = (1 - \beta^m)s_k . \tag{16}$$

For the periodic case, (13) becomes

$$Y = \lim_{l \to \infty} \left[\sum_{\nu=0}^{l} A^\nu \right] X, \tag{17}$$

where we continue to use the same symbols X and Y to represent the finite dimensional vectors.

In order to investigate the limit of (17), one must determine the behavior of the infinite series and its convergence properties. Moreover, if the limit does not exist, the question to be answered is whether or not the variance of Y has any limit. Other central moments may also be of interest.

In what follows, we show that the limit of (17) does not exist. This implies that the mean of Y is infinite. However, we shall show that the central moments always exist for any arbitrary m. We assume throughout this paper that averages over the sample values* are statistically identical to the averages over the ensembles.

A discussion of the properties of the linear transformation defined by (17) involves the study of a function of the matrix A. In order to discuss such a function, one must have a knowledge of the spectrum of the matrix. We study the spectrum of A in the next section.

V. SPECTRUM OF A

In this section, we prove the following theorem.

Theorem: The spectrum of A consists of two parts:

1. The maximum eigenvalue is located at $\lambda = 1$, and it is simple;

2. All other eigenvalues are such that their modulus is less than unity, i.e., $|\lambda_i| < 1$.

Proof: Observe that A is a stochastic matrix since the sum of each row is equal to one and all the elements of the matrix are nonnegative. Thus, $\lambda = 1$ is indeed an eigenvalue with eigenvector $\{1, 1, \cdots, 1\}$. It also follows that the entire spectrum of A is contained in the unit disk $|\lambda| \leq 1$. This can be observed in a simple manner by considering powers of matrix A and noting that the trace of A^n does not exceed m, the order of the matrix A. If there were any eigenvalue for $|\lambda| > 1$, one could find a large enough n such that the trace of A^n would exceed m. (We do not worry about cancellation because we can always choose the proper n to prevent this.) Hence, there are no eigenvalues outside the unit disk.

Next, we wish to show that there are no other eigenvalues ($\lambda \neq 1$) with modulus equal to one. We obtain a matrix equivalent to A by means of elementary transformations of interchanging rows as well as the corresponding columns. The eigenvalues of the matrix are invariant

---

* The values of the pulse displacements are referred to as the sample values, and the ensemble is the set of admissible sequences of pulse displacements. For justification of the above assumption in the general case, see Bennett, op. cit.

under such operations. We obtain a matrix of the form

$$B = \begin{bmatrix} A' & 0 \\ C & D \end{bmatrix}, \tag{18}$$

where A' is a square matrix all of whose elements are positive and D is a square null matrix. Only the eigenvalues of A' need be considered. To A' we apply Perron's theorem which, for a stochastic matrix with all elements positive, states that: the extremum eigenvalue is located at $\lambda = 1$; it is simple; and its modulus exceeds the moduli of all other eigenvalues. Q.E.D.

VI. MEAN, VARIANCE, ETC.

The solution to (17) can now be expressed in terms of the basis vectors of A in the form

$$Y = \lim_{l \to \infty} \sum_{\nu=0}^{l} \sum_{\mu=1}^{m} \lambda_\mu{}^\nu \alpha_\mu X^{(\mu)}, \tag{19}$$

where, $X^{(\mu)}$ is the eigenvector of A corresponding to the eigenvalue λ_μ of A. The coefficients α_μ are the expansion coefficients in

$$X = \sum_\mu \alpha_\mu X^{(\mu)}. \tag{20}$$

We have assumed, for the present, that A is of simple structure. There are no significant changes in the development when such an assumption is not made. We shall discuss this matter a little later.

In the previous section it has been proved that the extremum eigenvalue, say λ_1, is simple and is located at $\lambda_1 = 1$. The rest of the eigenvalues are strictly inside the unit circle. The mean value of Y is seen to approach infinity by considering only those terms that involve $\lambda_1 = 1$,

$$\bar{Y} = \alpha_1 X^{(1)} \sum_{\nu=0}^{\infty} \lambda_1{}^\nu + \sum_{\mu=2}^{m} \frac{\alpha_\mu}{1 - \lambda_\mu} \overline{X^{(\mu)}}, \tag{21}$$

where, $X^{(1)} = \{1, 1, \cdots, 1\}$.

The first term in (21) is a divergent series and $\bar{Y}$ approaches infinity as the number of repeaters increases indefinitely.* The behavior of the central moments is investigated by considering

$$[Y - \bar{Y}] = \sum_{\mu=2}^{m} \left(\frac{\alpha_\mu}{1 - \lambda_\mu} \right) [X^{(\mu)} - \overline{X^{(\mu)}}]. \tag{22}$$

---

* The statement is valid, in general, provided $\alpha_1 \neq 0$. We need only show that there exists at least one X such that $\alpha_1 \neq 0$. Consider a pulse train with all pulses present; then $X = \alpha_1 X^{(1)}$ with $\alpha_1 \neq 0$.

The value of $[Y - \bar{Y}]$ is finite since $|\lambda_\mu| < 1$. All powers of $[Y - \bar{Y}]$ are finite and $\overline{[Y - \bar{Y}]^k}$ will also be finite. We thus see that all the central moments, including the variance, are finite.

Now we consider the case when the structure of A is not simple. The only difference in this case concerns the vectors corresponding to eigenvalues other than λ_1. Let us, for simplicity, consider the basis vectors that correspond to an eigenvalue λ_μ of multiplicity two. Similar developments can be carried out when the multiplicity is greater than two. The normal form of A would have a Jordan block

$$\begin{bmatrix} \lambda_\mu & 1 \\ 0 & \lambda_\mu \end{bmatrix} \tag{23}$$

It is well known that there exist two linearly independent vectors $X_1^{(\mu)}$ and $X_2^{(\mu)}$ such that

$$\begin{aligned} A X_1^{(\mu)} &= \lambda_\mu X_1^{(\mu)} \\ A X_2^{(\mu)} &= \lambda_\mu X_2^{(\mu)} + X_1^{(\mu)}. \end{aligned} \tag{24}$$

The vector $X_1^{(\mu)}$ is an eigenvector of A and is transformed in the same manner as the vectors $X^{(\mu)}$ are, and it yields for Y a term of the form

$$\left(\frac{\alpha_\mu}{1 - \lambda_\mu} \right) X_1^{(\mu)}. \tag{25}$$

On the other hand, when A^ν operates on $X_2^{(\mu)}$ it yields

$$A^\nu X_2^{(\mu)} = \lambda_\mu{}^\nu X_2^{(\mu)} + \nu\lambda_\mu{}^{\nu-1} X_1^{(\mu)}. \tag{26}$$

Thus $X_2^{(\mu)}$ contributes to Y a term of the form

$$\begin{aligned} \alpha_\mu' \sum_{\nu=0} A^\nu X_2^{(\mu)} &= \alpha_\mu' \left[\sum_{\nu=0}^\infty \lambda_\mu{}^\nu X_2^{(\mu)} + \sum_{\nu=0}^\infty \nu\lambda_\mu{}^{\nu-1} X_1^{(\mu)} \right], \\ &= \alpha_\mu' \left[\left(\frac{1}{1 - \lambda_\mu} \right) X_2^{(\mu)} + \left(\frac{1}{1 - \lambda_\mu} \right)^2 X_1^{(\mu)} \right], \end{aligned} \tag{27}$$

since $|\lambda_\mu| < 1$.

The terms due to the basis vectors of A corresponding to λ_μ are shown to be bounded, and our results on the boundedness of the central moments remain valid regardless of the structure of A.

VII. SPACING AND MISALIGNMENT

Sometimes a more useful measure of jitter is the spacing jitter, which is defined as the deviations in the spacing between adjacent pulses or

pulse positions. This is obtained by taking the difference of the adjacent pulse position deviations. To do this operationally, let us define an operator S which shifts the elements in the vector Y such that the kth element appears as the $(k - 1)$th element and the first element appears as the mth element.

$$
S = \begin{bmatrix}
0 & 1 & 0 & 0 & \cdots & 0 \\
0 & 0 & 1 & 0 & \cdots & 0 \\
\vdots & & & & & \\
0. & 0 & 0 & 0 & 0 & 1 \\
1 & 0 & 0 & 0 & 0 & 0
\end{bmatrix},
\tag{28}
$$

The spacing jitter Y_s can then be represented in terms of the timing jitter Y by

$$
Y_s = [I - S]Y.
\tag{29}
$$

By using (19) and (29), we have

$$
Y_s = \lim_{l \to \infty} \sum_{\nu=0}^{l} \sum_{\mu=1}^{m} \lambda_\mu^\nu \alpha_\mu [I - S] X^{(\mu)}.
\tag{30}
$$

The operator $[I - S]$ annihilates $X^{(1)}$ and we obtain

$$
Y_s = \sum_{\mu=2}^{m} \left(\frac{\alpha_\mu}{1 - \lambda_\mu} \right) [I - S] X^{(\mu)}.
\tag{31}
$$

The spacing jitter is finite for all sample values, and so the mean and all other moments of this jitter are finite.*

Next, we briefly consider the misalignment which is defined as the difference between the timing errors at the output and at the input of a given repeater. The representation of the misalignment in the $(l + 1)$th repeater is given, in the periodic case, by modifying (12) to a finite dimensional one and obtaining

$$
[X_{l+1} - X_l] = A^l X_1,
\tag{32}
$$

where, X_k represents the jitter at the output of the kth repeater.

Equation (32) implies that the misalignment essentially amounts to a flat delay as l gets larger. Indeed, there is virtually no difference in the misalignment for different repeaters when the values of l are reasonably large.

---

* For periodic pulse patterns, this is intuitively obvious.

VIII. CONCLUSION

The general problem of timing errors in a string of repeaters has been expressed in terms of certain linear operators and functions of these operators. The simpler case of periodic pulse patterns is then studied in detail. We have shown, for the periodic case, that the mean value of jitter accumulation in a string of repeaters increases indefinitely but that the central moments of the jitter remain bounded. In fact, the divergence of the mean value for the infinitely long string stems from the accumulation of the flat delay occurring in each repeater. Once this flat delay is eliminated, the remaining part of the jitter is bounded. Consequently, all the central moments are bounded. All the moments of the spacing jitter are bounded for identical reasons. The misalignment behavior is also explained by the dominance and the invariance of the flat delay.

The question of evaluating the jitter accumulation will be discussed in a subsequent paper. We will show there that the spectrum of the operator A can be determined fairly simply even for very large periodicity. No polynomials of high degrees need be solved to determine the eigenvalues. We shall also discuss the computation errors involved in periodic approximation versus those involved in truncation of the infinite pulse train.

The general case of random pulse trains with no periodic structure will be examined in Part II. We shall have occasion to thoroughly examine the operator T. Since we shall be concerned with infinite dimensional space, the spectral properties of T are not so easy to determine. We shall compare the spectral properties of T with those of A in order to delineate the difference between the two cases.

REFERENCES

1. Sunde, E. D., Self-Timing Regenerative Repeaters, B.S.T.J., **36**, July, 1957, pp. 891–938.
2. Bennett, W. R., Statistics of Regenerative Digital Transmission, B.S.T.J., **37**, November, 1958, pp. 1501–1542.
3. Rowe, H. E., Timing in a Long Chain of Regenerative Binary Repeaters, B.S.T.J., **37**, November, 1958, pp. 1543–1598.
4. Rice, S. O., unpublished work.

Timing Errors in a Chain of Regenerative Repeaters, II

By B. K. KINARIWALA

(Manuscript received July 23, 1962)

The behavior of the timing jitter in a long chain of repeaters is shown to depend on the spectral properties of a linear operator which maps the space of bounded sequences into itself. As the number of repeaters increases indefinitely, so does the mean value of the jitter. The variation about this mean value remains bounded only for certain highly constrained pulse trains (e.g., periodic, finite, etc.), but it is otherwise unbounded.

I. INTRODUCTION

We showed in a previous discussion that the pulse displacements at the output of a chain of repeaters may be represented by a linear transformation of the pulse displacements at the output of the first repeater.* The linear transformation turns out to be a simple function of a basic operator T which, in essence, represents the action of the repeater on the incoming jitter. Though the operator T depends directly on the manner in which the repeater extracts its timing information from the incoming pulse train, it is believed that there would be no basic difference in the major results obtained or in the method of analysis for different timing extractors. We have assumed that the timing information extractor is a tuned circuit with a finite but fairly high Q and the source of jitter is the mistuning in the tuned circuit. Other sources of jitter often lend themselves to a similar mode of investigation.

The rest of the discussion in Part I concerned the class of periodic pulse trains. The problem reduces, in such cases, to a consideration of linear transformations in a finite dimensional space. For a periodic pulse train with period m, it was shown that the variance of the jitter remains bounded for an indefinitely long string of repeaters.

---

* We shall assume that the reader is familiar with the contents of Part I of this paper: B. K. Kinariwala, Timing Errors in a Chain of Regenerative Repeaters, I, this issue, pp. 1769–1780.

Unfortunately, the above results do not let us draw any conclusions for the behavior of the variance when the pulse train is not periodic, but infinite, in length. For example, if there existed a bound M, on the variance, which was not a function of m, then we can let the period become infinite and conclude that the variance was bounded for the indefinitely long random pulse train. However, it is not apparent whether M is dependent on m or not. The value of the variance is determined by the number of eigenvalues of the pertinent operator, their location, and the algebraic signs of the corresponding eigenvectors. It seems reasonable, therefore, that the bound on the variance is a function of the period m. The behavior of this function as m approaches infinity will determine whether the variance is bounded in the nonperiodic case. We do not pursue the matter in this direction because it is not easy to express the above function in a simple manner.

Instead, we investigate the general problem directly in the infinite dimensional space. We establish that the basic operator T maps the normed linear space l_p into l_p for $1 \leq p \leq \infty$. Next, we show that the domain of T for our problem is the space l_∞.* We determine the conditions under which the variance is bounded, and we conclude that there is no bound on the variance of the jitter for the random (infinite) pulse train. The conclusion remains valid for any specification of dependence or independence of the random variables α_n which take on the value one if a pulse is present at time $t = (-n\tau)$, but they are zero otherwise. Even a bound on the maximum number of successive zeros in the pulse trains does not seem to alter our result. Only when the operator T is restricted to a finite dimensional space does the variance remain finite. Such a restriction occurs for finite pulse trains, periodic pulse trains, nonperiodic pulse trains which eventually take on a periodic behavior, and so on.

The organization of the paper is in the nature of a proof with digressions. Though these digressions are extraneous to the discussion of the boundedness of the variance, they do serve to bring out some interesting points. We begin with the mathematical statement of the problem, which includes certain modifications of the previous statement. Next, we examine the elementary operator T and its properties such as boundedness, domain, and spectrum. We then proceed to the discussion of whether the variance of the jitter is bounded or unbounded. We close with a brief discussion of the results.

---

* The space l_∞ is a normed linear space which is complete. Hence, it is a Banach space.

II. STATEMENT OF PROBLEM

The purpose of a restatement of the problem here is to make certain desirable modifications. We also refer to a possible alternate formulation which, except for an occasional observation, we shall not pursue.

We are interested in studying the behavior of the equation

$$Y = \lim_{l \to \infty} \left[\sum_{\nu=0}^{l} T^{\nu} \right] X, \tag{1}$$

where X and Y represent the input and output jitter vectors, respectively, for a long chain of repeaters. By input jitter we mean input to the second repeater in the chain, and it is understood that the input to the first repeater is a jitter-free pulse train. The linear operator T represents the action of the repeater on the incoming jitter, and we shall describe it presently. The simple form of (1) is obtained by assuming that the mistunings, which appear as coefficients in the power series in T, are identical. This assumption does not alter the convergence properties of the relevant limit since the mistunings are of the same order of magnitude.*

The operator T in our previous discussion was obtained under the assumption that the jitter is observed in the neighborhood of time $t = 0$ with the pulse train extending back in time towards $t = -\infty$. We included in our description of T, X and Y the pulse position deviations regardless of whether a pulse was present or not. The operator T was defined by the matrix

$$T = \begin{bmatrix} \dfrac{\alpha_0}{s_0} & \dfrac{\alpha_1 \beta}{s_0} & \dfrac{\alpha_2 \beta^2}{s_0} & \cdots \\ 0 & \dfrac{\alpha_1}{s_1} & \dfrac{\alpha_2 \beta}{s_1} & \cdots \\ 0 & \cdots & \cdots & \cdots \\ \cdots & \cdots & \cdots & \cdots \end{bmatrix}, \tag{2}$$

where $\alpha_n = 1$ if a pulse is present at $t = -n\tau$ and equal to zero otherwise; β is a positive number slightly less than unity ($\beta \approx 1 - (\pi/Q)$); and

$$s_i = \sum_{n=0}^{\infty} \alpha_{n+i} \beta^n. \tag{3}$$

---

* The question of convergence should not be confused with the question of boundedness of the resulting operator or of the operator T.

When $\alpha_n = 0$, all the elements in the nth column of T are zero. As we observed in the periodic case, we can eliminate these columns and the corresponding rows without in any way affecting the results. Physically, this amounts to a consideration of jitter only at those positions where pulses were present in the original pulse train. With these minor changes, we represent T in the following manner.

$$
T = \begin{bmatrix} \dfrac{1}{S_0} & \dfrac{\beta^{i_1}}{S_0} & \dfrac{\beta^{i_1+i_2}}{S_0} & \cdots \\[2mm] 0 & \dfrac{1}{S_1} & \dfrac{\beta^{i_2}}{S_1} & \cdots \\[2mm] \cdots & \cdots & \cdots & \cdots \end{bmatrix},
\tag{4}
$$

where

$$
S_0 = 1 + \sum_{n=1}^{\infty} \prod_{\nu=1}^{n} \beta^{i_\nu},
\tag{5}
$$

and

$$
S_{n-1} = 1 + \beta^{i_n} S_n .
\tag{6}
$$

Vectors X and Y are also assumed to be suitably modified.

Though we are not concerned with it, we take note of the fact that an alternate formulation of the problem is possible by assuming that the pulse train starts at time $t = 0$ and extends towards $t = +\infty$. There are many disadvantages in such a formulation and we mention it here only for completeness. The operator of interest in this case takes the following form.

$$
T_2 = \begin{bmatrix} \dfrac{1}{S_{0+}} & 0 & 0 & \cdots \\[2mm] \dfrac{\beta^{i_1}}{S_{1+}} & \dfrac{1}{S_{1+}} & 0 & \cdots \\[2mm] \dfrac{\beta^{i_1+i_2}}{S_{2+}} & \dfrac{\beta^{i_2}}{S_{2+}} & \dfrac{1}{S_{2+}} & \cdots \\[2mm] \cdots & \cdots & \cdots & \cdots \end{bmatrix},
\tag{7}
$$

where

$$
S_{0+} = 1,
\tag{8}
$$

and

$$
S_{n+} = 1 + \beta^{i_n} S_{(n-1)+} .
\tag{9}
$$

Referring back to (1), we are interested in determining whether the mean and the variation about the mean of Y are bounded or not. The averages are to be taken over the components of Y. For our purposes, we shall not be concerned with evaluating any averages. As shown in Part I, the dominant part of $\bar{Y}$, the mean of Y, is the element representing flat delay in the jitter Y. All we need to know is whether the dispersion (or, the spread) about this flat delay remains bounded or not. Though this dispersion has some relation to the variance, it is not the variance. However, we shall continue to use the term variance for the dispersion about the flat delay. The relation between these quantities is shown in Part I. Moreover, the behavior of the dispersion also gives information about the spacing jitter. It also answers the question about the worst pattern.

III. BOUNDEDNESS OF T

We proceed now to examine the operator T to determine some of its important properties. It will be shown here that T is a bounded linear operator which maps the normed linear space $1_p(1 \leqq p \leqq \infty)$ into itself.*

Theorem: The norm of T (i.e., $|T|$) on 1_p is bounded for each p.†

Proof: Define a diagonal matrix

$$D = \mathrm{diag} \cdot \{S_0^{-1}, S_1^{-1}, S_2^{-1}, \cdots\},$$

and a matrix T_0 such that

$$T = DT_0 .$$

Then,

$$|T| = |DT_0| \leqq |D \| T_0|$$

$$\leqq |T_0|, \quad (|D| \leqq 1),$$

$$= |I + \mathrm{diag} \cdot \{\beta^{i_1}, \beta^{i_2}, \beta^{i_3}, \cdots\}S + \mathrm{diag} \cdot \{\beta^{i_1+i_2}, \beta^{i_2+i_3}, \cdots\}S^2$$

$$+ \cdots |;$$

---

* The space 1_p is the linear space of all sequences $x = \{\alpha_n\}$ of scalars for which the norm $|x| = \{\sum_{n=1} |\alpha_n|^p\}^{1/p}$ is finite. The norm for 1_∞ is

$$|x| = \sup_n |\alpha_n|.$$

For precise terminology and definitions as well as a basis for many of the statements made and concepts used in this paper, the reader should consult: N. Dunford and J. T. Schwartz, *Linear Operators — Part I: General Theory*, Interscience Publishers, Inc., New York, N. Y.; 1958.

† The bound or norm of T defined on a linear space χ is the $\sup_{|x| \leqq 1} |Tx|$, denoted by $|T|$. The operator T is bounded if $|T| < \infty$.

here

$$S = \begin{bmatrix} 0 & 1 & 0 & 0 & \cdots \\ 0 & 0 & 1 & 0 & \cdots \\ 0 & 0 & 0 & 1 & \cdots \\ \cdots & \cdots & \cdots & \cdots & \cdots \end{bmatrix}$$

is defined on 1_p with $|S| = 1$ for each value of p. Note that $0 < \beta < 1$ and $i_\nu \geqq 1$ for $\nu = 1, 2, 3, \cdots$. So

$$|T| \leqq |T_0|$$

$$\leqq \sum_{\nu=0}^{\infty} |(\beta S)^\nu|$$

$$\leqq \sum_{\nu=0}^{\infty} |\beta S|^\nu$$

$$= \frac{1}{1 - |\beta S|}$$

since $|\beta S| < 1$. The norm of T is shown to be bounded for each p.

As we shall see in the next section, the space 1_∞ is of particular interest to us. The norm of T on 1_∞ is given by the supremum of the sum of the absolute values of elements in a row. Since T is a stochastic matrix, $|T| = 1$ when it is defined on 1_∞.

IV. DOMAIN OF T

It has been stated before that for our problem the domain of the operator T is the space 1_∞. This is not a separable space and, hence, it is not the most convenient one to work with. It must clearly be understood, therefore, that the problem is defined on this space not due to preference but out of necessity. In our discussion of this matter, we begin with some observations in physical terms about the domain in question.

The operator T operates on the sequence representing the jitter at the output of the first repeater (or, the jitter input at the second repeater). The domain of T must include the set of all jitter sequences at the output of the first repeater.* The nature of these sequences is

---

* Here, we are concerned not with a specific operator but with the totality of the operators.

determined by two essential properties of the original pulse trains, viz., infinite length and random character. Since the pulse trains can be indefinitely long and completely random, the jitter sequences need not all converge to zero or to any other value. This conclusion is valid regardless of whether we consider jitter at all the possible pulse positions or only where the pulses are present. As a consequence of the above conclusion, and since the set of all the jitter sequences is certainly not a finite set, the domain cannot be any of the spaces 1_p with p finite. It also follows that the domain cannot be either c_0 (the space of sequences converging to zero), or c (the space of convergent sequences). These are separable spaces and they are to be preferred over 1_∞ if we are able to represent the problem in terms of any one of them. However, the above discussion shows that this is not possible.

On the other hand, if the jitter sequences are all bounded sequences, then the domain of T can be 1_∞. Obviously, the jitter sequences must be bounded in any realistic situation. In fact, the formulation of the problem assumes that the jitter introduced by a single repeater is quite small compared to 2π radians. Thus, the jitter sequences are all bounded and the domain of T is 1_∞.

A more precise bound on the jitter sequences can be obtained quantitatively. The jitter sequences are defined by

$$\{\beta \dot{S}_n S_n^{-1}\}, \tag{10}$$

where S_n are defined in (6) and $\dot{S}_n = (d/d\beta)S_n$. The bound on any sequence of the above type exists, and it can be obtained by determining the worst case as discussed by Aaron and Gray.* It is also clearly seen from (10) that the sequences need not all necessarily converge to zero (or, to any other value). We see now, in a precise manner, that the domain of T must indeed be 1_∞.

V. SPECTRUM OF T

So far we have established that all the jitter sequences at the input of the second repeater are elements of the space 1_∞, and the operator T is a bounded operator defined on 1_∞ with $|T| = 1$. We recall that the jitter accumulation in a string of repeaters is given in terms of a function of the operator T. In order to determine the properties of a function

---

* M. R. Aaron and J. R. Gray, Probability Distribution for the Phase Jitter in Self-Timed Reconstructive Repeaters for PCM, B.S.T.J., **41**, March, 1962; pp. 503–558.

of an operator it is necessary to start with some knowledge of the spectrum of the operator.*

The operator T is represented by a triangular matrix. We wish to emphasize that, for an infinite triangular matrix, the diagonal elements are not necessarily the eigenvalues of the matrix. Equally important is the observation that the set of eigenvalues may indeed include elements which are not to be found on the main diagonal.† Moreover, the spectrum of T may also contain points other than those in the point spectrum (i.e., the set of eigenvalues). Therefore, even though T is represented by a triangular matrix it is not a trivial matter to determine its spectrum.

Of course, T is a stochastic matrix and so $\lambda = 1$ is an eigenvalue of T with the corresponding eigenvector $x_0 = \{1, 1, 1, \cdots\}$. Some other results also follow from the stochastic nature of T. We shall denote the spectrum of T by $\sigma(T)$.

Theorem: The spectrum of T is a subset of the unit disk (i.e., $|\sigma(T)| \leqq 1$), and any pole λ of T with $|\lambda| = 1$ has order one.‡

Proof: The first statement follows immediately from the fact that $|T| = 1$. It is well known that for any λ such that $|\lambda| > |T|$ the resolvent operator $(\lambda I - T)^{-1}$ exists. Thus, the spectral radius of T, viz., $\sup |\sigma(T)|$ cannot exceed one. The spectrum is a subset of the unit disk, etc.

In order to prove the second statement, it suffices to treat the case that $\lambda = 1$ is a pole of T. Or else we treat a modified operator (T/λ) with norm one for $|\lambda| = 1$. Suppose that the order of the pole is at least two. Then there must exist an $x_0 \in E(1; T)\chi$, such that $(I - T)x_0 \neq 0$, but $(I - T)^2 x_0 = 0$.§ Consider a function of T corresponding to $f(\lambda) = \lambda^n/n$ in the neighborhood of $\lambda = 1$. We obtain a relation of the form

$$\frac{1}{n} T^n x_0 = \frac{1}{n} x_0 + (I - T)x_0.$$

Letting $n \to \infty$, we conclude that $(I - T)x_0 = 0$, which is a contradiction. Hence the poles of T which lie on the unit circle are simple poles.

---

* The spectrum $\sigma(T)$ of T is the complement of $\rho(T)$. The resolvent set $\rho(T)$ of T is the set of scalars λ, for which $(\lambda I - T)^{-1}$ exists as a bounded operator with domain χ, where χ is the domain of T. The function $R(\lambda; T) = (\lambda I - T)^{-1}$, defined on $\rho(T)$, is the resolvent of T.

† We hope to discuss elsewhere these statements and their implications in greater detail and with reference to linear operators in general.

‡ An isolated point λ_0 of $\sigma(T)$ is called a pole of T if $R(\lambda; T)$ has a pole at λ_0. By the order $\nu(\lambda_0)$ of a pole λ_0 is meant the order of λ_0 as a pole of $R(\lambda; T)$.

§ $E(\lambda_0; T)$ is a function of T which is identically one on a pole λ_0 of T but which vanishes on the rest of $\sigma(T)$. Observe that E is a projection operator, i.e., $E^2 = E$. The definition of E given here is a highly restricted one but it suits our purposes.

The next two theorems give us some more information about the spectrum. The first one shows that there cannot be a pole on the unit circle for $\lambda \neq 1$. The second one concerns the dimension of the eigen-manifold corresponding to the eigenvalue $\lambda = 1$.*

Theorem: All points on the unit circle except $\lambda = 1$ are in $\rho(T)$.

Proof: We already know that $\lambda = 1$ is in $\sigma(T)$. We also know that any λ such that $|\lambda| > 1$ is in $\rho(T)$. To show that any $\lambda \neq 1$ on the unit circle is in $\rho(T)$, consider

$$R(\lambda_0 ; T) = (\lambda_0 I - T)^{-1}, \qquad \{\lambda_0 \neq 1, \qquad |\lambda_0| = 1\}.$$

If we can show that $R(\lambda_0 ; T)$ exists for all x in χ with a bounded norm, we have proved the theorem. It is easy to verify that $R(\lambda_0 ; T)$ may be expressed as shown in (11).

$R(\lambda_0 ; T) =$

$$
\begin{bmatrix}
\dfrac{1}{(\lambda_0 - S_0^{-1})} & \dfrac{\beta^{i_1} S_0^{-1}}{(\lambda_0 - S_0^{-1})(\lambda_0 - S_1^{-1})} & \dfrac{\beta^{i_1 + i_2} S_0^{-1} \lambda_0}{(\lambda_0 - S_0^{-1})(\lambda_0 - S_1^{-1})(\lambda_0 - S_2^{-1})} & \cdots \\[3ex]
0 & \dfrac{1}{(\lambda_0 - S_1^{-1})} & \dfrac{\beta^{i_2} S_1^{-1}}{(\lambda_0 - S_1^{-1})(\lambda_0 - S_2^{-1})} & \cdots \\[3ex]
0 & 0 & \dfrac{1}{(\lambda_0 - S_2^{-1})} & \cdots \\[3ex]
\cdots & \cdots & \cdots & \cdots
\end{bmatrix}. \quad (11)
$$

Since λ_0 is a complex number, it follows that $(\lambda_0 - S_i^{-1}) \neq 0$ for any i. Next, we show that $R(\lambda_0 ; T)$ is a bounded operator. Observe that the norm is given by

$$|R(\lambda_0 ; T)| = \sup_i \sum_j |a_{ij}|, \qquad (12)$$

where, a_{ij} represents the element in the ith row and jth column of the matrix in (11), i.e., $R(\lambda_0 ; T) = \|a_{ij}\|$.

Consider the resolvent $R(\lambda_1 ; T)$ for $\lambda_1 = (1 + \epsilon)$ with $\epsilon > 0$. Obviously λ_1 is in $\rho(T)$ and $|R(\lambda_1 ; T)| < \infty$. We assert that, given any λ_0, there exists an $\epsilon > 0$ such that

$$|R(\lambda_0 ; T)| \leq |R(\lambda_1 ; T)| < \infty. \qquad (13)$$

The validity of our assertion is proven by first noting that $R(\lambda_1 ; T)$ is represented by the matrix in (11) with λ_0 replaced by λ_1. Let $R(\lambda_1 ; T) = \|b_{ik}\|$. Next we show that $|a_{ik}| \leq |b_{ik}|$, for all i and k, from which follows relation (13). Let $\lambda_0 = \cos\theta + j\sin\theta$, $(j = \sqrt{-1})$. Then

---

* If $\lambda = 1$ is a pole of T, this is the dimension of the range of projection $E(1; T)$.

$$\left|\frac{a_{mn}}{b_{mn}}\right| = \left|\frac{\lambda_0}{\lambda_1}\right|^{(n-m-1)} \prod_{\nu=m}^{n} \left|\frac{\lambda_1 - S_\nu^{-1}}{\lambda_0 - S_\nu^{-1}}\right|, \qquad n \geq (m+1),$$

$$= \left|\frac{\lambda_1 - S_m^{-1}}{\lambda_0 - S_m^{-1}}\right|, \qquad n = m,$$

for $m = 0, 1, 2, \cdots$. In any case, for $n \geq m$,

$$\left|\frac{a_{mn}}{b_{mn}}\right| \leq \prod_{\nu=m}^{n} \left|\frac{\lambda_1 - S_\nu^{-1}}{\lambda_0 - S_\nu^{-1}}\right| \quad \text{since} \quad |\lambda_0| < |\lambda_1|.$$

Consider a term of the form

$$\left|\frac{\lambda_1 - \alpha}{\lambda_0 - \alpha}\right|,$$

where $\alpha = (1 - \beta)$ is the lower bound on S_ν^{-1}. Then

$$\left|\frac{\lambda_1 - \alpha}{\lambda_0 - \alpha}\right| = \left|\frac{1 + \epsilon - \alpha}{\cos\theta - \alpha + j\sin\theta}\right|$$

$$= \left[\frac{(1 + \epsilon - \alpha)^2}{1 + \alpha^2 - 2\alpha\cos\theta}\right]^{\frac{1}{2}}$$

$$\leq 1$$

provided that

$$\epsilon^2 + 2\epsilon(1 - \alpha) - 2\alpha(1 - \cos\theta) \leq 0.$$

Since $0 < \alpha < 1$, the polynomial on the left side has one zero for $\epsilon > 0$ and one zero for $\epsilon < 0$. There exists, therefore, an $\epsilon > 0$ such that the above inequality is satisfied as long as $\theta \neq 0$. Since

$$\left|\frac{\lambda_1 - S_\nu^{-1}}{\lambda_0 - S_\nu^{-1}}\right| \leq \left|\frac{\lambda_1 - \alpha}{\lambda_0 - \alpha}\right|, \qquad \alpha \leq S_\nu^{-1} \leq 1,$$

$$\leq 1,$$

it follows that

$$\left|\frac{a_{mn}}{b_{mn}}\right| \leq \prod_{\nu=m}^{n} \left|\frac{\lambda_1 - S_\nu^{-1}}{\lambda_0 - S_\nu^{-1}}\right|, \qquad n \geq m$$

$$\leq \left|\frac{\lambda_1 - \alpha}{\lambda_0 - \alpha}\right|^{n-m+1}$$

$$\leq 1.$$

$$|a_{mn}| = |b_{mn}| = 0, \qquad \text{for } n < m.$$

The theorem is thus proved, and all the points on the unit circle except $\lambda = 1$ are in the resolvent set $\rho(T)$.

It follows from the above theorem that there are no poles on the unit circle except possibly at $\lambda = 1$. We know that such a pole, if it exists, must be of order one. The next theorem concerns the dimension of the eigenmanifold corresponding to $\lambda = 1$.

Theorem: There exists one and only one nontrivial element $x \in \chi$ such that $Tx = x$.

Proof: It is apparent that $x_0 = \{1, 1, 1, \cdots\}$ is one such element. If there exists another element $x \neq x_0$ (but, $|x| = |x_0|$), then some of its components must be unequal. Let $x = \{\xi_0, \xi_1, \xi_2, \cdots\}$. Then there is some $\xi_n \neq \xi_{n+1}$. We will show that this is impossible.

If $Tx = x$, it follows that [cf. (4)]

$$\xi_n = S_n^{-1}\xi_n + S_n^{-1}\beta^{i_{n+1}}\xi_{n+1} + S_n^{-1}\beta^{(i_{n+1}+i_{n+2})}\xi_{n+2} + \cdots$$

and

$$\xi_{n+1} = S_{n+1}^{-1}\xi_{n+1} + S_{n+1}^{-1}\beta^{i_{n+2}}\xi_{n+2} + \cdots.$$

Substituting the second equation into the first we obtain

$$\xi_n = S_n^{-1}\xi_n + S_n^{-1}\beta^{i_{n+1}}S_{n+1}\xi_{n+1}.$$

Or, since from (6)

$$S_n - 1 = \beta^{i_{n+1}}S_{n+1},$$

we have a contradiction

$$\xi_n = \xi_{n+1}.$$

This proves the theorem, and the eigenmanifold corresponding to $\lambda = 1$ is of dimension one.

The results obtained in this section about the spectrum of T are quite general and remain valid under any restriction of the domain 1_∞ assuming, of course, that x_0 is in such a restriction. The all-important question not answered in this section is whether or not T has a pole at $\lambda = 1$. This is a crucial question indeed and, on the basis of the results already obtained, the answer determines the behavior of the variance of the jitter. We delay the discussion of the existence of a pole at $\lambda = 1$ in order to first show its pivotal character. Next, we show that the existence of the pole depends upon a certain suitable restriction of the domain of T. These two points lead us to our final conclusions.

VI. BOUNDEDNESS OF VARIANCE

Let us consider now what happens to the output jitter as the number of repeaters approaches infinity. We obtain the results, at first, under the assumption that T has a pole at $\lambda = 1$. We discuss later the case where $\lambda = 1$ is not a pole of T.

Theorem: If $\lambda = 1$ is a pole of T, then there exists a bound on the variance of

$$y = [\sum_{m=0}^{\infty} T^m]x. \tag{14}$$

Proof: Let $\lambda = 1$ be a pole of T. Then $\sigma(T)$ may be decomposed into the union of a closed set σ, which lies inside a circle $|Z| < \alpha_0 < 1$, and the simple pole at $\lambda = 1$. Let us put $E_1 = E(1; T)$, $E_D = (I - E_1)$ and $D = TE_D$.* The range of E_1 is one-dimensional, and the iterates of T are given by

$$T^m = E_1 + D^m, \tag{15}$$

since for a simple pole at $\lambda = 1$

$$f(T)E_1 = f(1)E_1,$$

and

$$T^m E_D = D^m.$$

It also follows that $\sigma(D) = \sigma + \{0\}$, and so $\sigma(D)$ is contained in the disk $|Z| < \alpha_0$ for some $\alpha_0 < 1$. From the definition of spectral radius, this implies that $\lim \sup_{m \to \infty} |D^m|^{1/m} < \alpha_0$, from which it follows that for $m \geq 1$,

$$|D^m| \leq M\alpha_0^m \tag{16}$$

for some positive number M.

Next, observe that the space χ is a direct sum of subspaces $\chi_1 = E_1\chi$ and $\chi_D = E_D\chi$, which are invariant under T since T commutes with E_1 and E_D. It follows from (15) and (16) that

(a) $Tx = x$, for x in χ_1;

(b) $T^n x \to 0$ exponentially fast, for x in χ_D.

Every x in (14), then, is given by

$$x = x_1 + x_D,$$

where $x_1 = E_1x$ and $x_D = E_Dx$. The element x_1 except for a constant

---

* Observe that E_D is also a projection operator since $E_D^2 = E_D$.

multiplier is the eigenvector $\{1, 1, 1, \cdots\}$. Then

$$y = \lim_{n\to\infty} [\sum_{m=0}^{n} T^m](x_1 + x_D).$$

Obviously, the mean of y increases indefinitely* since

$$\bar{y} = \lim_{n\to\infty} [\sum_{m=0}^{n} T^m]x_1 + \bar{y}_D, \tag{17}$$

where

$$y_D = \lim_{n\to\infty} [\sum_{m=0}^{n} T^m]x_D. \tag{18}$$

The first term on the right-hand side of (17) increases indefinitely, and so $\bar{y} \to \infty$. The limit in (18) exists [cf. (16) and statement (b) above] and so

$$[y - \bar{y}] = y_D - \bar{y}_D \tag{19}$$

is bounded. Hence, the variance is bounded, if $\lambda = 1$ is a pole of T, as was to be proved. The physical interpretations of this case are discussed in the concluding section.

It must be observed that the bound on the variance is shown to exist for all elements x in χ. Hence, the result is valid for the admissible elements, viz., the jitter sequences.

The boundedness of the variance is a consequence of the inequality (16). As a function of α_0, the bound varies as $(1 - \alpha_0)^{-1}$ and increases indefinitely as α_0 approaches one. Therefore, we ask whether infinity is, indeed, the least upper bound on the variance when $\lambda = 1$ is *not* a pole of T. We anticipate the results of the next section to state that there is no bound (finite) on the variance when 1 is not a pole of T. We first show that given any number M, there exists an element x in χ, such that the variance of y exceeds M. Next, we show that there exist admissible elements for which the same conclusion holds.

VII. UNBOUNDED VARIANCE

We show, at first, that $\lambda = 1$ is not a pole of T in the general case. By the general case, we mean that the domain is not restricted in any way.

Theorem: The point $\lambda = 1$ is the limit point of the point spectrum of T.

---

* As discussed in Part I, there exists at least one X such that $x_1 \neq 0$.

Proof: We first determine the conditions that x must satisfy for $Tx = \lambda x$. Let $x = \{\xi_0, \xi_1, \cdots\}$. Then, if $Tx = \lambda x$,

$$\lambda \xi_n = S_n^{-1}\xi_n + S_n^{-1}\beta^{i_{n+1}}\xi_{n+1} + S_n^{-1}\beta^{(i_{n+1}+i_{n+2})}\xi_{n+2} + \cdots$$

and

$$\lambda \xi_{n+1} = S_{n+1}^{-1}\xi_{n+1} + S_{n+1}\beta^{i_{n+2}}\xi_{n+2} + \cdots.$$

Substituting the second equation into the first, we obtain

$$(\lambda - S_n^{-1})\xi_n = \lambda S_n^{-1}S_{n+1}\beta^{i_{n+1}}\xi_{n+1}.$$

Or, since

$$S_n - 1 = \beta^{i_{n+1}}S_{n+1},$$

we have

$$\xi_{n+1} = \frac{S_n - (1/\lambda)}{S_n - 1}\,\xi_n, \qquad (n = 0, 1, 2, \cdots). \tag{20}$$

From (20) we note that when $\lambda = S_n^{-1}$ we obtain an eigenvector x with $(n + 1)$ nonzero elements $\xi_k(k = 0, 1, \cdots, n)$. Hence, if the diagonal elements S_n^{-1} approach one as $n \to \infty$, then $\lambda = 1$ is a limit point of the set of eigenvalues. However, of greater physical importance is the case when the number of successive zeros in the admissible pulse trains has a finite upper bound. In such cases, the diagonal elements have an upper bound less than unity, i.e.,

$$S_n^{-1} \leqq \alpha < 1. \tag{21}$$

Even in these cases, there exists an eigenvector x for every λ such that $\alpha < \lambda \leqq 1$. We obtain the vector x from (20), starting with $\xi_0 = 1$. Since $S_n^{-1} < \lambda \leqq 1$, we find that the sequence $\{\xi_n\}$ is a strictly decreasing sequence, i.e.,

$$0 \leqq \xi_{n+1} < \xi_n \neq 0.$$

The sequence $x = \{\xi_n\}$ converges to zero, and hence it is a member of the space c_0 and has norm one. A simple substitution of x, obtained from (20), into the equation $Tx = \lambda x$ shows that x is indeed an eigenvector. Since an eigenvector x exists for every λ such that $\alpha < \lambda \leqq 1$, the point $\lambda = 1$ is the limit point of the point spectrum of T. The proof is complete and $\lambda = 1$ is not a pole of T.

It immediately follows that when all x in χ are admissible elements, there exists no bound on the variation of y about the flat delay. If it does, let M be such a bound. Then we can always find an eigenvector x,

corresponding to a $\lambda_1 > \alpha$, such that $(1 - \lambda_1)^{-1} > M$. Since x_1 is a member of c_0, the flat delay in the jitter is zero. The dispersion is given by

$$y_1 = \left(\frac{1}{1 - \lambda_1} \right) x_1 ;$$

and

$$| y_1 | > M | x_1 |,$$

which is a contradiction. Hence, there is no bound, etc.

To show that the same conclusion holds when the admissible elements x are the jitter sequences, we need merely show that there exists an admissible jitter element x in c_0 such that $(x - x_1)$ is nonnegative, i.e., nonnegative elements in the sequence $(x - x_1)$. Then, since all elements of T are nonnegative, $| Tx | \geqq | Tx_1 | > M | x_1 |$. Such an element x can be constructed easily by letting all pulses be present for a long enough time and then letting one of the pulses be absent, after which there is a string of alternating pulse and space, and then two pulses are absent, and so on. The sequence x for this case is a member of c_0 since the jitter will ultimately approach zero. The elements of x are assuredly greater than those of x_1 provided we make the string of pulses long enough between spaces.*

Similar conclusions are valid when the number of successive zeros in the original pulse train does not exceed a specified finite number. In this case, we use a member of the space c, $x = x_0 + x_1$, where x_1 is defined above and x_0 is the eigenvector corresponding to $\lambda = 1$. The dispersion is, as before,

$$y_1 = \left(\frac{1}{1 - \lambda_1} \right) x_1 .$$

The admissible jitter sequence is one that converges to x_0 but otherwise has properties similar to the previous case. Physically, the pulse train converges to a periodic pulse train with one pulse and at most the maximum number of successive zeros in each period.

We have thus shown that the bound on the variation of the jitter about the mean exists if T has a pole at $\lambda = 1$ and that there exists no such bound otherwise. At this point, we recall that a somewhat different formulation of the problem is obtained in (7). Let us note here that in the alternate formulation somewhat different but similar

---

* In fact, numerous admissible sequences with the same properties can be easily constructed. Their linear combination would also be such a sequence, and so on.

development takes place. In the alternate formulation, the point $\lambda = 1$ is not a limit point of the point spectrum. But, in general, neither is it a pole of T. It can be shown that every neighborhood of $\lambda = 1$ contains points in the spectrum of T. From this fact, the rest of the conclusions follow.

VIII. DISCUSSION OF RESULTS

The results may be stated simply in terms of the existence of a pole of T at $\lambda = 1$. If $\lambda = 1$ is in the point spectrum of T and it is an isolated point of the spectrum of T (i.e., it is a pole), then the variance of the jitter is bounded. Otherwise, the jitter dispersion has no bound. We show that, in the random case, $\lambda = 1$ is not a pole of T. The same result is obtained when a constraint is put on the number of successive zeros in the pulse train. Thus, there exists no bound on the variation of the jitter about its mean value for the truly infinite and random pulse trains.

On the other hand, of some physical importance are the cases which may be approximated by periodic pulse trains or nonperiodic pulse trains which either are finite or become periodic after a finite interval.* For such cases, the operator T is restricted to a finite dimensional space and $\lambda = 1$ is necessarily a pole of T. The variance is, therefore, bounded. Of course, the bound is a function of the dimension of the space as well as of the other eigenvalues in the spectrum. Each case must be investigated separately to determine the corresponding bound. Such a bound may be all that is important in the usual situation where a finite chain of repeaters is present in the system. Some practical means of determining the bounds will be discussed in a subsequent paper. We shall also discuss there many other practical matters, such as errors involved in our model, transients, etc.

To sum up, as the number of repeaters gets larger, the dimension of the space gets larger (since the effective pulse train gets longer), and the maximum dispersion of the jitter increases. Thus, there is such a thing as a worst pattern when there are a finite number of repeaters. However, the worst value of the jitter keeps on increasing.

The rate at which the variance increases as a function of the number of repeaters is not investigated in this paper. It is, of course, not possible for the dispersion to grow faster than n, the number of repeaters. This conclusion follows from the fact that the norm of T is equal to one.

---

* Many other physical constraints may be used to restrict T to a finite dimensional space. The variance is bounded in all such cases.

More precise determination of the rate of growth would depend upon a particular distribution of the random variables involved. We do not pursue this aspect of the problem.*

The conclusions about the spacing jitter (cf. Part I) follow along the same lines as above for the finite and infinite dimensional spaces. The misalignment, $T^n x$, in the nth repeater is also influenced by the dimensionality of the domain of T. When the dimension is finite, the misalignment is merely a flat delay (since $\lambda = 1$ is an isolated eigenvalue) for reasonably large n. However, when there is no pole at $\lambda = 1$, the misalignment is not so simply stated, but it is different from repeater to repeater.

We conclude with the observation that the approach proposed here should be potentially useful for many problems of signal processing encountered in data systems.

----

* For some partial results, for a somewhat different model, refer to C. J. Byrne, B. J. Karafin and D. B. Robinson, Jr., Pattern Induced Timing Jitter in T-1 PCM Repeaters, to be published. This paper uses a model proposed, in an unpublished report, by R. C. Chapman, Jr.

The Use of Solar Radio Emission for the Measurement of Radar Angle Errors

By J. T. KENNEDY and J. W. ROSSON

Space guidance and instrumentation have placed stringent demands on the pointing accuracy of tracking systems. One of the basic problems encountered is the calibration of the angle indicators of the tracking antenna to the true direction of the radio line of sight. A method of calibration is discussed which uses the sun as a primary directional reference.

I. INTRODUCTION

Historically, celestial bodies have been used as primary directional references for optical instruments such as navigational sextants, surveying theodolites, etc. Since celestial bodies are also sources of radio emission, they may be used directly as primary radio directional references. "Radio sextants" use the sun and moon as microwave directional references for all-weather marine navigation.[1] Conventional microwave tracking systems can also track these sources. For example, an X-band monopulse radar having an 8-foot antenna and crystal mixer receiver tracks the sun with an accuracy limited only by atmospheric effects. Moon tracking is of poorer quality because of the lower signal-to-noise ratio, but improvements in noise figure and a larger time-bandwidth product could make moon tracking competitive with present sun tracking.

The major limitation in using the sun as a precise reference has been the uncertainty of the position of its "radio center." This uncertainty is caused by regions of enhanced radio emission associated with sunspots. A method and experimental results will be described which overcome this limitation by taking advantage of the apparent rotation of the solar disk. This makes possible highly accurate alignment and zero setting without the usual optical aids.

II. SUN TRACKING PROCEDURE

Fig. 1 shows the comparison of the spectrum of solar radio emission with those of the moon and the brightest "radio stars." The plot is flux density vs wavelength. At 3 cm, for example, the power from the quiet sun is −164 dbm per square meter of effective antenna area in each cycle per second of bandwidth. This is the level of thermal noise which would be received at the earth if the sun were a black body at 18,000°K. We may say therefore that the sun has an equivalent radio temperature of 18,000°K at 3 cm. The average radio temperature of the moon at this wavelength is 180°K, so that the received power is 20 db less than the power from the sun. Even the brightest "radio stars" at 3-cm wavelength are extremely weak, the received power being about 20 db less than that from the moon.

In order to use celestial sources as directional references, the tracking system must be capable of determining the angle of arrival of the noise signal. Manasse[2] has shown that the optimum procedure is to perform
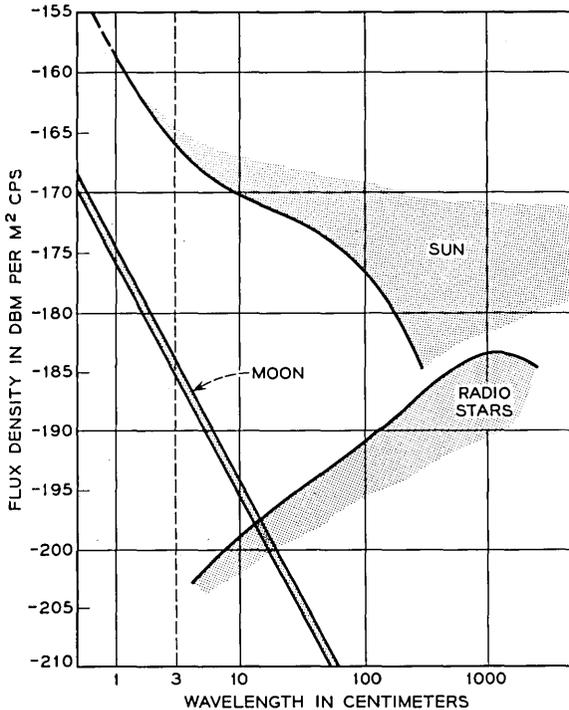
Fig. 1 — Radio emission from celestial bodies.

a simple correlation of the odd and even components of the antenna output. Since this is the technique of angle determination used in monopulse radar,* a monopulse system is well suited to the tracking of celestial noise sources. This was demonstrated in tracking experiments using an X-band monopulse radar. The theoretical sun and moon tracking performance are given in Appendix A. The calculated performance indicates that this system is theoretically capable of tracking the sun with a precision of better than 5 microradians.

To understand how an extended source such as the sun can be used as a precise reference, consider the simple case of more than one point source present in the antenna beam. These sources are not resolved and therefore appear as a single source located at the intensity centroid. Two point sources of equal intensity will appear as a single source midway between the two. Consider the typical difference pattern response of a monopulse antenna as in Fig. 2. A signal source to the left of the antenna null axis produces a positive error signal, a source to the right a negative signal. Zero error signal is obtained in autotracking multiple sources when the positive and negative signal contributions cancel each other. An extended source such as the sun can be considered as a collection of point sources. In this case, regions to the left will contribute a positive signal, regions to the right a negative signal.
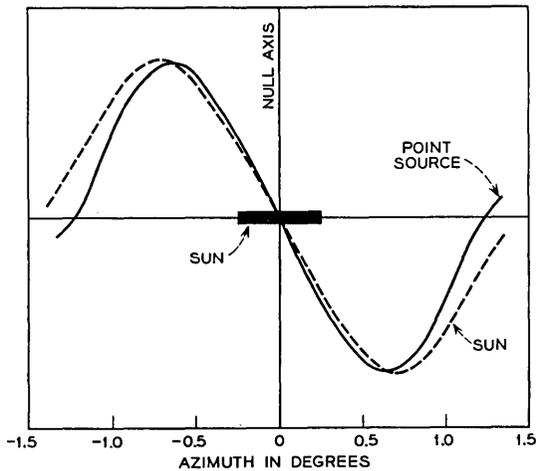
Fig. 2 — Typical monopulse difference patterns.

* In a monopulse system, the sum (even) and difference (odd) signals are correlated in the angle error detector.

Thus, when the radar is used passively to track the sun, the radio line of sight follows the point which corresponds to the centroid of radio emission, or "radio center." Although extended sources tend to broaden the difference pattern, the effect is surprisingly small for sources less than a beamwidth in extent. The effect is shown exaggerated in the dashed curve in Fig. 2. Actually, the effect of the $\frac{1}{2}$-degree sun within a one-degree beamwidth is barely discernible.

Over the surface of the sun, the radio emission is not uniform, and for this reason the "radio center" is displaced from the geometric center. Fig. 3 is a "radio picture"[3] of the sun which shows regions of enhanced radio emission superimposed on a background level. The background level is constant with time, whereas the enhancements evidence growth, decay and movement much like the sunspots with which they are associated. In the presence of regions of enhanced emission, the radio center is displaced from the visible center. Each region has the effect of pulling the radio center in its direction by an amount proportional
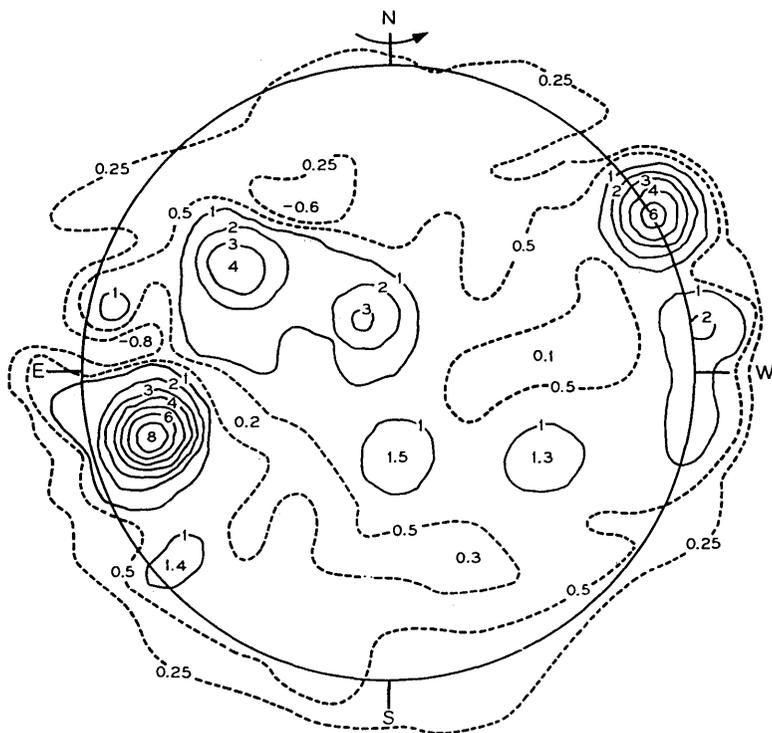
Fig. 3 — Radio picture of the sun.

to the amplitude and area of the enhancement, and its distance from the center. Because of the rotation of the sun about its axis in a period of 28 days, these regions move from left to right in about 14 days. The intensity of the enhancements is wavelength dependent, being most prominent at about 10 cm. For this reason, the resulting displacement of the radio center depends on wavelength. Measurements have been reported[4] which give in one case a maximum displacement of 1.2 mils at 3.2 cm and 0.9 mil at 2.0 cm during the peak of sunspot activity in 1957–58, and in another case 1.05 mils at 3.2 cm and 0.57 mil at 1.6 cm.

Some radio center observations made during the early part of this study are shown in Fig. 4. This is a plot of radio center displacement caused by sunspot activity during a two-week period in November 1960. In order to make these measurements, the antenna was first accurately aligned. Movement of the radio center was associated with a large sunspot which appeared on the eastern limb of the sun on November 5. Then, because of the rotation of the sun on its axis, the sunspot moved across the central meridian of the sun on November 12 and subsequently passed from view off the western limb on November 18. It can be seen that the radio center position changes slowly because of the long life-
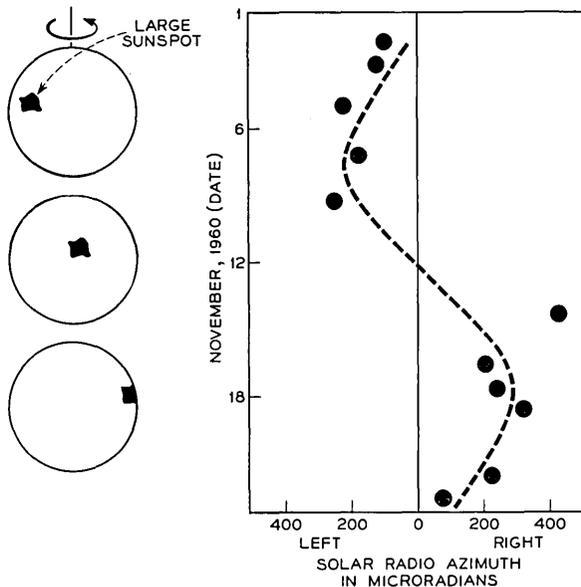
Fig. 4 — Radio center movement.

time of the enhanced regions and their slow movement with the solar
rotation. Actually, the variation over a period of several hours is small
enough to be neglected.

Unless corrected, this pulling effect imposes a major limitation on
the accuracy of radio direction finding using the sun. However, a method
has been found which makes it possible to determine the radio center
displacement and also antenna alignment errors from data obtained in
tracking the sun over a period of a few hours. That is, without previous
antenna alignment, it is possible to determine not only the radio center
displacement, but also the antenna alignment errors. The method makes
use of the apparent motion of celestial bodies caused by the rotation
of the earth. The effect is perhaps most easily visualized in the case of
the stars. For an observer in northern mid-latitudes, stars which rise
in the east reach a maximum elevation angle when they cross the ob-
server's meridian to the south and then set in the west (Fig. 5). Con-
sider two stars which rise one after the other at the same point on the
horizon. As they rise, the later one will be below and left of the earlier
one. At meridian crossing, the two stars are side by side. When they
are setting, the later star is above and to the left of the earlier one.
To the observer, the later star has moved clockwise relative to the ear-
lier one. A quantitative description of this rotation is given in Appendix
B.

This same rotational effect is also observed in the case of the sun.
That is, any point displaced from the center of the sun will appear to
rotate around the center. This suggests that if angle measurements
on the radio sun are compared to the azimuth and elevation of the geo-
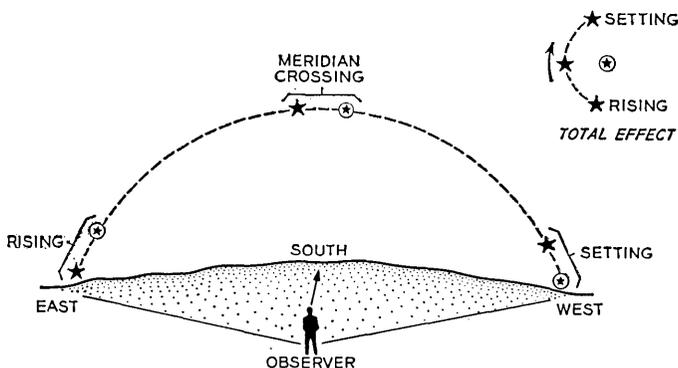
Fig. 5 — Apparent rotation of celestial bodies.

metric center of the sun,* the differences between the measured and
calculated values will show the motion of the displaced radio center.
An elevation versus azimuth plot of these differences is made to look
for this rotational effect. Typical data obtained in sun tracking on
August 8, 1961, are shown in Fig. 6. The abscissa is actually the azimuth
differences times the cosine of the elevation to refer the azimuth up to
the viewing plane. Each point is the mean difference in a 24-second sam-
ple. Since the antenna had not been previously aligned, an initial align-
ment is made on the first observation, which results in zero differences
for the first data point. The rotation with time apparent in the curved
pattern of the data points is attributable to the apparent rotation of the
radio center. Data points for 11 AM, noon, and 1 PM are indicated.

A simple graphical method was used to examine these data. An over-
lay template was constructed for this particular day and latitude and
fitted to the data as shown in the shaded area. Four independent de-
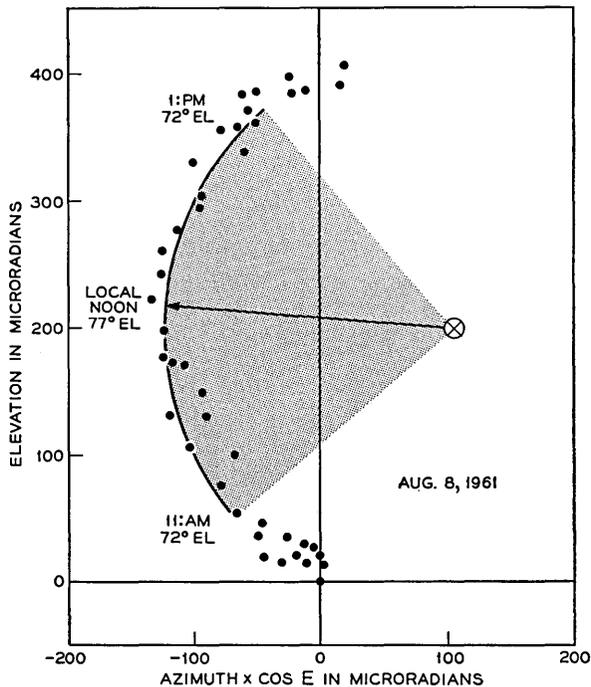
Fig. 6 — Typical sun tracking data, August 8, 1961, with initial zero set.

* The position of the sun can be calculated accurately from the ephemeris, as
described in Appendix C.

terminations were averaged to obtain the "best" estimate of the radio center displacement and error in the initial zero setting. If the initial zero set had been correct, the center of curvature would have been at the origin. Therefore the final zero settings can be determined from the offset in Fig. 6. Fig. 7 shows the same data after making the final zero set adjustment.

The radio center displacement may be described in a coordinate system which is independent of time by resolving the displacement vector at noon into horizontal and vertical components. The horizontal component becomes the displacement in hour angle and the vertical component the displacement in declination. A summary of the values of radio center displacements obtained is given in Table I. The last column in Table I shows the probable error in the radio center determination and therefore indicates the accuracy attainable in using the sun as an X-band directional reference.

Radio center displacement is most easily determined around local noon when the solar disk rotation rate is maximum, making the effect

Fig. 7 — Data of Fig. 6 after final zero set adjustment.

TABLE I — RADIO CENTER DISPLACEMENT AT LOCAL NOON

Date	Displacement		Standard Deviation
	Hour Angle	Declination	
	(Microradians)	(Microradians)	(Microradians)
April 24, 1961	−125	+50	14
May 25, 1961	+85	+40	8
June 1, 1961	+95	+20	12
June 15, 1961	−95	+15	9
June 21, 1961	+135	+40	16
July 25, 1961	+95	+50	30
August 8, 1961	−235	+20	26

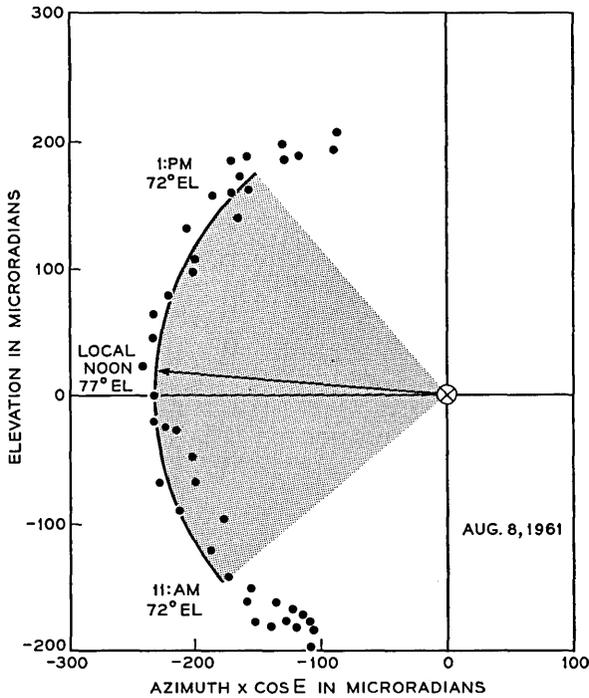more easily recognized than at any other time of day. Also, since the sun is at its maximum elevation angle at this time, atmospheric effects are minimized. Another important advantage of noontime observations is that the elevation angle is changing very slowly, which means that elevation-dependent systematic errors can be considered essentially constant.

Azimuth zero set errors are compressed at high elevation angles by the cosine of the elevation angle. For this reason, azimuth zero set accuracy is better at lower elevation angles.

The most important advantage in using celestial microwave directional references is the direct measurement of the radio axis to angle indicator relationship without going through the involved intermediate steps of determining systematic errors between the radio axis and the optical line-of-sight and the systematic errors between the optical line-of-sight and the angle indicators. These experiments have demonstrated that the limitations of using the sun can be overcome to make direct measurements possible.

III. APPLICATIONS AND LIMITATIONS

The sun serves as a useful tracking source in investigating atmospheric refraction and other low-angle effects on angle tracking.

Directional measurements of celestial bodies is the classical method of position determination in celestial navigation. The accuracy obtained in high-angle sun tracking enables the geodetic position of the tracking antenna to be determined to an accuracy of about 600 feet.

Some of the limitations in using the sun as a precise reference are given below.

(a) *Solar flares:* Although the level of solar radio emission can generally be considered substantially constant over a period of several hours, intense outbursts are sometimes observed at the time of large solar

flares. These outbursts can exert a strong pulling effect on the radio center, but fortunately they are generally of short duration (several minutes) and are easily recognizable in tracking data. Of the approximately 200 data points in seven days tracking, only one was affected by a suspected outburst. This occurred on June 15, 1961, at 1641 Universal Time at the same time as an "Outstanding occurrence" reported by Ottawa[5] on 10-cm wavelength. The effect was a brief displacement of the radio center amounting to about 150 microradians.

(b) *Solar disk rotation:* Because of the geometry of the solar disk rotation, the determination of radio center displacement is more easily accomplished at the higher elevation angles of the sun. For this reason, radio center displacement is more easily determined in the summer at low latitudes. Longer observing times are required at higher latitudes in the winter.

(c) *Antenna beamwidth:* Sun or moon tracking with antenna beam widths of less than $\frac{1}{2}$ degree will suffer from decreased angle sensitivity caused by the large source distribution. In the extreme case of beamwidths of the order of $\frac{1}{10}$ degree, less extended sources such as the "radio stars" would be more attractive.

IV. SUMMARY

Celestial radio sources are attractive as microwave directional references; however, two major aspects must be investigated in considering them. The first aspect is the ability to track the source. The second aspect deals with the precise knowledge of the position of the celestial radio source. For a conventional X-band radar receiver utilizing a crystal mixer, the sun is most suitable from the standpoint of "noise signal"-to-noise ratio. The moon presents a marginal condition. By tracking the sun in a time-continuous mode (i.e., range gate disabled), the tracking quality becomes limited only by the atmospheric noise.

In examining the second aspect, the radio center of the sun is not coincident with the actual center, but is displaced by local regions of enhanced radio emission associated with sunspot activity. Although the sunspot activity is random on a day-to-day basis, the effect upon the radio center displacement is small enough to be considered constant over a period of several hours. A technique was developed to utilize the diurnal motion of the earth to enable the radio displacement to be determined independently of other sources of error.

V. ACKNOWLEDGMENT

System Description and Tracking Performance

A conventional monopulse tracking system was used for the experiments which have been described. Normally, the radar receiver samples the input only during the very short interval of time when the returning pulse is expected. This is, of course, not the optimum procedure to use in the case of a continuous, low-level signal. However, by means of a simple modification, the receiver can be kept open to optimize system performance with signals which are present continuously.

Since the microwave signals from celestial radio sources are quite constant in level and cover a broad spectrum, neither automatic gain nor frequency control are required.

With these modifications, the performance of the tracking system can be expressed as a function of the system parameters as follows:

$$\delta\Theta = \Theta_b \frac{\sqrt{1 + S/N}}{2S/N\sqrt{2B\tau}}$$

where $\delta\Theta$ = rms angle fluctuations
Θ_b = antenna beamwidth
S/N = input signal-to-noise power ratio
B = receiver bandwidth
τ = post detection integration time.

This result is based on the assumption of a point source of noise in the presence of external background and internal receiver noise, but does not include the effects of transmission through the atmosphere.

The noise power, N, received from the sun is the product of the solar flux density, S, and the effective antenna area, A, thus:

$$N = S \times A \times \tfrac{1}{2} = 4.37 \times 10^{-20} \text{ watts/cps}$$

where the factor $\tfrac{1}{2}$ accounts for the fact that the antenna accepts only the vertically polarized component of the randomly polarized solar radio emission. It is useful to consider the temperature, T_{eq}, of an equivalent network, replacing the antenna, which would have an available noise power equal to that from the sun. In this case,

$$kT_{eq} = N$$

where k is Boltzmann's constant, 1.38×10^{-23} watts/°K cps. The resulting effective antenna temperature from the sun is thus 3150°K.

The receiver noise temperature, assuming a nominal 11-db noise figure, is:

$$T_R = (F - 1)T_0 = 11.6 \times 290°\text{K} = 3360°\text{K}$$

where F is the system noise figure expressed as a power ratio and T_0 is the reference temperature, 290°K. Thus, the signal-to-noise ratio is about unity. Assuming a typical 1° beamwidth, 10-mc bandwidth, and $\frac{1}{2}$-second time constant, the resulting tracking performance is about 5 microradians. In actual tracking however, this performance cannot be realized because of atmospheric limitations which are believed to be in the order of 20 to 50 microradians.

When this system is used with a three-second time constant to track the moon, the short-term angle uncertainties are about 400 microradians. This agrees essentially with the theoretical value, indicating that the system performance when tracking the moon is limited by receiver noise rather than by atmospheric effects.

APPENDIX B

Apparent Solar Disk Rotation

The apparent rotation of the solar disk can be derived from the spherical triangle shown in Fig. 8. The orientation of the sun remains fixed with respect to the great circle passing through the sun and the celestial pole, whereas the orientation to an observer in azimuth-elevation coordinates is always referred to the great circle passing through the sun and the zenith. The apparent rotation of the solar disk is described by the variable angle, p. From the Law of Sines:

$$\sin p = \frac{\cos \phi}{\cos \delta} \sin A.$$

For a given set of observations, the observer's latitude, ϕ, and the declination angle of the sun, δ, remain constant; therefore the apparent rotation of the sun is a simple function of the azimuth angle, A. Fig. 8 and the above equation show that the displaced radio center of the sun will trace through the arc of a circle whose radius is the magnitude of the radio center displacement.

The apparent solar disk rotation can also be expressed in terms of the local hour angle, H, which changes with earth's rotation uniformly at about 15° per hour. The expression is:

$$\tan p = \frac{\sin H}{\sin \delta \cos H - \cos \delta \tan \phi}.$$

A plot of this equation is given for 28.5 degrees North latitude in Fig. 9 for several values of declination. From these curves, the maximum

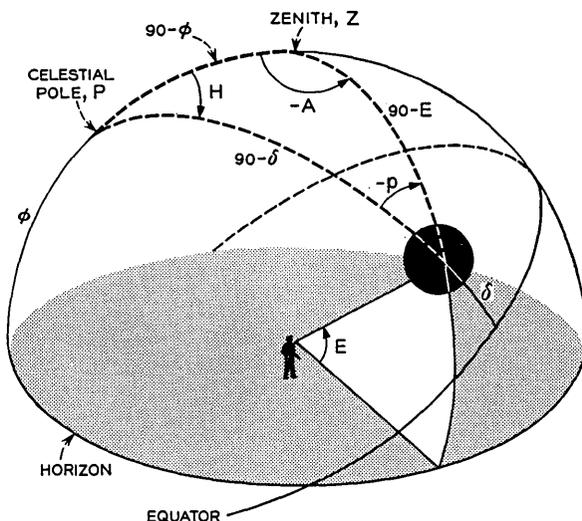Fig. 8 — Spherical geometry used to derive apparent rotation of solar disk.

rate of rotation occurs at local noon; hence the optimum time to observe the radio center displacement is around local noon.

The latter equation is used to make the overlay template which is fitted to the plotted data to locate the center of rotation of the observed data points.
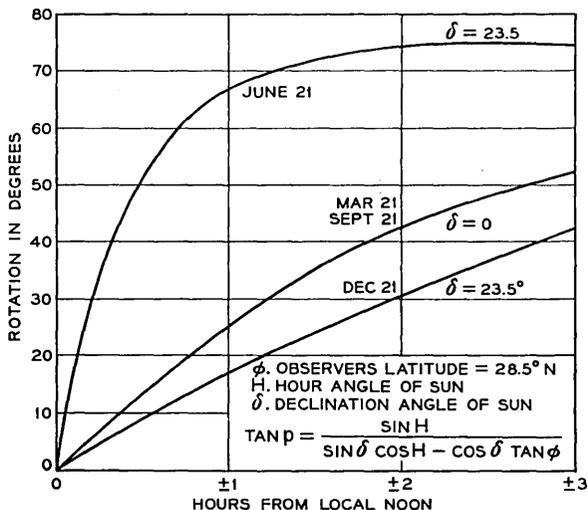

Fig. 9 — Apparent solar disk rotation.

APPENDIX C

Determination of the True Angular Position of the Sun

In the experiment, the tracking system measures the azimuth and elevation angles and records these data along with the time of measurement on magnetic tape. This tape becomes the input to a digital computer which performs the computations described below and compares the measured values with the calculated true position of the sun.

Primary position data for the sun are taken from the *American Ephemeris and Nautical Almanac*. These data are referred to the true equinox and equator of date and contain a correction for aberration. Corrections must be computed for solar parallax, the difference between Ephemeris Time and Universal Time, and the local deflection of the vertical. These corrections are applied in the spherical coordinates of hour angle and declination. The estimated accuracies in these coordinates are 0.02 second of time in hour angle and 0.2 second of arc in declination. During the experiments, time is recorded for each of the angle observations to an accuracy of about 0.05 second. This brings the total accuracy of the computed position of the sun to about 4 microradians.

The hour angle and declination, together with the latitude, are used to calculate the azimuth and elevation angles.

In order to compare the observed values with the computed angular positions of the sun, it is necessary to correct the observed values of elevation for atmospheric refraction. The correction used is

$$\Delta E = -N_0 \cot E$$

where N_0 is the index of refraction determined from observations at the tracking site and E is the observed elevation angle. This equation is adequate for elevation angles above 10 degrees.

REFERENCES

1. Marner, G. R., Automatic Radio Celestial Navigation, Jour. of the Inst. of Navigation, **12**, Nos. 3 and 4, July–Oct. 1959, pp. 249–259.
2. Manasse, R., Maximum Angular Accuracy of Tracking a Radio Star by Lobe Comparison, I.R.E. Trans. on Antennas and Propagation, **AP-8**, No. 1, Jan. 1960, pp. 50–56.
3. Swarup, G., Stanford Microwave Spectroheliograms for 1960 June, Stanford Radio Astronomy Institute Publication No. 11.
4. Molchanov, A. P., The Spectrum of Local Sources of Solar Radio Emission, Soviet Astronomy, **5**, No. 5, March–April 1962, pp. 651–654.
5. National Bureau of Standards, Central Propagation Laboratory, Solar Geophysical Data, **CRPL-F 203**, part B, July 1961, p. IVa.

Integral Representation of Zero-Memory Nonlinear Functions

By J. C. HSU

Integral representation of zero-memory nonlinear functions offers prom-ise as an analytical method for nonlinear control systems study. A review of work performed at Bell Laboratories and elsewhere on the use of these representations is presented, with particular emphasis on nonlinearities often encountered in feedback control systems. In general, the integral representations are useful only insofar as the resulting expression can be readily evaluated. The use of Bennett functions systematized the formulation of these integrals. The numerical results of a large class of the integrals can then be given by the tabulated Bennett functions. A comprehensive bibliography is appended.

I. INTRODUCTION

Integral representation of zero-memory nonlinear functions has been extensively used by Bennett, Rice and others (see References) in the solving of problems such as the finding of modulation products when one or more sinusoids appear at the input, and the finding of the output autocovariance function when sine wave and random noise are applied. In relation to the necessary calculations which occur in the use of these integral representations, a class of functions known as Bennett functions, after W. R. Bennett, has been defined. A selected representation of these functions has been tabulated and plotted.

While the original studies were carried out in relation to problems encountered in communications, the methods and the results can cer-tainly be applied to advantage in control problems. Some work in this regard has been done by J. C. Lozier in unpublished notes on the analysis of the oscillating control servomechanism. On the whole, however, it appears that these approaches are not known to investigators in the controls field. The present paper represents an attempt to summarize in a unified manner the work that has been done and to indicate the

scope of applications and limitations of the integral representations, particularly with respect to controls usage.

II. INTEGRAL REPRESENTATION ARISING FROM FOURIER TRANSFORMS

It is known that the function

$$f_1(u) = \frac{u}{2} + \frac{u}{\pi} \int_0^\infty \frac{\sin u\lambda}{\lambda} \, d\lambda \tag{1}$$

is discontinuous in its first derivative with respect to u, its value as a function of u being:

$$
\begin{aligned}
f_1(u) &= u \qquad u > 0 \\
&= 0 \qquad u < 0.
\end{aligned} \tag{2}
$$

The plot of $f_1(u)$ vs u is in the form of an ideal half-wave rectifier.

Using $f_1(u)$ as a basic unit, other discontinuous functions can be generated. For example

$$
\begin{aligned}
f_2(u) &= \frac{1}{2} + \frac{1}{\pi} \int_0^\infty \frac{\sin u\lambda}{\lambda} \, d\lambda = 1 \qquad u > 0 \\
&= 0 \qquad u < 0
\end{aligned} \tag{3}
$$

and is in the form of an off-on relay as a function of u.

From (3) the bang-bang type of relay is readily created as:

$$
\begin{aligned}
f_3(u) &= \frac{2A}{\pi} \int_0^\infty \frac{\sin u\lambda}{\lambda} = A \qquad u > 0 \\
&= -A \qquad u < 0.
\end{aligned} \tag{4}
$$

A relay with dead zone is

$$
\begin{aligned}
f_4(u) &= \frac{A}{\pi} \int_0^\infty \frac{\sin (u - c)\lambda + \sin (u + c)\lambda}{\lambda} \, d\lambda \\
&= \frac{2A}{\pi} \int_0^\infty \frac{\sin u\lambda \cos c\lambda}{\lambda} \, d\lambda =
\begin{aligned}
&= A & u > & \;\; c \\
&= 0 & -c < u < & \;\; c \\
&= -A & u < & -c.
\end{aligned}
\end{aligned} \tag{5}
$$

A limiter (linear characteristic with saturation) is

$$
f_5(u) = \frac{2}{\pi} \int_0^\infty \frac{\sin \mu\lambda \sin A\lambda}{\lambda^2} \, d\lambda
\begin{aligned}
&= -A & u < -A \\
&= u & -A < u < A \\
&= A & u > A
\end{aligned} \tag{6a}
$$

$$
= \frac{2u}{\pi} \int_0^\infty \frac{\cos u\lambda \sin A\lambda}{\lambda} \, d\lambda + \frac{2A}{\pi} \int_0^\infty \frac{\sin u\lambda \cos A\lambda}{\lambda} \, d\lambda. \tag{6b}
$$

Equation (6b) is readily obtained by manipulating two functions of the form of (1). That (6a) is equivalent to (6b) is seen by integrating (6a) once by parts. Other discontinuous functions can be generated from the above five functions by appropriate shifting (bias) of each individual characteristic, or by combining several characteristics. In fact, simply multiplying by an appropriate $g(u)$ can create quite general discontinuous characteristics.

It is noted that u may be viewed as the input to the nonlinear element, and $f(u)$ then gives the response to this input. If $u(t)$ is a function of time, for each $u(t_1)$ the function $f[u(t_1)]$ yields the instantaneous value of the output (i.e., $f(u)$ is a functional of u). While $f(u)$ is no more convenient for use in the evaluation of the output as a function of time than equations of the form (2), giving the discontinuous function as a set of equations, it is very useful for the purpose of spectral analysis since $f[u(t)]$ is in a compact form suitable for Fourier series expansion.

As an example, we seek to find the output spectral component for the relay with dead zone, when input is in the form $u = P \cos x$.

Using (5), the output Fourier coefficients are found by:

$$a_n = \frac{1}{\pi} \int_{-\pi}^{\pi} \left\{ \frac{2A}{\pi} \int_0^{\infty} \frac{\sin (\lambda P \cos x) \cos c\lambda}{\lambda} \, d\lambda \right\} \cos nx \, dx$$

$$= \frac{2A}{\pi^2} \int_0^{\infty} \frac{d\lambda}{\lambda} \cos c\lambda \int_{-\pi}^{\pi} \sin (\lambda P \cos x) \cos nx \, dx$$

$$= \begin{cases} 0 & n \text{ even} \\[2mm] \dfrac{A}{4\pi} (-1)^{(n-1)/2} \displaystyle\int_0^{\infty} \frac{J_n(\lambda P) \cos c\lambda}{\lambda} \, d\lambda & n \text{ odd} \end{cases}$$

where $J_n(z)$ is Bessel function of the first kind of order n.

Since it is known that[1]

$$\int_0^{\infty} \frac{J_n(at) \cos bt}{t} \, dt = \begin{cases} \dfrac{1}{n} \cos \left\{ n \sin^{-1} \left(\dfrac{b}{a} \right) \right\} & b < a \\[4mm] \dfrac{a^n \cos \dfrac{n\pi}{2}}{n\{b + \sqrt{b^2 - a^2}\}^n} & b > a, \end{cases} \tag{7}$$

then, for n odd:

$$a_n = \frac{A}{4\pi} (-1)^{(n-1)/2} \left\{ \frac{1}{n} \cos \left[n \sin^{-1} \left(\frac{c}{P} \right) \right] \right\} \qquad c < P$$

$$= 0 \qquad\qquad\qquad\qquad\qquad\qquad\qquad P < c.$$

Certain of the nonlinear characteristics expressed in the integral form are also amenable to a double frequency type of analysis in which the input is of the form

$$u(t) = P \cos (\omega_1 t + \theta_1) + Q \cos (\omega_2 t + \theta_2).$$

Bennett[2] in particular has contributed extensively to double frequency studies.

In control systems analysis, a double frequency study becomes necessary in (a) the oscillating servomechanisms[3] and (b) the dual input describing function approach to closed loop servos.[4,5,6] In what follows, the fundamental components (i.e., components in ω_1 and ω_2 of the output) from a bang-bang type of relay are found. The approach follows closely that of Lozier.

The input u is a function of two frequencies ω_1 and ω_2 ; this is brought to light by setting $x = \omega_1 t + \theta_1$, $y = \omega_2 t + \theta_2$, and letting $Q/P = k$. Thus

$$u(x, y) = P(\cos x + k \cos y). \tag{8}$$

In passing through a bang-bang type relay, it is recognized that the amplitude P in (8) does not influence the output; thus without loss of generality it may be set to unity.

The output $f(u)$, written as $f(x,y)$ is:

$$f(x,y) = +A \qquad \cos x + k \cos y > 0$$

$$f(x,y) = -A \qquad \cos x + k \cos y < 0$$

which may be expressed as a double Fourier series[2,7] as:

$$f(x,y) = \sum_{n=0}^{\infty} \sum_{m=0}^{\infty} [A_{\pm mn} \cos (mx \pm ny) + B_{\pm mn} \sin (mx \pm ny)] \tag{9}$$

where

$$A_{\pm mn} = \frac{1}{2\pi^2} \int_{-\pi}^{\pi} \int_{-\pi}^{\pi} f(x,y) \cos (mx \pm ny) \, dy \, dx \tag{9a}$$

$$B_{\pm mn} = \frac{1}{2\pi^2} \int_{-\pi}^{\pi} \int_{-\pi}^{\pi} f(x,y) \sin (mx \pm ny) \, dy \, dx \tag{9b}$$

$$A_{00} = \frac{1}{\pi^2} \int_{-\pi}^{\pi} \int_{-\pi}^{\pi} f(x,y) \, dy \, dx, \qquad B_{00} = 0. \tag{9c}$$

From symmetry of the bang-bang relay, $B_{\pm mn} \equiv 0$ for all m and n; moreover the integral representation of (4) can here be used, thus:

$$A_{\pm mn} = \frac{A}{\pi^3} \int_{-\pi}^{\pi} \int_{-\pi}^{\pi} \left[\int_0^\infty \frac{d\lambda \sin{(\cos x + k \cos y)} \lambda}{\lambda} \right]$$

$$\cdot \cos{(mx \pm ny)}\, dy\, dx.$$

The interchange of integration can be carried out here in view of the finite limits of the outer integral and the bounded nature of the inner integral, whence:

$$A_{\pm mn} = \frac{A}{\pi^3} \int_0^\infty \frac{d\lambda}{\lambda} \int_{-\pi}^{\pi} dx \int_{-\pi}^{\pi} dy \left\{ \sin{[(\cos x + k \cos y)\lambda]} \cos{(mx \pm ny)} \right\}.$$

Upon expanding, collecting nonzero terms, and integrating, the result is (as $A_{+mn} = A_{-mn}$ for all m, n, the $\pm$ signs are henceforth dropped.):

$$A_{mn} = \frac{4A}{\pi} (-1)^{(m+n-1)/2} \int_0^\infty \frac{J_n(k\lambda)J_m(\lambda)}{\lambda}\, d\lambda, \qquad m + n \text{ odd} \tag{10}$$

$$= 0 \qquad\qquad\qquad\qquad \text{otherwise}$$

where use has been made of the following definite integrals:[8,1]

$$\frac{2}{\pi} \int_0^{\pi/2} \cos{(z \sin \varphi)} \cos 2n\varphi d\varphi$$

$$\tag{11a}$$

$$= (-1)^n \frac{2}{\pi} \int_0^{\pi/2} \cos{(z \cos \varphi)} \cos{(2n\varphi)}\, d\varphi = J_{2n}(z)$$

$$\frac{2}{\pi} \int_0^{\pi/2} \sin{(z \sin \varphi)} \sin{(2n + 1)\varphi d\varphi}$$

$$\tag{11b}$$

$$= (-1)^n \frac{2}{\pi} \int_0^{\pi/2} \sin{(z \cos \varphi)} \cos{(2n + 1)\varphi d\varphi} = J_{2n+1}(z).$$

The integral in (10) may be evaluated by means of formulas attributed to Sonine and Schafheitlin[9] (also known as the Weber-Schafheitlin integrals[8]), the result being expressed in the form of hypergeometric functions $F(\alpha,\beta,c,x)$:

$$\int_0^\infty \frac{J_n(a\lambda)J_m(b\lambda)}{\lambda^r}\, d\lambda = \frac{a^n \Gamma\left(\dfrac{n + m - r + 1}{2}\right)}{2^r b^{n-r+1}\, \Gamma\left(\dfrac{-n + m + r + 1}{2}\right)\Gamma(n + 1)} \tag{12a}$$

$$\cdot F\left(\frac{n + m - r + 1}{2}, \frac{n - m - r + 1}{2}, n + 1, \left(\frac{a}{b}\right)^2\right)$$

if $n + m - r + 1 > 0$, $r > -1$, and $0 < a < b$,

$$\int_0^\infty \frac{J_n(a\lambda)J_m(a\lambda)}{\lambda^r}\,d\lambda$$

$$= \frac{\left(\dfrac{a}{2}\right)^{r-1}\Gamma(r)\,\Gamma\left(\dfrac{n+m-r+1}{2}\right)}{2\Gamma\left(\dfrac{-n+m+r+1}{2}\right)\Gamma\left(\dfrac{n+m+r+1}{2}\right)\Gamma\left(\dfrac{n-m+r+1}{2}\right)} \quad (12b)$$

if $n + m + 1 > 0$, $r > 0$, and a real; and

$$\int_0^\infty \frac{J_n(a\lambda)J_m(b\lambda)}{\lambda^r}\,d\lambda = \frac{b^m\Gamma\left(\dfrac{n+m-r+1}{2}\right)}{2^r a^{m-r+1}\Gamma\left(\dfrac{n-m+r+1}{2}\right)\Gamma(m+1)}$$

$$\cdot F\left(\frac{n+m-r+1}{2},\,\frac{-n+m-r+1}{2},\,m+1,\,\frac{b^2}{a^2}\right) \quad (12c)$$

if $(n + m - r + 1) > 0$, $r > -1$, and $0 < b < a$.

   Accordingly,

$$A_{mn} = \frac{2A}{\pi}\,(-1)^{(n+m-1)/2}\,\frac{k^n\Gamma\left(\dfrac{n+m}{2}\right)}{\Gamma\left(\dfrac{2-n+m}{2}\right)\Gamma(n+1)}$$

$$\cdot F\left(\frac{n+m}{2},\,\frac{n-m}{2},\,n+1,\,k^2\right) \quad \text{for } k < 1 \qquad (13a)$$

$$= \frac{2A}{\pi}\,(-1)^{(n+m-1)/2}$$

$$\cdot\frac{\Gamma\left(\dfrac{n+m}{2}\right)}{\Gamma\left(\dfrac{2-n+m}{2}\right)\Gamma\left(\dfrac{2+n+m}{2}\right)\Gamma\left(\dfrac{n-m+2}{2}\right)} \qquad (13b)$$

$$\text{for } k = 1$$

$$= \frac{2A}{\pi}\,(-1)^{(n+n-1)/2}\,\frac{\Gamma\left(\dfrac{n+m}{2}\right)}{k^m\Gamma\left(\dfrac{n-m+2}{2}\right)\Gamma(m+1)}$$

$$\cdot F\left(\frac{n+m}{2},\,\frac{m-n}{2},\,m+1,\,\left(\frac{1}{k}\right)^2\right) \quad \text{for } k > 1. \qquad (13c)$$

The three cases of (13) are essentially equivalent if one recognizes that

$$F(a,b,c,1) = \frac{\Gamma(c)\Gamma(c - a - b)}{\Gamma(c - a)\Gamma(c - b)}$$

and that, for $k > 1$, the situation is identical to that of inverting the role of n and m, and defining a new quantity $k' = 1/k$.

The output fundamental components are A_{10} and A_{01} ; from (13) one has:

$$A_{10} = \frac{2A}{\pi} \frac{\Gamma\left(\frac{1}{2}\right)}{\Gamma\left(\frac{3}{2}\right)\Gamma(1)} F\left(\frac{1}{2}, -\frac{1}{2}, 1, k^2\right) \tag{14a}$$

$$= \frac{4A}{\pi}\left(1 - \frac{1}{4}k^2 - \frac{3}{64}k^4 - \frac{5}{256}k^6 \cdots\right)$$

$$A_{01} = \frac{2A}{\pi} \frac{k\Gamma\left(\frac{1}{2}\right)}{\Gamma\left(\frac{1}{2}\right)\Gamma(2)} F\left(\frac{1}{2}, \frac{1}{2}, 2, k^2\right) \tag{14b}$$

$$= \frac{2Ak}{\pi}\left(1 + \frac{1}{8}k^2 + \frac{3}{64}k^4 \cdots\right).^\dagger$$

Considered together with the input (8), this yields Lozier's oft-quoted result,[3,10] that the equivalent "gain" of the relay, for small values of k, is 6 db higher for the "carrier" than for the "signal."

It is not difficult to see that the Weber-Schafheitlin integrals also occur for two frequency inputs applied to the characteristics (1) and (3), but that integrals of the form

$$\int_0^\infty \frac{J_n(a\lambda)J_m(b\lambda)}{\lambda^r} \begin{Bmatrix} \sin A\lambda \\ \cos A\lambda \end{Bmatrix} d\lambda \tag{15}$$

occur for characteristics of (5) and (6). Moreover, inputs with more than two frequency components will result in generalized Weber-Schafheitlin integrals of the form

$$\int_0^\infty \prod_{i=1}^N J_i(a_i\lambda)\lambda^{-r}\, d\lambda \tag{16}$$

---

† Equations (14a) and (14b) can also be expressed in terms of the complete elliptic integrals for which tables are available. See Refs. 3, 21, and 22.

for characteristics (1), (3), and (4), and generalized integrals of the form

$$\int_0^\infty \prod_{i=1}^N J_i(a_i\lambda)\lambda^{-r} \begin{Bmatrix} \sin A\lambda \\ \cos A\lambda \end{Bmatrix} d\lambda \tag{17}$$

result for characteristics (5) and (6).

Unfortunately no general solutions have been found to represent (15), (16) or (17) in known functions. In such cases, numerical solutions can be used. Numerical solutions in terms of Bennett functions and their tabulation are described in Section IV of this paper.

III. INTEGRAL REPRESENTATION ARISING FROM LAPLACE TRANSFORM[11],[12]

The integral representation of Section II is closely related to the Fourier transform. An alternate approach using the Laplace transform is more convenient in some cases and has been extensively used by Bennett and Rice, among others. We mention some results of this approach for the sake of completeness.

Expressing the output of a nonlinear device in response to an input u as $f(u)$, it is possible to find the (possibly two-sided) Laplace transform of $f(u)$, denoted $F(s)$, or,

$$F(s) = \int_{-\infty}^\infty e^{-su} f(u)\ du. \tag{18}$$

The inverse transform is then

$$f(u) = \frac{1}{2\pi j} \int_C e^{us} F(s)\ ds \tag{19}$$

where C is some suitably chosen contour of integration. If $F(s)$ exists, then (19) is an explicit expression for $f(u)$ which may be used to advantage. In the case of solving for modulation products, $f(u)$, written explicitly in x and y, may thus be used directly to compute the double series coefficients.

To compute A_{mn}, for example, using double Fourier Series expansion in response to an input $u = P \cos x + Q \cos y$, one has

$$A_{mn} = \frac{\epsilon_m \epsilon_n}{4\pi^2} \int_{-\pi}^\pi \int_{-\pi}^\pi \cos mx \cos ny\ dx\ dy \left[\frac{1}{2\pi j} \int_C e^{s(P\cos x + Q\cos y)} F(s)\ ds \right]^\dagger$$

$$= \frac{\epsilon_m \epsilon_n}{8\pi^3 j} \int_C F(s)\ ds \int_{-\pi}^\pi e^{sP\cos x} \cos mx\ dx \int_{-\pi}^\pi e^{sQ\cos y} \cos ny\ dy.$$

---

† ϵ_m is the Neumann factor, defined as:

$$\epsilon_m = 1 \quad m = 0$$
$$\epsilon_m = 2 \quad m = 1, 2, \cdots .$$

Since

$$\frac{j^{-n}}{\pi} \int_0^\pi e^{jz \cos \alpha} \cos n\alpha \, d\alpha = J_n(z) \tag{20}$$

and letting $s = j\omega$, one obtains,

$$A_{mn} = \frac{\epsilon_m \epsilon_n}{2\pi} j^{m+n} \int_C F(j\omega) J_m(P\omega) J_n(Q\omega) \, d\omega \tag{21}$$

and the required coefficients are evaluated by contour integration.

The above result can readily be generalized. For example, where there is a dc bias of b units superimposed on the $P \cos x + Q \cos y$ in the input, (i.e., $u = b + P \cos x + Q \cos y$), the net result is to insert a factor $e^{jb\omega}$ under the integral of (21).

Inputs of the form $u = b + \sum_{i=1}^r P_i \cos x_i$ will result in coefficients of the form

$$A_{n_1, \cdots n_r} = \frac{\prod_{i=1}^r \epsilon_{n_1} j \exp \sum_{i=1}^r n_i}{\pi} \int_C e^{jb\omega} F(j\omega) \prod_{i=1}^r J_{n_1}(P_i\omega) \, d\omega \tag{22}$$

whenever $f(u)$ is Laplace transformable. The contour C is a function only of the nonlinear device, as may be expected. The Laplace transform of several ordinarily encountered ideal nonlinear devices, as well as their associated contour of integration C has been given in Rice[11] in his appendix 4A.

The nonlinear devices expressed as in (19) may be used fruitfully in certain investigation in noise problems. These are briefly described here. Reference may be made to Rice's classic papers of 1944 and 1945.[11]

For inputs that include narrowband noise, the input waveform will be of form

$$u = R \cos (\omega_m t + \theta) \qquad R \geq 0$$

where R and θ are functions of time whose variation is slow as compared to $\cos \omega_m t$. ($\omega_m/2\pi$ is approximately the midband frequency.)

The output $f(u)$ then is

$$f(u) = \frac{1}{2\pi} \int_C F(j\omega) \exp [j\omega R \cos (\omega_m t + \theta) \, d\omega].$$

By means of the relation

$$e^{jz \cos \varphi} = \sum_{n=0}^\infty \epsilon_n j^n \cos n\varphi J_n(z) \tag{23}$$

the equation above may be written:

$$f(u) = \sum_{n=0}^{\infty} A_n(R) \cos (n\omega_m t + n\theta) \qquad (24)$$

where

$$A_n(R) = \epsilon_n \frac{j^n}{2\pi} \int_C F(j\omega) J_n(\omega R) \ d\omega. \qquad (25)$$

In this representation, important conclusions may be reached concerning the properties of the output without undertaking laborious computations. For $A_n(R)$ whose variation is of the order of that of R, the output spectrum has bands which are centered at f_m, $2f_m \cdots$. A narrow-band filter centered about nf_m will then yield a slowly varying cosine wave with envelope $A_n(R)$. A narrow-band low-pass filter will yield the level $A_0(R)$.

In some cases the probability density function $P(R)$ of R is known. (For narrow-band Gaussian noise, for example, $P(R)$ is the Rayleigh distribution.) The probability density of the output envelope $A_n(R)$ is simply:

$$P[A_n(R)] = \frac{P(R)}{\left| \dfrac{dA_n(R)}{dR} \right|}. \qquad (26)$$

Another application in which the representation of (19) is useful is the calculation of the autocovariance function of the output of a zero-memory nonlinear device. From this the output power spectrum is found by taking the Fourier cosine transform.

The autocovariance function of the output is:

$$\Psi(\tau) = \lim_{T \to \infty} \frac{1}{T} \int_0^T f[u(t)] f[u(t + \tau)] \ dt . \qquad (27)$$

By (20):

$$\Psi(\tau) = \lim_{T \to \infty} \frac{1}{4\pi^2 T} \int_0^T \int_C F(j\omega_1) \exp [j\omega_1 u(t)] \ d\omega_1 \int_C F(j\omega_2)$$
$$\cdot \exp [j\omega_2 u(t + \tau)] \ d\omega_2 \ dt.$$

If an exchange of limits is justifiable, the above becomes

$$\Psi(\tau) = \frac{1}{4\pi^2} \int_C F(j\omega_1) \ d\omega_1 \int_C F(j\omega_2) \ d\omega_2$$
$$\cdot \left[\lim_{T \to \infty} \frac{1}{T} \int_0^T \exp [j\omega_1 u(t) + j\omega_2 u(t + \tau)] \ dt \right].$$

The quantity in the bracket is the (time) average value of

$$\exp j[\omega_1 u(t) + \omega_2 u(t + \tau)]$$

which, in the event that $u(t)$ satisfies the ergodic hypothesis, is equal to the characteristic function of the two variables $u(t)$ and $u(t + \tau)$. Denoting this quantity by $g(\omega_1, \omega_2, \tau)$, one has:

$$\Psi(\tau) = \frac{1}{4\pi^2} \int_C F(j\omega_1) \, d\omega_1 \int_C F(j\omega_2) g(\omega_1, \omega_2, \tau) \, d\omega_2. \qquad (28)$$

This gives an interesting approach to the computation of the output autocovariance function.

It is interesting to note, incidentally, that the characteristic function of $u(t) = P \cos pt$ is

$$J_0\big(P\sqrt{\omega_1^2 + \omega_2^2 + 2\omega_1\omega_2 \cos p\tau}\big),$$

and for

$$u(t) = P \cos pt + Q \cos qt$$

where p and q are incommensurable, the characteristic function is

$$J_0\big(P\sqrt{\omega_1^2 + \omega_2^2 + 2\omega_1\omega_2 \cos p\tau}\big) \times J_0\big(Q\sqrt{\omega_1^2 + \omega_2^2 + 2\omega_1\omega_2 \cos q\tau}\big).$$

Here, as elsewhere, one is limited by his ability to integrate. The autocovariance function, however, has been solved for particular nonlinear characteristics, for example, the square-law device.

IV. NUMERICAL SOLUTIONS AND BENNETT FUNCTIONS

Since it has not yet been found possible to express the modulation coefficients in a more general case in terms of known functions, it is often necessary to resort to numerical computations. The numerical approaches have been tackled by Sternberg, Kaufman, Feuerstein, Shipman, among others.[13-19] Some of their results have been tabulated and a class of generalized functions encountered in these investigations are christened Bennett functions.[14]

The original approach of Sternberg and Kaufman is along the lines of direct integration, summarized below.

If the output $f(u)$ can be expressed in the form of a continuous $N + 1$-sided polygonal function over a closed interval $-a \leq u \leq a$, i.e.,

$$f(u) = f(-a) + \sum_{i=1}^{N} g_i U_{-2}(u - u_i) \quad i = 1, \cdots N \qquad (29)$$

where u_i and g_i are constants, u_i being the "break-points" of the polygo-

nal function

$$-a \leqq u_1 < u_2 < u_3 \cdots u_N < a \tag{30}$$

and $U_{-2}(u - u_i)$ are unit ramp functions:

$$U_{-2}(u - u_i) = 0 \qquad u < u_i$$

$$U_{-2}(u - u_i) = u - u_i \qquad u \geqq u_i \qquad (i = 1, 2 \cdots N). \tag{31}$$

If the input is of form $u = P \cos x + Q \cos y$, one can confine his attention piecewise to N functions of the type

$$f_i(x,y) = f(P \cos x + Q \cos y; u_i) \qquad i = 1, 2 \cdots N. \tag{32}$$

The over-all function is then

$$f(x,y) = f(-a) + \sum_{i=1}^{N} g_i f_i(x,y). \tag{33}$$

Factoring out P in each term, and introducing parameters $h_i = u_i/P$, $k = Q/P$, we express $f_i(x,y)$ as the double Fourier series:

$$f_i(x,y) = \tfrac{1}{2} P A_{00}(h_i,k) + P \sum_{m,n=0}^{\infty *} A_{\pm mn}(h_i,k) \cos (mx \pm ny) \dagger \tag{34}$$

where

$$A_{\pm mn}(h_i,k) = \frac{1}{2\pi^2 P} \int_{-\pi}^{\pi} \int_{-\pi}^{\pi} f_i(x,y) \cos (mx \pm ny) \, dx \, dy,$$

$$m,n = 0, 1, 2 \cdots ; i = 1, 2 \cdots N$$

and for $f(x,y)$ we carry out another expansion:

$$f(x,y) = \tfrac{1}{2} C_{00} + \sum_{m,n=0}^{\infty *} C_{\pm mn} \cos (mx \pm ny). \tag{35}$$

The C's and the A's are then related by

$$\tfrac{1}{2} C_{00} = f(-a) + \tfrac{1}{2} P \sum_{i=1}^{N} g_i A_{00}(h_i,k) \tag{36}$$

$$C_{\pm mn} = P \sum_{i=1}^{N} g_i A_{\pm mn}(h_i, k).$$

As $A_{+mn}(h_i,k) = A_{-mn}(h_i,k)$ for all m and n, the $\pm$ sign can be dropped.

---

† $\sum_{m,n=0}^{\infty *}$ denotes a summation without the A_{00} term; in addition, terms whose index is such that $m \cdot n = 0$ are to be weighed by a factor of $\tfrac{1}{2}$.

By considering the function

$$f_i(x,y) = \begin{cases} P(\cos x + k \cos y - h_i); & \cos x + k \cos y \geqq h_i \\ 0 & \cos x + k \cos y < h_i \\ & i = 1, 2 \cdots N \end{cases}$$

the zones over which integration for the evaluation of A_{mn} must be carried out is seen to be bounded by the curve

$$\cos x + k \cos y = h; \quad h = h_i$$

over the closed square

$$R_0 : \begin{cases} -\pi \leqq x \leqq \pi \\ -\pi \leqq y \leqq \pi. \end{cases}$$

Five cases need to be considered; two are degenerate:

$$\text{(d1)} \quad 1 + k \quad \leqq h$$

$$\text{(d2)} \quad -(k + 1) \geqq h$$

In the first instance the integrand vanishes everywhere except possibly over a set of zero measure, and hence the coefficients are identically zero. In the second instance the integration is to be carried out throughout the zone (excepting possibly a set of zero measure), which means the output is the same as the input except for a constant multiplying factor.

The three nondegenerate cases are:

$$\text{(}i\text{)} \quad h < 1 + k, \quad \text{or}$$

$$h > 1 - k.$$

The integral here is to be carried out over a zone R of the x,y plane bounded by a closed curve lying wholly within R_0.

$$\text{(}ii\text{)} \quad h \geqq k - 1, \quad \text{or}$$

$$h \leqq 1 - k$$

The integral here is to be carried out over a zone R bounded by two open curves (i.e., two opposite segments of the boundary of R also constitute the boundary of R_0).

$$\text{(}iii\text{)} \quad h < k - 1, \quad \text{or}$$

$$h > -(k + 1)$$

The area of integration is bounded by four open curves. The integra-

tion can thus be carried out for these nondegenerate cases by formulas of the type:

$$A_{mn}(h,k) = \frac{2}{\pi^2} \int_{R_1} \left[\int (\cos x + k \cos y - h) \cos mx \, dx \right] \cos ny \, dy$$

$$+ \frac{2}{\pi^2} \int_{R_2} \left[\int (\cos x + k \cos y - h) \cos mx \, dx \right] \cos ny \, dy$$

$$m, n = 0, 1, 2 \cdots$$

$$A_{mn}(h,k) = \frac{2}{\pi^2} \int_{R_3} \left[\int (\cos x + k \cos y - h) \cos ny \, dy \right] \cos mx \, dx$$

$$+ \frac{2}{\pi^2} \int_{R_4} \left[\int (\cos x + k \cos y - h) \cos ny \, dy \right] \cos mx \, dx$$

$$m, n = 0, 1, 2 \cdots$$

where R_1, R_2, R_3, R_4 are zones appropriate for each of the cases.

It is seen that the inner integrals can be performed, after which suitable manipulation will yield a set of recurrence relationship first derived by Rice.[20] Except for misprints, they are:

$$(m - n + 3)A_{m+1,n-1} \equiv -(m + n - 3)A_{m-1,n-1} + 2mhA_{m,n-1}$$

$$- 2mkA_{mn} \qquad m,n \geq 1$$

$$(m + n + 1)A_{mn} \equiv -(m - n - 3)A_{m-2,n} - 2(m - 1)kA_{m-1,n-1}$$

$$+ 2(m - 1)hA_{m-1,n} \qquad m \geq 2, n \geq 1$$

$$(n + m + 1)A_{mn} \equiv -(n - m - 3)A_{m,n-2}$$

$$- 2(n - 1)\frac{1}{k} A_{m-1,n-1} + 2(n - 1)\frac{h}{k} A_{m,n-1}$$

$$m \geq 1, n \geq 2$$

$$(n - m + 3)A_{m-1,n+1} \equiv -(n + m - 3)A_{m-1,n-1}$$

$$+ 2n\frac{h}{k} A_{m-1,n} - 2n\frac{1}{k} A_{mn} \qquad m,n \geq 1.$$

(37)

With the aid of these relationships, the higher-order coefficients can be expressed in terms of the first four coefficients $A_{00}(h,k)$, $A_{10}(h,k)$, $A_{01}(h,k)$ and $A_{11}(h,k)$.

For cases such as the ideal limiter, the antisymmetric condition

$f(-u) = -f(u)$ is observed; u_i are now symmetric and the "gains" g_i are antisymmetric. Here:

$$A_{00}(-h,k) \equiv A_{00}(h,k) + 2h$$

$$A_{10}(-h,k) \equiv 1 - A_{10}(h,k)$$

$$A_{01}(-h,k) \equiv k - A_{01}(h,k)$$

$$A_{mn}(-h,k) \equiv (-1)^{m+n}A_{mn}(h,k) \qquad (m + n > 1).$$

(38)

The function $A_{mn}(h,k)$ are called by Sternberg the Bennett functions of multiplicity two and order m,n. In part II of Sternberg's paper,[14] the functions $A_{00}(h,k)$, $A_{10}(h,k)$, $A_{01}(h,k)$ and $A_{11}(h,k)$, have been tabulated for h between -2 and $+2$ in 0.2 steps and k with values of 0.001, 0.01, 0.1 and 1.0. The values $A_{20}(h,k)$, $A_{02}(h,k)$, $A_{30}(h,k)$, $A_{21}(h,k)$. $A_{12}(h,k)$, $A_{03}(h,k)$ are tabulated for k of 0.1 and 1.0. All values are tabulated to six decimal places. The accuracy of the first set of tables is held to be to one unit in the last place, while for the second set the accuracy is about three units in the last place.

The above approach is extendable to devices with continuous and smooth characteristics if it can be approximated in a piece-wise linear form. As long as the characteristic may be approximated to within a pre-chosen $\epsilon > 0$ uniformly on the interval $-a \leq u \leq a$ by

$$S(u,\epsilon) = f(-a) + \sum_{i=1}^{N(\epsilon)} g_i U_{-2}(u - u_i), \qquad (39)$$

Sternberg and Kaufman show that the approximate modulation product amplitudes computed as per (33), (34) and (35) will not differ from the true values by more than $4\epsilon/\pi$ in all cases, and the output will be within ϵ of the true value for all time if it is obtained by summing over the approximate expansions.

For a symmetrical ideal limiter

$$f(u) = \begin{cases} -gu_0 & u \leq -u_0 \\ gu & -u_0 < u \leq u_0 \\ gu_0 & u \geq u_0 \end{cases} \qquad 0 < u_0 < 2P, g > 0.$$

The approaches described above can be applied to the range

$$-a \leq x \leq a$$

$$a \geq 2P.$$

Sternberg, in part II of his paper,[14] gives the results relating the coefficients C_{mn} and A_{mn} as:

$$C_{\pm mn} = 0 \qquad\qquad m + n = 0, 2, 4 \cdots \qquad (40\text{a})$$

$$C_{10} = Pg[1 - 2A_{10}(h,k)] \qquad\qquad (40\text{b})$$

$$C_{01} = Pg[k - 2A_{01}(h,k)] \qquad\qquad (40\text{c})$$

$$C_{\pm mn} = -2PgA_{mn}(h,k) \qquad m + n = 3, 5, 7, \cdots. \qquad (40\text{d})$$

Here $H = u_0/P$, $k = Q/P$ and input are in the form

$$u(t) = P \cos (pt + \theta p) + Q \cos (qi + \theta q)$$
$$0 < P < P + Q \leqq 2P.$$

In Ref. 17, Bennett functions of the νth kind, denoted $A_{mn}^{(\nu)}(k)$, are defined. These are the coefficients for the output of a νth law rectifying function in response to a two-frequency input. ν is usually taken to be an integer. $A_{mn}^{(\nu)}(k)$ for $\nu = 1, 2$ have been tabulated.[17] Bennett functions of a given kind can be obtained from those of the lower kinds by means of recursion formulas.

By extending the above, Bennett functions with multiplicities of three or higher (i.e., modulation coefficients when the input has three or more distinct frequency components) can readily be defined. For input of the form

$$u(t) = P(\cos x + k_1 \cos y + k_2 \cos z) \qquad (41)$$

for example, the output from a piece-wise linear nonlinear element can be expressed in terms of the Bennett functions of the first kind,

$$A_{mnl}(h, k_1, k_2), \qquad h = \frac{u_0}{P}$$

where, as before, u_0 is the breakpoint for an individual segment. Similarly, for a νth law rectifier subjected to inputs of the form (41), Bennett functions of the νth kind

$$A_{mnl}^{(\nu)}(h, k_1, k_2)$$

can be defined.

A number of interesting relations have been derived for the three frequency Bennett functions of the νth kind.[19] These include recurrence relations and integrals linking three-frequency Bennett functions with two-frequency ones. No tabulation of the three or more frequency Bennett functions is known to have been attempted.

Relationships between the "Fourier" representation and the "Laplace" representations for nonlinear characteristics have also been revealed by Feuerstein.[18] He has shown that, in many cases, the contour integration in the "Laplace" formulation can be reduced to integrals

over the infinite real line. The results are generalized Weber-Schafheitlin integrals of the form (16) and (17). This is perhaps not a surprising result from intuitive grounds.

It is interesting to note, however, that for a ν-law rectifier, the Bennett function of the νth kind of arbitrary multiplicity is given by

$$A_{m_0}{}^{(\nu)}{}_{,\ldots m_N}(h,k_1, \cdots, k_N) = \nu! j^{M-\nu-1} \frac{2}{\pi} \int_0^\infty \lambda^{-(\nu+1)} \cos \lambda h$$

$$\cdot \prod_{i=0}^N J_{m_i}(k_i\lambda) \, d\lambda$$

<div align="center">

for ν integer,   (42a)

$M \geqq \nu + 1$, and

$M + \nu$ odd,

</div>

and

$$A_{m_0}{}^{(\nu)}{}_{,\ldots m_N}(h,k_1, \cdots, k_N) = \nu! j^{M-\nu-2} \frac{2}{\pi} \int_0^\infty \lambda^{-(\nu+1)}$$

$$\cdot \sin \lambda h \prod_{i=0}^N J_{m_i}(k_i\lambda) \, d\lambda$$

(42b)

<div align="center">

for ν integer,

$M \geqq \nu$, and

$M + \nu$ even,

where $M = \sum_{i=0}^N m_i$ and $k_0 = 1 \geqq k_i$.

</div>

By these formulas, the generalized integrals of (17) are related directly to Bennett functions.

Feuerstein in fact did not stop with the considerations of integer ν. The formulas of the Bennett functions of the νth kind, with noninteger ν and with M taking in values other than those shown above, are related to the generalized integrals of (17), though in a more complicated form.

V. ACKNOWLEDGMENT

REFERENCES

1. Bennett, W. R., and Rice, S. O., Note on Methods of Computing Modulation Products, Philosophical Magazine, **18**, 1934, pp. 422–424.

2. Bennett, W. R., New Results in the Calculation of Modulation Products, B.S.T.J., **12**, April, 1933, pp. 228–243.
3. MacColl, L. A., *Fundamental Theory of Servomechanisms*, Van Nostrand, 1945, p. 80.
4. West, J. C., Douce, J. L., and Livesley, R. K., The Dual Input Describing Function and Its Use in the Analysis of Nonlinear Feedback Systems, Proc. I.E.E., **103B**, 1956, pp. 463–474.
5. Bonenn, Ze'ev, Frequency Response of Feedback Relay Amplifiers, Proc. I.E.E. **108B**, 1961, pp. 287–295.
6. Gibson, J. E., and Sridhar, R., A New Dual-Input Describing Function and an Application to the Stability of Forced Nonlinear Systems, paper delivered at the Joint Automatic Control Conference, June 27–29, 1962, New York University.
7. Hobson, E. W., *The Theory of Functions of a Real Variable*, **2,** Dover Publications, pp. 698–719.
8. Watson, G. N., *Theory of Bessel Functions*, Cambridge University Press, 1948, pp. 20–21, 398–406.
9. Magnus, W., and Oberhettinger, F., *Formulas and Theorems for the Functions of Mathematical Physics*, Chelsea, 1954, p. 35.
10. Tsien, H. S., *Engineering Cybernetics*, McGraw-Hill, 1954, p. 77.
11. Rice, S. O., Mathematical Analysis of Random Noise, B.S.T.J., **23**, July, 1944, pp. 282–332; B.S.T.J., **24**, Jan., 1945, pp. 46–156. Also found in Wax, N., Editor, *Selected Papers on Noise and Stochastic Processes*, Dover Publications, pp. 133-294.
12. Davenport, W. B., Jr., and Root, W. L., *An Introduction to the Theory of Random Signals and Noise*, McGraw-Hill, 1958, pp. 277–308.
13. Sternberg, R. L., and Kaufman, H., A General Solution of the Two-Frequency Modulation Product Problem, I, J., Math. and Phys., **32**, 1953, pp. 233–242.
14. Sternberg, R. L., A General Solution of the Two-Frequency Modulation Product Problem, II, III, J. Math and Phys., **33**, 1954, pp. 68–79, 199–206.
15. Kaufman, H., Harmonic Distortion in Power Law Devices, Math. Mag., **28,** 1955, pp. 245–250.
16. Sternberg, R. L., Shipman, J. S., and Thurston, W. B., Tables of Bennett Functions for Two-Frequency Modulation Product Problems for the Half-Wave Linear Rectifier, Quart. J. Mech. Appl. Math., **7**, 1954, pp. 505–511.
17. Sternberg, R. L., Shipman, J. S., Kaufman, H., Tables of Bennett Functions for the Two-Frequency Modulation Product Problem for the Half-Wave Square Law Rectifier, Quart. J. Mech. and Appl. Math., **8**, 1955, pp. 457–462.
18. Feuerstein, E., Intermodulation Products for ν-Law Biased Wave Rectifier for Multiple Frequency Input, Quart. Appl. Math., **15**, 1957, pp. 183–192.
19. Sternberg, R. L., Shipman, J. E., and Zohn, S. R., Multiple Fourier Analysis in Rectifier Problems, Quart. Appl. Math., **16**, 1959, pp. 335–359.
20. Bennett, W. R., The Biased Ideal Rectifier, B.S.T.J., **26**, Jan., 1947, pp. 139–169.
21. Bennett, W. R., Note on Relations between Elliptic Integrals and Schlömilch Series, Bull. Am. Math. Soc., **38**, Dec., 1932, pp. 843–848.
22. Kalb, R. M., and Bennett, W. R., Ferromagnetic Distortion of a Two-Frequency Wave, B.S.T.J., **14**, Apr., 1935, pp. 322–359.
23. Middleton, D., The Response of Biased, Saturated Linear and Quadratic Rectifiers to Random Noise, Jour. Appl. Phys., **17**, 1946, pp. 778–801.
24. Middleton, D., Some General Results in the Theory of Noise Through Nonlinear Devices, Quart. Appl. Math., **5**, 1948, pp. 445–498.
25. Lampard, D. G., Harmonic and Intermodulation Distortion in "Power Law" Devices, Proc. I.E.E., Pt. IV, **100**, 1953, pp. 3–6.
26. Shipmen, J. S., On Middleton's Paper "Some General Results in the Theory of Noise Through Nonlinear Devices," Quart. Appl. Math., **18**, 1955, pp. 200–201.
27. Gelb, Arthur, The Dynamic Input-Output Analysis of Limit Cycling Control Systems, paper delivered at the Joint Automatic Control Conference, June 27–29, 1962, New York University.

The Solid-State Receiver in the TL Radio System

By W. E. BALLENTINE, V. R. SAARI, and F. J. WITT

The availability of reliable high-frequency solid-state devices and the application of new circuit concepts have made possible the development of completely solid-state IF and baseband circuits for the TL microwave radio system. These include (1) a 70-mc IF amplifier with 20-mc 3-db bandwidth, 105 db of gain, and 60 db of automatic gain control, (2) a remodulation-type limiter, (3) discriminator, automatic frequency control, and squelch circuits, and (4) two 6-mc baseband feedback amplifiers. All circuits have been designed to operate over a temperature range of at least −20°C to +60°C. It has been demonstrated that electrical performance comparable to or better than that obtained with electron tube circuits may be achieved while gaining considerably in power drain and reliability. The new circuit techniques and the design considerations which led to their development are presented.

I. INTRODUCTION

When the junction transistor was first announced, it was apparent to many that it would eventually replace the electron tube as an active element in many communications systems. Its small size, low power drain, ruggedness, reliability, and potentially low cost all contribute to its widespread usefulness in the development of new electronic circuits and in the redesign of existing apparatus. The growth in diversity of applications is directly related to the properties of the devices which become available or can be made available in production quantities. This article reports on another step in this expansion — solid-state circuits for a wideband microwave communications system. The development of this new system became both technically feasible and economically practical when diffused-base transistors with excellent high-frequency performance and reliability became available in large quantities at low cost.

Although improvements in device capabilities were very important, the success of the development described herein is due also to the application of new circuit design concepts which differ considerably from conventional electron tube circuit design practice. These innovations and their supporting philosophy will be discussed.

The TL radio relay system as a whole will be described in another article.[1] That article should be consulted for an over-all system description and for the results of early field applications. The present article is restricted to a description of the IF and baseband circuits.

II. TL IF AND BASEBAND CIRCUITS

2.1 *General Description*

A simplified block diagram of the TL receiver is shown in Fig. 1. Let it be mentioned that, in the entire radio system, the only nonsolid-state components are the beating oscillator and transmitting klystrons. Attention in this article is directed to the solid-state circuits which are enclosed by a dashed line in Fig. 1. The IF signal is amplified by the IF
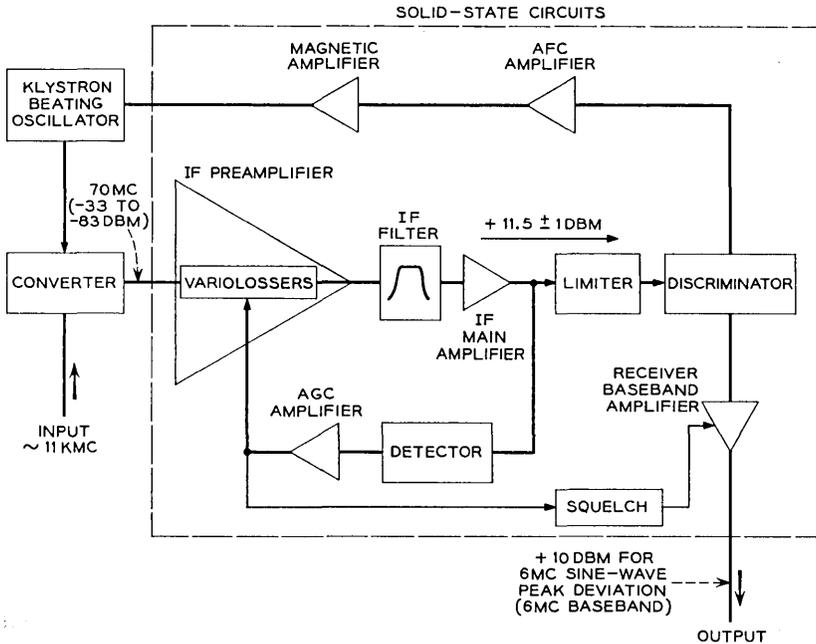

Fig. 1 — Simplified block diagram of wideband FM receiver.

preamplifier and IF main amplifier. A passive filter located between these amplifiers limits the bandwidth. AM noise and an AM component arising from FM-to-AM conversion in the IF amplifiers are suppressed by the limiter. Baseband intelligence is detected in the discriminator. The resulting signal is amplified in the receiver baseband amplifier and is then applied to the transmitter at a repeater or delivered to appropriate terminal equipment. In the transmitter, baseband signals are amplified by the transmitter baseband amplifier (a transistor circuit not shown in Fig. 1). This amplifier drives the repeller electrode of the transmitting klystron.

Three other circuits are included in the receiver: (1) an automatic gain control (AGC) circuit which adjusts the gain of the IF preamplifier to compensate for variations in received signal level; (2) an automatic frequency control (AFC) circuit which controls the voltage on the repeller electrode of the beating oscillator klystron, adjusting its oscillating frequency in such a way as to keep the IF carrier frequency centered in the IF passband; and (3) a squelch circuit which prevents noise from feeding through the receiver during abnormal fades or periods of absence of the incoming carrier.

Fig. 2 is a photograph of the IF and baseband circuits, except for the transmitter baseband amplifier. The four compartments, from bottom to top, contain (1) the IF preamplifier; (2) the passive filter; (3) the IF main and AGC amplifiers; and (4) the squelch circuit, transistor AFC amplifier, limiter, discriminator, and receiver baseband amplifier.
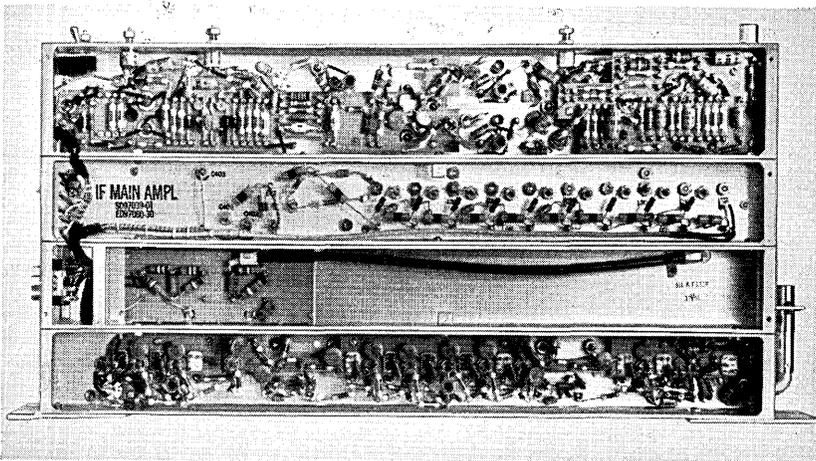

Fig. 2 — IF and baseband circuits.

The transmitter baseband amplifier is packaged separately and is shown in Fig. 3.

2.2 *Some Departures from Conventional Design Philosophy*

2.2.1 *IF Amplifiers and Automatic Gain Control*

In order to utilize the microwave medium efficiently, it is necessary to have a wide IF band which is precisely positioned and defined. In the usual wideband electron tube IF amplifier, the passive interstage coupling networks define the IF band. Variable dc bias can be applied to the tubes to change the gain electronically for AGC without changing the normalized frequency response. This convenient property is due to the fact that the principal band-limiting mechanisms in electron tube IF amplifier circuits — namely, the input and output capacitances — are not strongly bias-dependent. Lossless interstage networks are designed to include these capacitances as elements, and gain-bandwidth product is preserved.
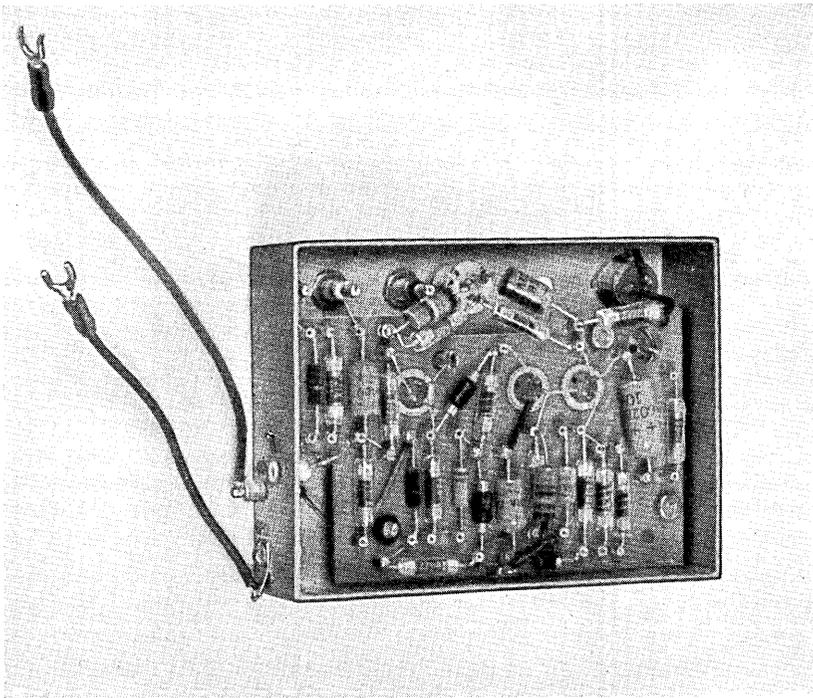

Fig. 3 — Transmitter baseband amplifier.

2.2.1.1 *Inherent Transistor Characteristics.* Certain inherent charac-
teristics of transistors dictate a departure from the conventional electron
tube approach.* These characteristics are listed below:

A. The principal mechanism which causes the gain of a transistor
amplifier to fall off at high frequencies is transit time — i.e., the finite
time it takes minority carriers in the base region to complete their
journey from emitter to collector. (This effect occurs in electron tubes,
but it has only secondary importance up to 100 mc for electron tubes
used in IF service.)

B. Not only are the input and output impedances quite frequency-
dependent, but they also depend on the dc bias and on the gain of the
transistor. Hence, it is generally not possible to design interstage band-
limiting coupling networks which would be satisfactory for a wide range
of transistors and dc operating points.

C. A transistor stage exhibits both forward and reverse transmission;
hence, the input impedance depends on the load impedance, and the
output impedance depends on the generator impedance.

D. A transistor IF amplifier using presently available diffused-base
transistors has a wider inherent bandwidth capability than a conven-
tional electron tube IF amplifier.

2.2.1.2 *Design Considerations.* Some design considerations for transistor
wideband IF amplifiers are stated below. These follow rather naturally
from the characteristics listed above.

A. For wideband applications, the transistor amplifier configuration
should be a low-pass rather than a bandpass structure.† Useful low-
pass configurations are discussed in the Appendix. The cutoff frequency
of the low-pass amplifier is above the upper edge of the IF band, and
the over-all IF characteristic is determined by imbedding a passive
bandpass filter in the cascade of IF stages. The transistor amplifier
stage has a sufficiently large inherent bandwidth to make this technique
practical. Because transit-time effect is the primary cause of gain
rolloff at high frequencies, extending the bandwidth on the low side
does not reduce the gain obtained in the ultimate band.

By using a low-pass configuration, envelope delay distortion, a pri-
mary limitation in FM systems, is minimized; and the small amount
present is of such a nature that it is easily equalized. A low-pass tran-

---

* It is assumed in the following discussion that the IF band falls between the
beta and alpha cutoff frequencies of the transistor. This condition is satisfied for
the TL radio IF amplifiers.

† This does not mean low-pass in the strictest sense; i.e., the amplifier chain
need not pass dc. By low-pass is meant that the frequency rolloff above the IF
band is determined by a low-pass structure.

sistor wideband IF amplifier has proven to be far superior to an elec-
tron tube IF amplifier from the standpoint of envelope delay distortion.

A further advantage of the use of the low-pass configuration is that
adjustment is greatly simplified, because the IF band is a small part
of the passband of the active circuits. Also, a wide range of transistor
parameters can be tolerated.

The passive bandpass filter, which may include a simple envelope
delay equalizer, can be adjusted prior to installation in the IF system
if the IF amplifier is designed to present controlled terminating impe-
dances for the filter. The position of the passive bandpass filter should
be near enough to the output of the amplifier to prevent out-of-band
noise, originating in the IF stages following the filter, from contributing
appreciable noise power at the IF output. On the other hand, it must
be near enough to the IF amplifier input to prevent intermodulation
of out-of-band noise from occurring during weak signal conditions.

B. To obtain a low receiver noise figure, the IF amplifier input tran-
sistor stages should be designed to utilize as much available power gain
as possible while, of course, taking into account such factors as stability
and input impedance. This technique will minimize the effect of the
noise figures of the second and third stages on the over-all noise figure.
The undesirable departure from the ideal "flat" transmission charac-
teristic, which is inherent in obtaining high gain, can be compensated
with an equalizer network following the second or third stage. See the
Appendix for a discussion of the "doublet circuit," which uses this
principle.

C. The gain variation of the IF amplifier for AGC purposes should
be achieved by using separate wideband variolossers. As in the TL
system, these may employ semiconductor diodes. This is a departure
from the standard technique of varying the gain by changing the dc
bias on the amplifier stages. Generally, an intolerable amount of change
in the normalized IF transmission characteristic will result if the latter
method of gain control is used. The wideband variolossers are passive
attenuator networks whose IF transconductances are controlled by the
direct current flowing through them. Variolossers can be designed so
that the normalized IF transmission characteristic changes only slightly
over a wide range of loss settings. The required loss range (60 db for
the TL system) must generally be split up between two or more vario-
lossers. The number of variolossers used and their position in the IF
chain must be chosen carefully in accordance with the system require-
ments and the limitations of the variolossers. The maximum IF input
level to the variolossers must be restricted so that the diodes remain

reasonably linear; otherwise, undesirable IF transmission characteristic changes and excessive AM-to-PM conversion will result. However, the loss must not be allowed to accumulate too close to the input end of the amplifier; otherwise, the system noise figure under strong signal conditions will be unnecessarily high.

As illustration, consider what happens as the input carrier level increases: The automatic gain control system will increase the loss in the variolossers in order to hold the IF amplifier output level constant. Because of this increased variolosser loss, and because of the noise generated in the IF amplifier stages which follow the variolossers, the receiver noise figure will increase. Of course, the IF output signal-to-noise ratio is also increased and a better output signal is obtained. However, the receivers spend most of the time operating under strong signal conditions, so the strong signal S/N ratio (which varies inversely with noise figure) must be kept considerably better than that allowed during localized deep signal fades.* It is important, therefore, to use enough variolossers and to locate them properly in the IF amplifier chain.

It is good design practice to have the passive bandpass filter located between the last variolosser and the output of the IF amplifier to prevent any spurious out-of-band distortion products that might be generated in the variolossers during strong signal conditions from being remodulated into the desired band in a later part of the amplifier.

2.2.2 *Limiter*

The conventional technique for suppressing the AM component of modulation on the IF amplifier output signal is to pass the signal through one or more amplitude limiters. In recent years, these limiters have taken the form of clippers containing semiconductor diodes. When more than one limiter is used, it is necessary to provide buffering amplifiers between them in order to achieve adequate limiting action. Ruthroff[2] has pointed out that this process is inefficient, and he has proposed an improved circuit which has been called *the remodulation limiter*. This circuit derives its efficiency from the fact that it senses the AM present on the incoming IF waveform and then amplitude modulates this IF signal in such a way that the original AM is canceled. A version of a particular form of the remodulation limiter is described in more

---

* The requirement on strong signal noise figure is based on the cumulative effects of noise in a multihop system, and it is therefore related to the number of hops. On the other hand, the weak signal noise figure requirement is relatively independent of the number of hops because of the localized nature of deep fades.

detail later in this paper. Whereas the clipper-type of circuit typically requires four diodes and two transistor-amplifying stages for 25 db of AM index suppression, a remodulation limiter with equivalent performance contains just two diodes.

2.2.3 *Automatic Frequency Control*

The receiver AFC circuit* in the TL radio system is conventional insofar as it provides a negative feedback loop which centers the IF signal in the IF passband. The klystron-beating oscillator frequency is controlled by an error signal which is sensed at the discriminator, amplified, and impressed on the klystron repeller. The part of the feedback loop between the discriminator and the klystron repeller must necessarily be direct-coupled; other considerations dictate that the repeller voltage be a high negative voltage, about -500 volts. The problem of direct-coupling the transistor circuits, which operate near zero volts, to the klystron repeller has been overcome by the use of a magnetic amplifier (magamp). The magamp serves to completely isolate the low- and high-voltage circuits while effectively maintaining direct coupling and adding to the AFC feedback loop gain.

2.3 *Circuit Description*

2.3.1 *IF Amplifiers*

2.3.1.1 *IF Preamplifier*. The input circuit of the IF preamplifier (Fig. 4) consists of a pair of direct-coupled common-emitter stages followed by a high-pass filter. The principal advantage of this combination, which is called a "doublet," is that it yields the best noise figure of the various circuits investigated† as well as an acceptable input return loss. The remaining stages of IF amplification consist of wideband common-base, transformer-coupled circuits. To obtain good transistor interchangeability and insensitivity to temperature change, the stages are padded and mismatched, resulting in a power gain for each common-base stage of about 6 db. Two diode attenuator networks, the variolossers, are included in the preamplifier, dividing it into three approximately equal gain segments. Their placement is such that they have a negligible (<0.1

---

* Transmitter AFC is not required in the TL radio system because of the specially designed klystron and klystron cooling system.[3]

† Circuits investigated included the common-base stage with a wideband transformer interstage network, the doublet circuit, and the common-emitter stage with frequency-dependent shunt feedback. These configurations are compared in the Appendix.
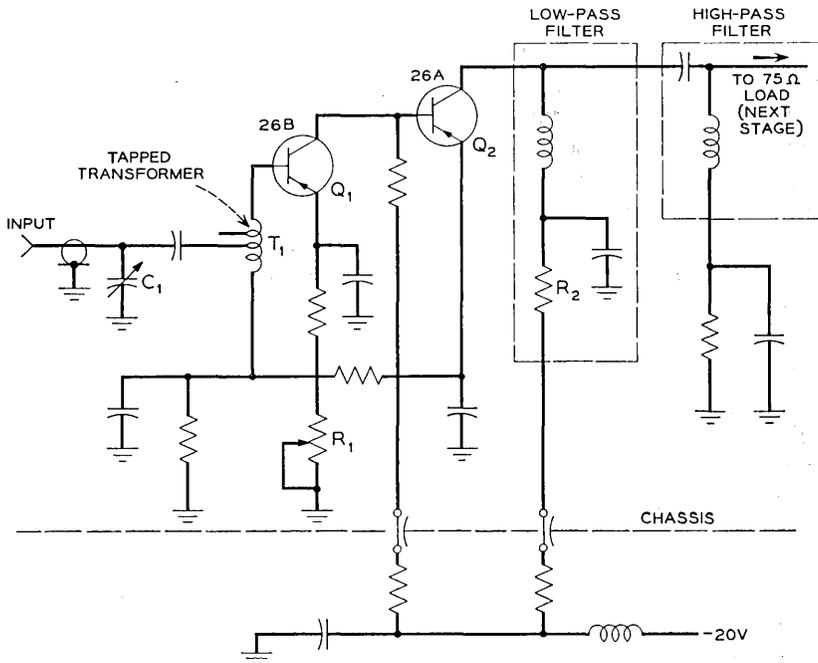
Fig. 4 — Low-noise input section.

db) effect on the noise figure under weak-signal conditions and remain sufficiently linear under strong-signal conditions. The preamplifier maximum gain is adjusted at room temperature to 57 db, flat between 64 and 76 mc within about ±0.2 db.

Input return loss adjustments are applied in the form of potentiometer R_1 (which varies the bias current in transistor Q_1), taps on transformer T_1, and variable capacitor C_1 (Fig. 4).

The two common-emitter stages of the doublet exhibit a downward transmission slope approaching 12 db per octave in the IF band; the high-pass filter, which has a cutoff at approximately 100 mc, equalizes this rolloff. This combination yields a very good noise figure because the available power gain provided between the preamplifier input jack and the input of transistor Q_2 is relatively large, thus minimizing the influence of the second transistor on the over-all noise figure. The constant resistive load for transistor Q_2 consists of a high-pass network and a low-pass network, which have complementary input impedances. Resistor R_2 is the termination for the low-pass network, and the third transistor stage terminates the high-pass network.

A diagram of a typical common-base stage is shown in Fig. 5. In this configuration, the transistor has a current gain slightly less than unity in the IF band. The interstage transformer, which is a ferrite-core distributed autotransformer,[4,5,6] provides a current step-up ratio of approximately 1:2, making the over-all power gain slightly less than 6 db per stage. Since a transistor of the type used is capable of providing a maximum unilateral gain of about 15 db at 80 mc, there is evidently a considerable sacrifice of gain in order to obtain a high degree of stability and transistor interchangeability. The slope of the gain-frequency characteristic in the IF band can be adjusted by changing the damping resistor R_2, which is introduced to control gain peaking at higher frequencies. (Also, a variable inductor is added in the base lead of some of the stages to provide a small, continuous, additional slope adjustment.)

Fig. 6 indicates the make-up of the complete preamplifier. Potentiometer R_4 is a gain control having 16 db range. Used to adjust the over-all IF amplifier gain to 105 db, it does not unduly affect the good output return loss of the preamplifier. (A good termination is needed for proper filter operation.)

2.3.1.2 *Variolossers.* Two variable-loss pi networks of germanium point-contact diodes are included in the preamplifier (Fig. 6) to maintain a constant level out of the main amplifier. The input levels from the converter may vary from about -33 dbm to less than -83 dbm. Each variolosser is able to insert from 1 to 30 db of flat loss over the IF band. This loss range, greater than that required to correct for IF input level variations, allows for temperature and aging effects on the gain of the amplifier.

The impedance of each variolosser diode to signal frequencies is

TYPICAL VALUES:

$R_1 = 825$, $R_2 = 464$, $R_3 = 2150$

$R_4 = 1780$, $R_5 = 10$, $L_1 = 7$

$C_1 = 0.0005$, $C_2 = 0.005$, $C_3 = 0.001$, $C_4 = 1$

RESISTANCE IN OHMS

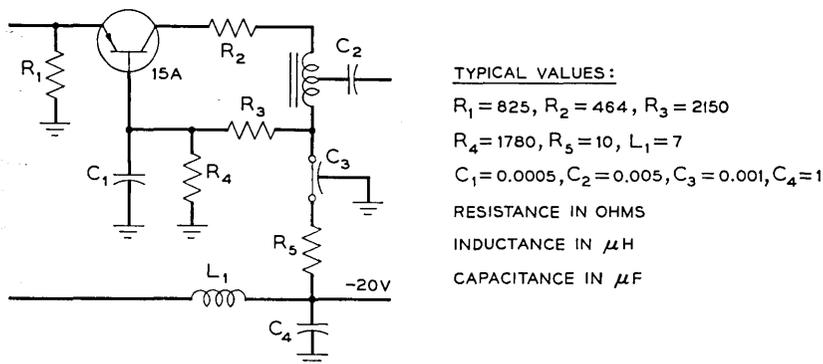INDUCTANCE IN μH

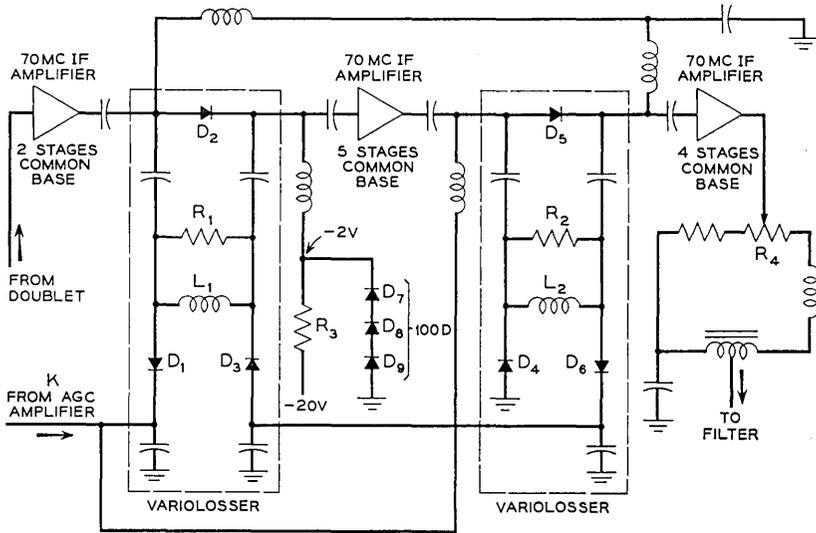CAPACITANCE IN μF

Fig. 5 — Typical common-base stage.

Fig. 6 — Gain control circuits in the preamplifier.

controlled by the direct current passing through it. Direct current is caused to flow in such a manner that as the current increases in the shunt diodes, it decreases in the series diodes (and vice versa). Since the diodes appear in pi networks at IF, variable loss is obtained without producing much variation of the input and output impedances of the variolossers. The currents are controlled by the output of the AGC amplifier (see Fig. 8 below), which responds to amplitude-modulation frequencies ranging from dc up to about 50 cps. Diodes D_7, D_8 and D_9 are used as a -2.0-volt dc supply and are forward-biased through resistor R_3. (These diodes become starved of current under fade conditions, and the reduced voltage ensures a low minimum IF loss in the variolossers.) The series and shunt diode sets are connected in parallel for incremental currents supplied from the K lead; but the -2.0-volt source is placed within a loop passing through all six attenuator diodes, thus providing a condition wherein their dynamic resistances can simultaneously equal about 130 ohms. This condition occurs when the input dc lead from the AGC amplifier carries no current, and it corresponds to a medium loss condition in the variolossers. The two variolossers are so interconnected that they conduct the same dc currents, thereby forcing their loss values to track together. Inductors L_1 and L_2 carry control current and also counteract the effect of the series-diode capacitance, which is important when the diode resistances reach their

highest level. Resistors R_1 and R_2 provide an upper limit for the series path impedance, thereby forcing the shunt diodes to carry more of the loss burden at higher IF input signal levels.

A network containing a thermistor applies a temperature-dependent bias voltage in series with the shunt diodes of the variolossers. The effect is to equalize the drift which tends to occur in the AGC amplifier output current, and thus to prevent drift in the squelch firing level. The thermistor network, not shown in Fig. 6, is inserted between diode D_4 and ground.

2.3.1.3 *IF Filter* (Fig. 1). The main functions of the IF filter are to delimit the IF bandwidth precisely with a minimum of ripple or slope within the band and to equalize the delay of the over-all IF amplifier. Besides limiting thermal noise, it also prevents out-of-band interfering signals and harmonics generated in the variolossers from entering the main amplifier. Systems considerations[1] dictate that the 3-db frequencies be 60 and 80 mc, and that the loss be flat to within ±0.1 db from 64 to 76 mc. It is designed to work between precise 75-ohm terminations.

2.3.1.4 *IF Main Amplifier* (Fig. 7). The IF main amplifier is a cascade of nine common-base stages, each developing slightly less than 6 db of gain, and a parallel common-base output stage capable of delivering a maximum power of +13 dbm into the limiter. The nominal power gain of this amplifier is 48 db, flat to within ±0.2 db over the 64- to 76-mc IF band.

The driver stage Q_9 is similar to the earlier stages, except that it is followed by an additional transformer to give an over-all 4:1 current step-up at the last interstage (for driver linearity). Resistors R_2 and R_3 ensure equal driving currents for the parallel transistors. Resistor R_4 helps to provide a good output return loss for a 200-ohm load (the limiter).

2.3.2 *Automatic Gain Control Circuit* (Fig. 8)

For proper operation of the limiter, it is necessary that the output level of the IF main amplifier be held nearly constant regardless of changes in RF signal level and temperature. Furthermore, the IF amplifier stages preceding the output stage must not be overdriven; otherwise, too much spurious phase modulation will result. These desired conditions are achieved through the use of an automatic gain control circuit consisting of an IF detector, a direct-coupled amplifier called the AGC amplifier, and the variolossers described in Section 2.3.1.2. The AGC amplifier, excited by the detector, feeds back a current (K lead) to control the loss due to the variolossers and thereby

Fig. 7 — Main IF amplifier.

Fig. 8 — AGC amplifier.

compensates any tendency for the IF output level to change. The dc amplifier has sufficient gain to multiply the small current increment drawn from the detector to the relatively large current needed to drive the variolossers. This circuit holds the limiter input level to $+11.5$ dbm ± 1 db for IF input levels ranging from -83 dbm to -33 dbm over the temperature range from $-20°C$ to $+60°C$.

A masking resistor R_1 is inserted to partially isolate the output of the IF main amplifier from the nonlinear input impedance of the AGC detector. This reduces the AM-to-PM conversion of the receiver. The detector-diode voltage varies almost linearly with the IF output voltage and is therefore used as a limiter input level monitor.

The dc amplifier consists of a differential stage followed by a common-emitter stage. The differential stage is used to minimize the drift in IF output level due to changes in temperature. The amplifier has one net phase reversal, providing negative feedback around the AGC loop. The closed-loop bandwidth of the AGC system is limited to about 50 cps by capacitors C_1 and C_2, which produce the only significant cutoffs occurring in the feedback-vs-frequency characteristic of the AGC system.

A switch is incorporated in the differential stage to permit the AGC loop to be opened for test purposes. The potentiometer R_2 serves a dual purpose. With the AGC loop closed (switch on), it sets the dc reference to which the detector output level is compared; and since the variolossers are automatically adjusted to make the difference between these levels zero, this potentiometer sets the IF output level. When the loop is open, the potentiometer is used to manually adjust the loss of the variolossers.

The collector voltage of transistor Q_3 is a monotonic function of the received carrier level. This voltage is used to trigger a squelch circuit (lead S), to excite a diversity switching circuit (lead L) and to drive a signal strength meter (also lead L). Potentiometer R_3 serves as a calibration control for this voltage, and potentiometer R_4 provides an additional adjustment for the voltage on lead L.

2.3.3 Limiter (Fig. 9)

The output signal of the IF main amplifier will contain both AM and FM components of noise and baseband signals.* Since the discriminator will respond to AM signals as well as to FM signals, a limiter is used to greatly reduce the AM component of the signal entering the discriminator.

---

* The AM baseband signal component is due to the action of a non-flat system transmission characteristic on the FM signal.
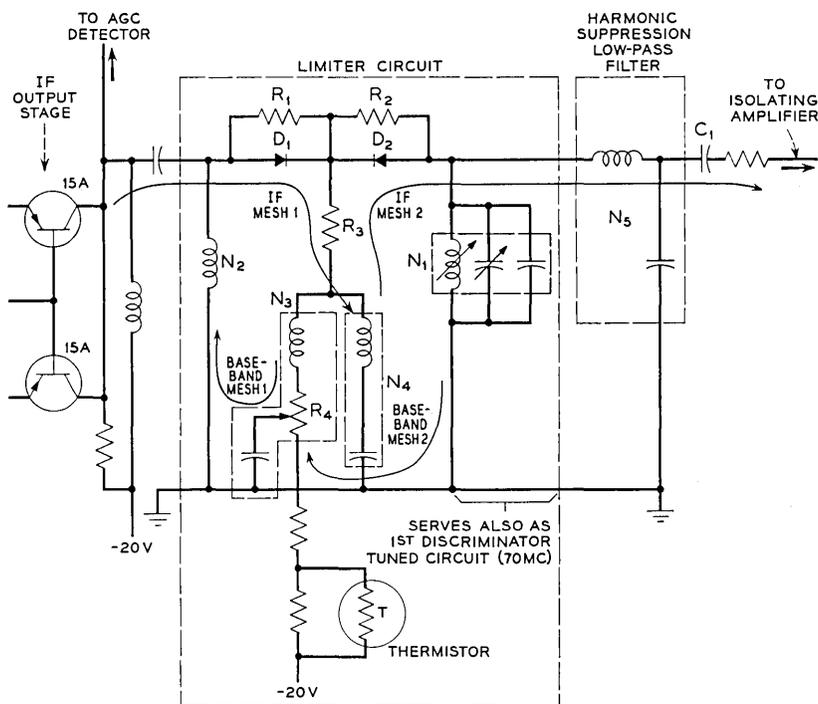
Fig. 9 — Remodulation-type limiter circuit.

The operation of the limiter can be understood from a consideration of Fig. 9.[2] The limiter resembles a simple series diode clipper in which the diodes are used to open up the transmission path after a certain level threshold is reached. One can think of the first and second diodes as an amplitude detector and an amplitude modulator, respectively. This process of detection and modulation is so performed that the net AM on the limiter output signal is minimized. Some of the incoming AM sideband energy is coupled from the IF mesh 1 to IF mesh 2 through the shunt path consisting of resistor R_3 and bandpass network N_4. The envelope of the IF signal is detected by diode D_1 in baseband mesh 1 and this baseband signal is coupled through the shunt path consisting of resistor R_3 and low-pass network N_3 to baseband mesh 2. There the baseband signal is impressed on the IF carrier by diode D_2 and appears across the load at sideband frequencies in phase opposition to the energy coupled from IF mesh 1. Note that networks N_1 and N_5 are required to cause the baseband and sideband signals to flow in the proper meshes and to attenuate undesirable modulation products. (Also, N_1 is a 70-mc

antiresonant tank circuit which serves as a corrective circuit for linearizing the discriminator characteristic.) Potentiometer R_4 is adjusted to achieve cancellation of the AM. The dc source in the baseband shunt path is used to bias the diodes D_1 and D_2 and hence set the limiter output level. The thermistor compensates for temperature drift in the gain (or loss) of the limiter, discriminator and baseband amplifiers. The FM signal behaves in the same manner as the carrier, suffering only loss in passing through the limiter. Insertion loss of the limiter is about 10 db, and the circuit has been designed for acceptable limiting for input levels ranging from +10 to +13 dbm.

Resistors R_1 and R_2 shunt the diodes, thereby permitting the use of diodes with a wide range of reverse impedances. These resistors, being in parallel with the low forward impedances, do not affect diode performance in the forward bias state. The load driven by the limiter is the input network of the discriminator. Capacitor C_1 tunes out the reactive part of the input impedance of the limiter-discriminator isolating transistor at the IF center frequency.

2.3.4 Triple-Tuned Balanced Discriminator (Fig. 10)

The discriminator extracts the baseband information from the input FM signal. After passing through the first common-base isolating amplifier, the FM signal traverses a wide-band transformer and then drives two separate branches. Each of these paths contains a common-base isolating amplifier, a parallel resonant circuit, an amplitude detector, a low-pass filter, and two terminating resistors. The discriminator output baseband signal is the sum of the output currents of the two paths. Two outputs are provided: an ac-coupled output to the receiver baseband amplifier and a direct-coupled output to the AFC amplifier.

Circuit N_1 (Fig. 9) is tuned approximately to the 70-mc carrier frequency, circuit N_2 (Fig. 10) to 85 mc, and circuit N_3 to 55 mc. The use of circuits N_2 and N_3 alone yields the familiar "S" curve; however, the low-Q tuned circuit N_1 significantly improves the linearity of the discriminator.[7] Since the attainment of adequate linearity requires precise adjustment of both the Q and resonant frequency of the tuned circuits, both the inductor and capacitor of each tank are adjustable. Proper phasing of the outputs of the two paths is accomplished by connecting the discriminator diodes as indicated. (This connection avoids the use of a costly and large-size broadband transformer.)

Negative-coefficient capacitors are used to maintain the proper resonant frequencies of the two tuned circuits of Fig. 10 as the temperature changes. Equal forward-bias voltages of approximately 0.3 volt are
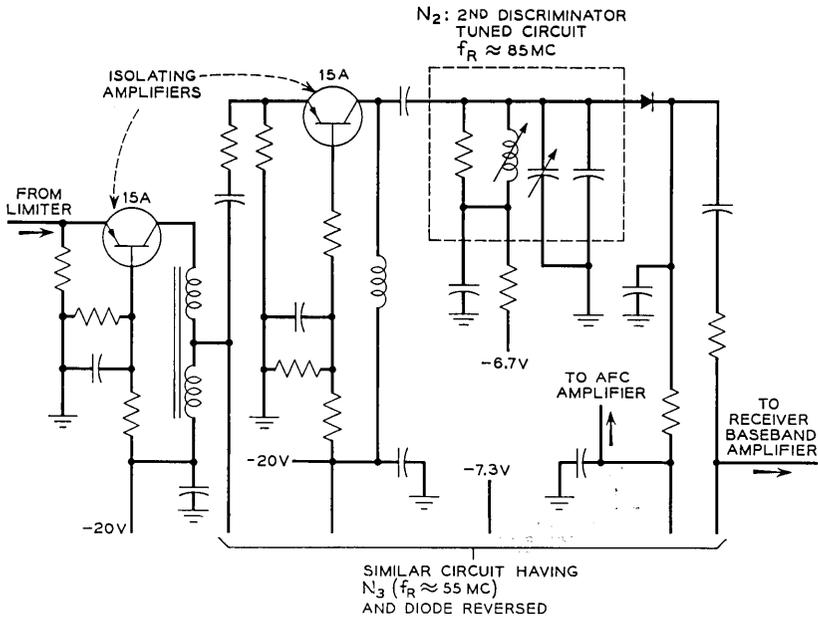
Fig. 10 — Balanced discriminator.

maintained across each of the diodes to improve the linearity of the detectors.

2.3.5 *Automatic Frequency Control Amplifier* (Fig. 11)

The AFC loop contains two cascaded amplifier circuits, a two-transistor amplifier followed by a magnetic amplifier. The primary purpose of the transistor AFC amplifier is to isolate the discriminator and baseband amplifier from the magnetic amplifier, since the latter amplifier produces a substantial 1800-cycle signal rich in harmonics which must be attenuated to avoid spurious baseband amplifier output tones.

The transistor AFC amplifier consists of a common-emitter stage direct-coupled to a common-collector stage. Shunt negative feedback provides bias and gain stabilization and low input and output impedances. (The low input impedance helps isolate the two paths of the balanced discriminator, and it simultaneously stabilizes the bias applied to the discriminator diodes.) Attenuation of undesirable tones from the magnetic amplifier is provided by the low output impedance of the transistor AFC amplifier and by an RC filter between the discriminator and the transistor AFC amplifier. The input current from the discrimi-
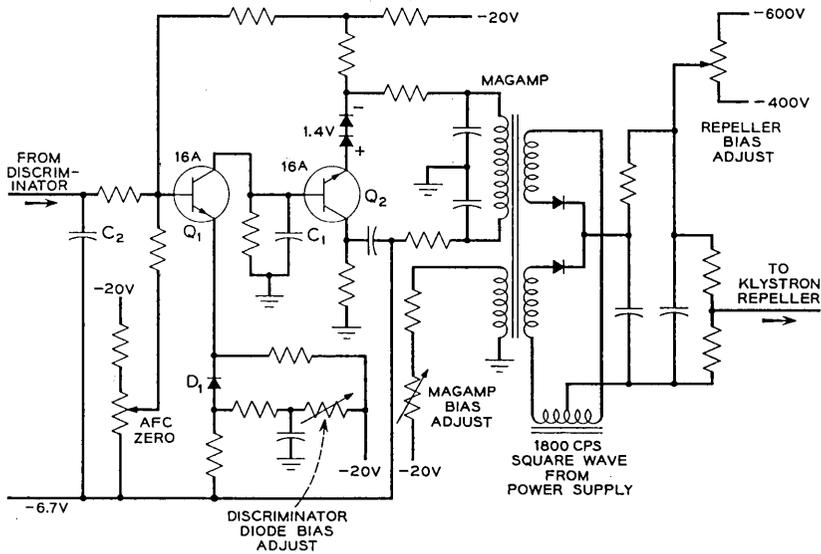
Fig. 11 — AFC amplifier.

nator is very nearly zero when the IF carrier frequency is 70 mc be-
cause the discriminator diodes are oppositely poled.

Since the transistor AFC amplifier output voltage must be bipolar
and since the dc power supply has only one polarity (−20 volts) with
respect to dc ground, a −6.7 volt dc voltage source is used as the transis-
tor AFC amplifier "dc ground." The dc output of the AFC amplifier
is relatively insensitive to variations in both the −20-volt power sup-
ply and the −6.7-volt source. The transistor AFC amplifier output
is approximately 40 mv/mc of carrier deviation.

Temperature stability of the transistor AFC amplifier is achieved by
canceling Q_1 base-emitter voltage-drop changes with diode D_1 and by
achieving beta drift compensation by making the collector current of
Q_1 and the base current of Q_2 approximately equal in magnitude. Ca-
pacitor C_1 is used to shape the feedback versus frequency characteristic
of the transistor AFC amplifier and assures stability. Capacitor C_2
reduces 1800-cycle energy originating in the magnetic amplifier.

The main gain-producing element of the AFC loop is the magamp,
which provides a voltage gain of about 950. Its cutoff frequency, which
controls the response time of the AFC loop, is about one cycle per
second. The 1800-cycle square wave required for operation of the

magamp is obtained from a winding on the dc-to-dc converter which supplies high voltage for the klystrons.

2.3.6 Receiver Baseband Amplifier (Fig. 12)

The receiver baseband amplifier follows the discriminator. It is a direct-coupled cascade of three common-emitter transistor stages with shunt feedback through a "T" network. Two virtually identical input currents are applied to the amplifier from the two branches of the discriminator. The external current gain of the amplifier is given, to a good approximation, by the ratio of the feedback network short-circuit transfer impedance (13 to 25 kilohms) to the output-lead resistance (145 ohms). The gain may be varied over a 5-db range by adjusting potentiometer R_5.

The output stage is a parallel combination of a pnp germanium unit
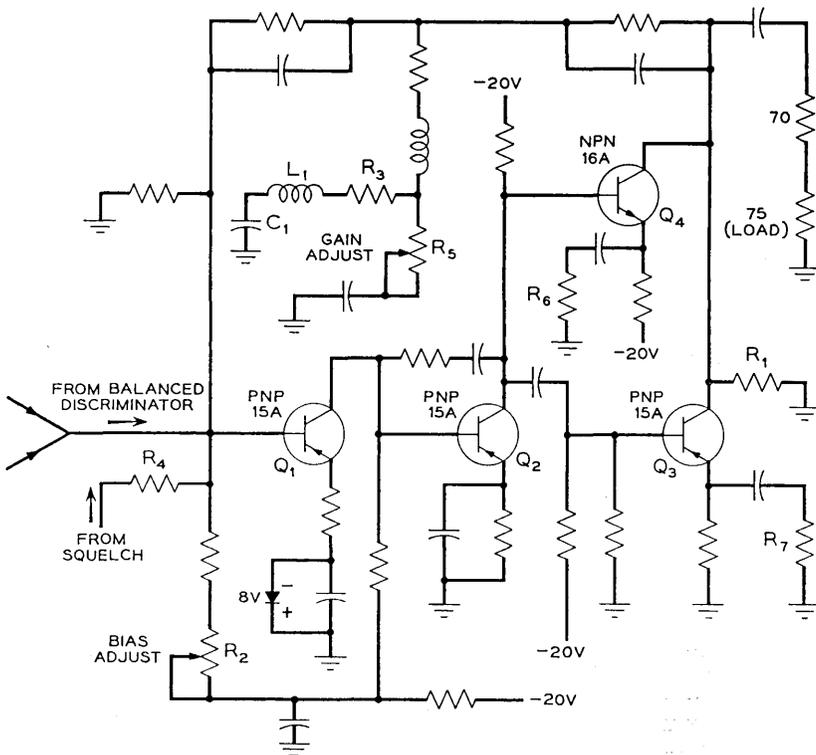
Fig. 12 — Receiver baseband amplifier.

having a common-emitter current-gain cutoff at about 15 mc and an npn silicon unit with a cutoff at about 3 mc. Both transistors contribute substantially to the ac load current out to 6 mc (the highest baseband frequency), with the result that more current can be driven into the load under given distortion limits than can be provided by one transistor alone. The dc current passed by transistor Q_3 into the collector node is drawn out of that node by transistor Q_4, allowing a reduction of the output admittance shunting the load. The available output power is thus increased. Resistor R_1 sets the amount by which the bias current in the silicon transistor Q_4 exceeds that in the germanium transistor Q_3. The small emitter resistors R_6 and R_7 ensure that the two transistors share the load equally by making their input impedances proportional to their respective incremental current gains.

The local shunt feedback in the second stage allows the circuit to accommodate high-gain units in the output stage without becoming unstable; and it also compensates, to some degree, for the drop in incremental gain of the output stage during part of the signal cycle, maintaining the over-all feedback and thereby reducing distortion.

Because of the large amount of over-all shunt feedback, the output impedance of the amplifier is roughly 5 ohms augmented by the 70-ohm padding resistance, which yields a good output return loss. Potentiometer R_2 adjusts the dc collector voltage of transistors Q_3 and Q_4. The network formed by resistor R_3, inductor L_1 and capacitor C_1 improves the stability margins when potentiometer R_5 is set for maximum resistance.

The amplifier is switched off during deep carrier fades by an input from a squelch circuit sufficient to drive it into saturation. This input current is passed through resistor R_4, which is large enough to mask out the output capacitance of the squelch circuit.

2.3.7 *Transmitter Baseband Amplifier* (Fig. 13)

A baseband amplifier immediately precedes the transmitter klystron in the TL system. This amplifier provides an adjustable voltage gain of 27 ± 4 db between a 75-ohm source and the klystron repeller load (which, including wiring capacitance, behaves like a 35-$\mu\mu$f capacitor).

The amplifier uses three transistors. The first stage uses the common-base configuration; the second stage is common-collector; and the third stage is common-emitter, providing the net phase reversal needed for negative shunt feedback. Because of the very low input impedance provided by the common-base stage and the over-all negative feedback, a 75-ohm resistor is added to give excellent input return loss.
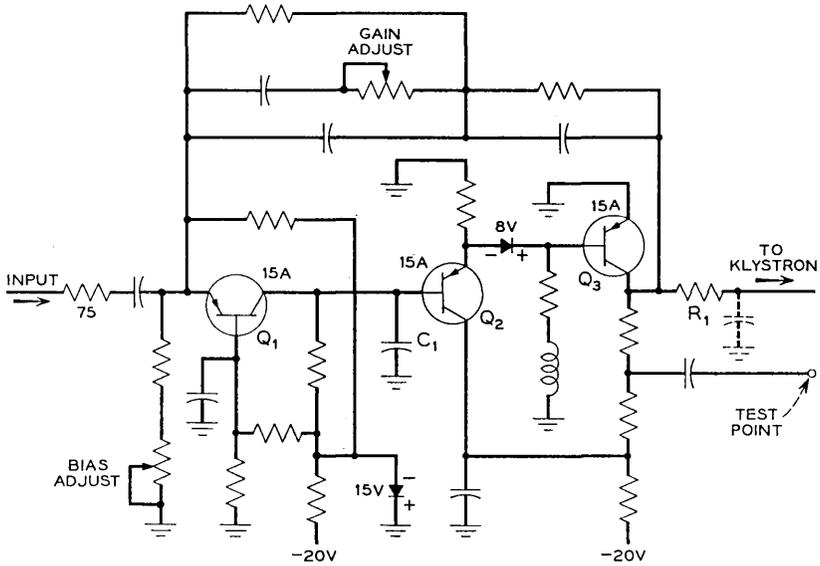
Fig. 13 — Transmitter baseband amplifier.

Capacitor C_1 provides the initial feedback cutoff (at about 5 mc). This cutoff slides to compensate for changes in the current gains of Q_2 and Q_3 since it depends on the input impedance of the common-collector stage. Resistor R_1 improves the phase margin of the feedback ($A\beta$) by halting the falling asymptote due to the 35-$\mu\mu$f load capacitance at about 47 mc.

2.3.8 *Squelch Circuit* (Fig. 14)

The receiver contains a bistable trigger circuit which renders the baseband amplifier inoperative during deep radio path fades. This
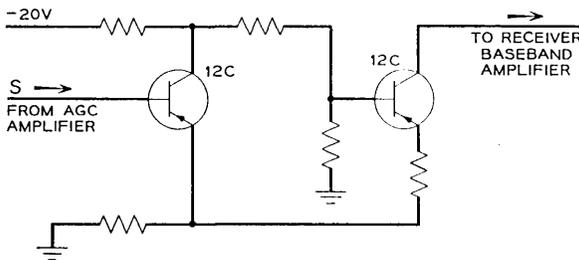
Fig. 14 — Squelch circuit.

circuit is a Schmitt trigger operating from the variolosser-control voltage produced by the AGC amplifier. This voltage, which appears at the collector of transistor Q_3 in Fig. 8, becomes less negative as the IF input carrier fades, and the circuit is designed to trigger in the vicinity of −2.8 volts. This voltage level is caused to correspond to a carrier level of from −80 to −95 dbm by means of potentiometer R_3 in Fig. 8. When the Schmitt trigger circuit fires, it injects about 1.5 ma of current into the summing node of the receiver baseband amplifier, driving this amplifier into saturation since as little as 0.8 ma will saturate it.

2.4 *Circuit Performance*

2.4.1 *IF Amplifier*

The most important electrical performance features of the IF amplifier in the TL radio receiver may be described by graphs showing the over-all gain-frequency characteristic at different incoming signal levels and at extremes of temperature.

All of the curves in Fig. 15 are normalized with respect to the gain at 70 mc and 25°C with the passive filter in. The data show that both the in-band and wideband spectral distortion is small as the ambient temperature is changed from −20°C to +60°C. Furthermore, the gain level at 70 mc without AGC varies a maximum of 2 db over the same temperature range. Between 50 and 90 mc the "bowed" shape of the curves is primarily due to the output circuit of the IF amplifier (Fig. 7); the in-band effect is negligible.
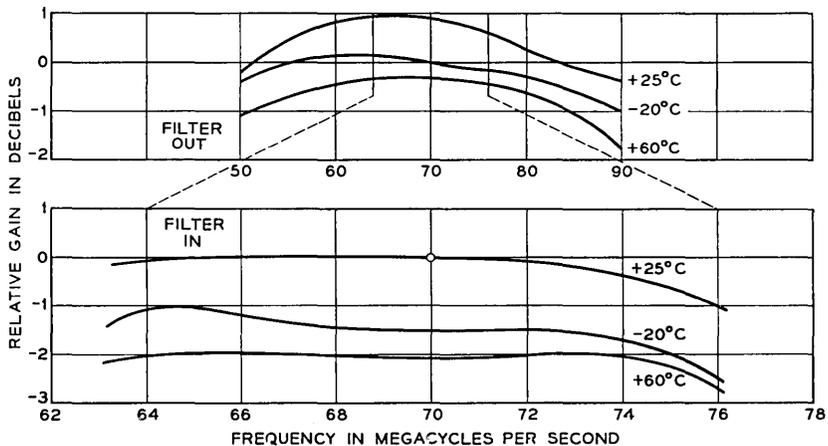
Fig. 15 — Gain-frequency characteristic of IF amplifier.

The IF amplifier output level vs frequency at different input levels and temperature extremes is shown in Fig. 16. These curves demonstrate the tightness of the AGC.* The output power is set to +11.5 dbm at 70 mc, 25°C with an input level of −58 dbm. The maximum level shift encountered at 70 mc as temperature and input level vary is ±0.6 db, and the maximum tilt is 0.13 db/mc across the band. The IF main amplifier provides +11.5 dbm of power with less than 0.5 db compression working into the 200-ohm limiter input impedance.

In addition to transmission-shape and output-level stability, another important requirement is that the envelope delay distortion be small. Fig. 17 shows the envelope delay in nanoseconds at two input levels and at temperature extremes. The maximum change in envelope delay over the 64- to 76-mc band is observed to be 12 nanoseconds. Most of the change with frequency occurs during deep fades where noise, rather than delay distortion, is controlling. The envelope delay characteristic of the IF filter is presented in Fig. 18 along with the insertion and return loss characteristics. The 70-mc loss is about one db, and the envelope delay shift across the 64- to 76-mc band is 6 nanoseconds.

The noise figure of the IF amplifier during fades, measured from a 75-ohm source impedance, is typically about 6 db. Fig. 19 is a plot of noise figure as a function of input carrier level in dbm at 25°C. The
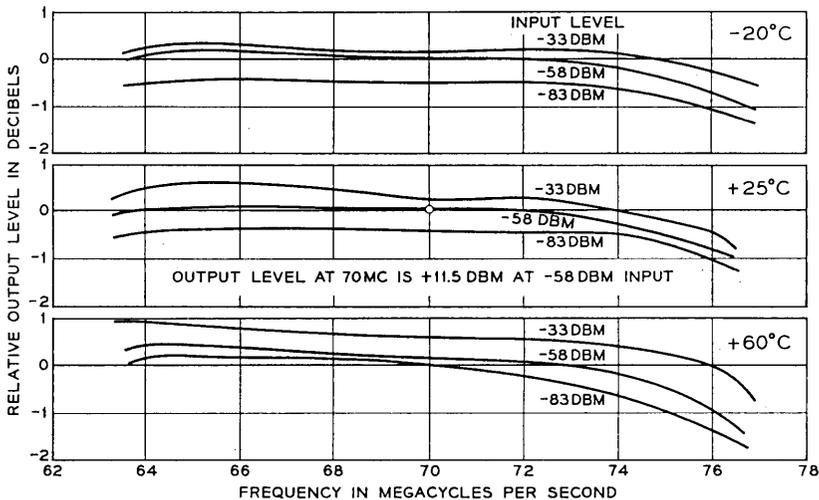
Fig. 16 — IF output level versus frequency (with filter and AGC).

* The frequency response of the AGC system, for the purpose of this measurement, is made much lower than the sweep frequency of the signal source.
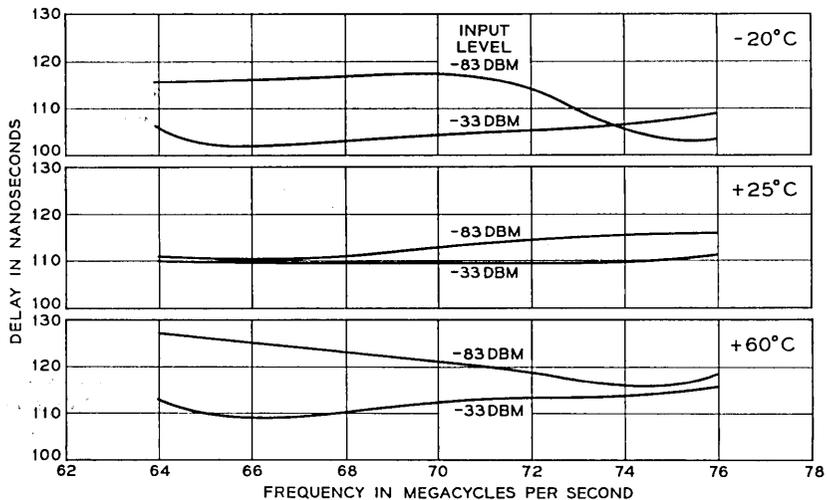
Fig. 17 — Delay-frequency characteristic of IF amplifier (with filter and AGC).

input circuit is adjusted so that a compromise is reached between low noise figure and return loss, typically 26 db from 64 to 76 mc.

2.4.2 AGC Circuit

The stability of the closed AGC feedback loop may be measured by applying a step function from a current source at the K lead of the AGC amplifier (Fig. 8) and observing the output voltage on the collector of Q_3 as a function of time. Fig. 20 shows a sketch of this waveform for three input level conditions representing different amounts of AGC loop gain. An input level of -58 dbm yields the worst transient response. The amount of overshoot is a measure of the stability margins, and the rise time and ripple frequency relate to the response time. The AGC system cuts off at approximately 50 cps, and the maximum overshoot of 6 db suggests a minimum phase margin of about 20 degrees.

2.4.3 Limiter

Measurements of AM suppression of the limiter for three temperatures and three drive levels into the IF preamplifier are given as functions of baseband frequency in Fig. 21. The limiter has been optimized for maximum AM suppression at 100 kc, room temperature, and a +11.5-dbm drive level and still provides at least 18-db suppression over the
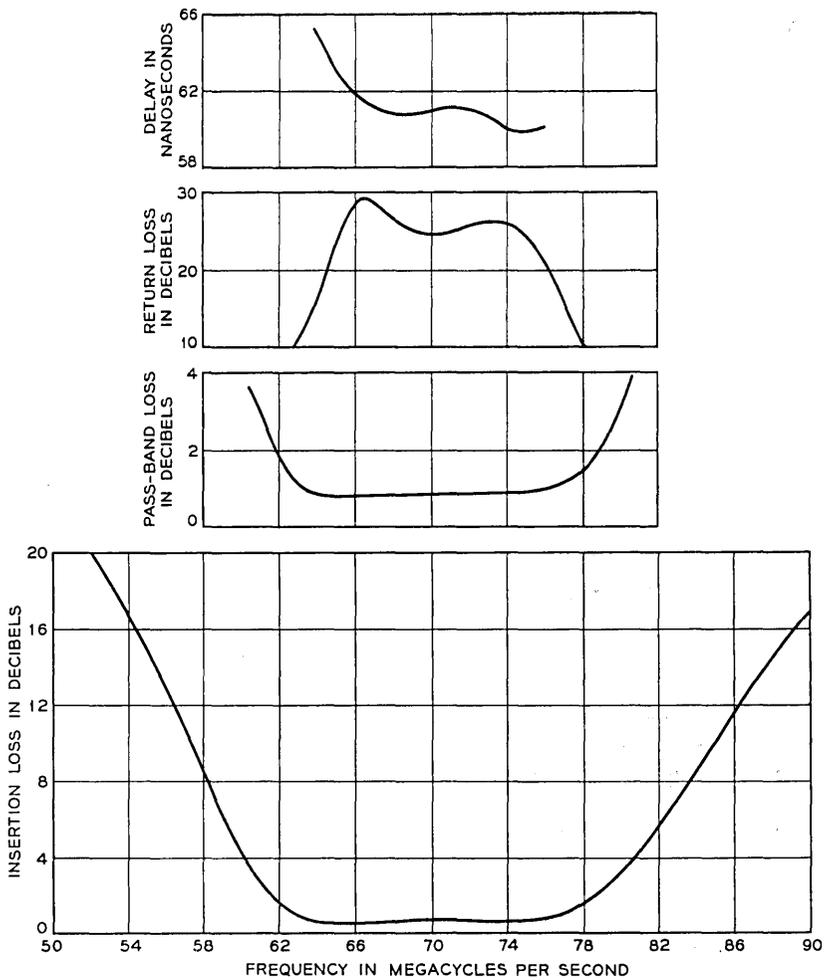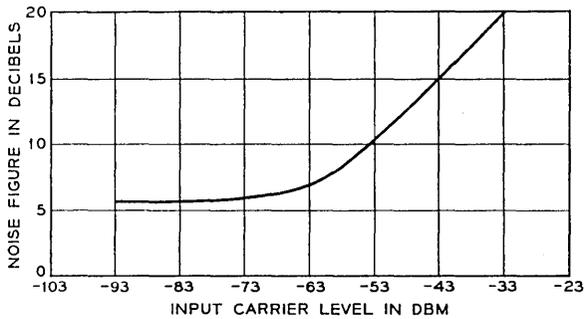
Fig. 18 — Loss, delay and return loss of IF filter.

Fig. 19 — Noise figure versus input carrier level, 25°C.
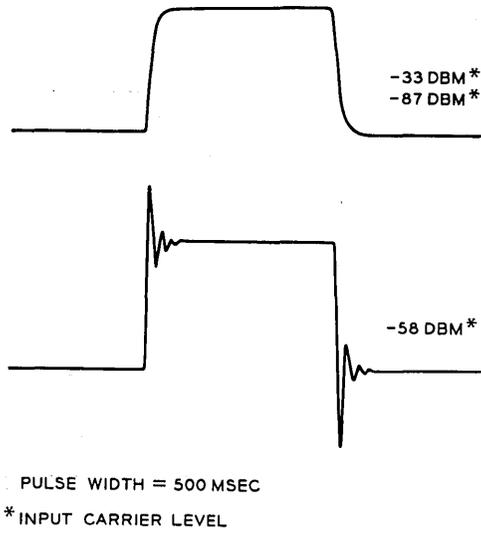
PULSE WIDTH = 500 MSEC

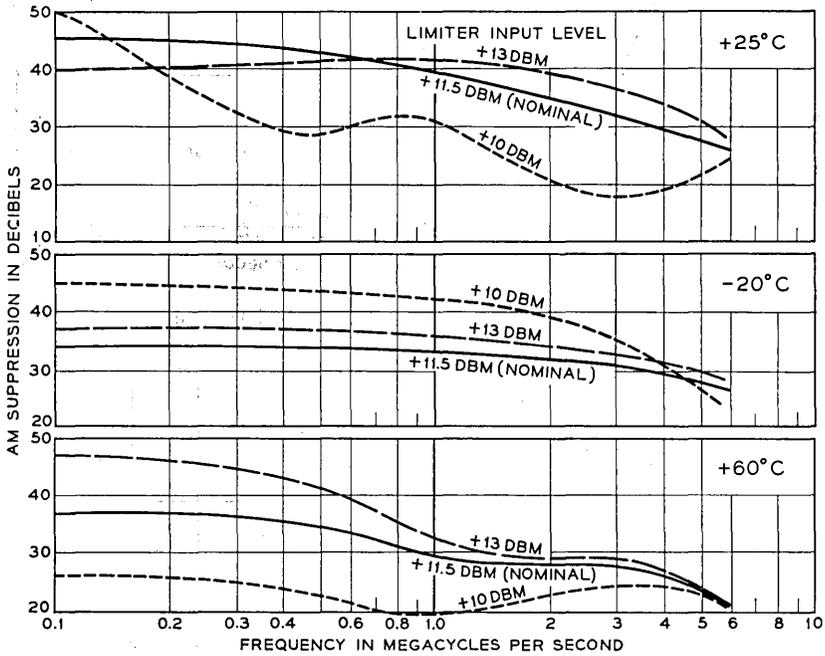*INPUT CARRIER LEVEL

Fig. 20 — Step response of AGC system.

Fig. 21 — Limiter AM suppression

6-mc baseband under the worst conditions of temperature and of drive level permitted by the AGC.

2.4.4 Discriminator and Transistor AFC Amplifier

A discriminator is judged primarily by its linearity, stability of its zero crossover frequency and sensitivity.[7] The over-all receiver nonlinearity is typically measured to be better than 4, 7 and 4 per cent at temperatures of +25, −20 and +60°C, respectively, for a peak deviation of 6 megacycles; and this is approximately the nonlinearity of the discriminator.

Measurements on the composite discriminator-transistor AFC amplifier indicate that the shift in zero crossover frequency is ±200 kc, and the nominal sensitivity of 40 mv per megacycle changes ±2 mv per megacycle over this temperature range. The rejection of the 1800-cycle signal and harmonics of this frequency generated by the magnetic amplifier is sufficient to keep the level of this signal at the receiver-baseband output down to the order of −50 dbm.

2.4.5 AFC Loop

The AFC loop performance, aside from drift which was discussed in the previous section, is relatively independent of temperature. A typical circuit has a loop gain of 30 db, 10-db gain margin and 60 degrees phase margin.

2.4.6 Receiver Baseband Amplifier

The open-loop gain and phase vs frequency characteristics of a typical receiver baseband amplifier are shown in Fig. 22 for a medium gain setting and room temperature. The closed-loop gain curves for −20°C, +25°C and +60°C are also shown. It is clear that the external gain from 200 cps to 2 mc stays constant within ±0.08 db over the temperature range, and between 2 mc and 6 mc it is constant within ±0.23 db. The open-loop characteristic exhibits a 6-db per octave rolloff, which is desirable when flatness of external gain near the unity feedback crossover frequency is important. The feedback amounts to 31 db at midband and 13 db at 6 mc. The phase and gain margins are 47° and 6 db, respectively. (A small gain margin such as this can be tolerated when a large part of the phase shift tracks well with the f_T's of the transistors* and, hence, with the crossover frequency.) Since feedback is maintained down to dc, there is no question of low-frequency oscillation.

* f_T is defined as the frequency at which the common-emitter short-circuit current gain is unity. It is a convenient figure of merit for the bandwidth of the transistor.
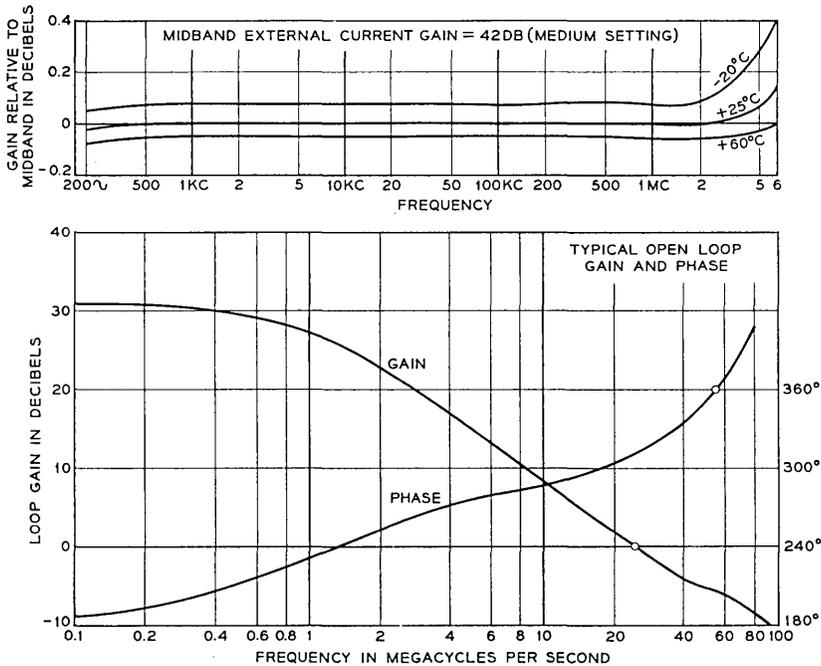
Fig. 22 — Gain-frequency curves — typical receiver baseband amplifier.

The second- and third-harmonic distortion products are down at least 37 db and 46 db, respectively, for maximum external gain (minimum feedback condition) and full output level of $+10$ dbm at 6 mc. These figures become better rapidly as frequency decreases, reaching -60 dbm and -70 dbm, respectively, at 500 kc. The output noise power of the amplifier in a 500-cycle band for frequencies above 100 kc is approximately -92 dbm.

2.4.7 Transmitter Baseband Amplifier

Measurements similar to those made on the receiver baseband amplifier were made on the transmitter amplifier. Fig. 23 displays the gain-frequency characteristics of a typical transmitter baseband amplifier at a medium gain setting and room temperature. This particular model contains transistors with average f_T's; thus, it represents a typical case. The phase and gain margins are 53° and 8 db, respectively.

Distortion measurements taken on the transmitter baseband amplifier indicate that the second and third harmonics are, respectively, at
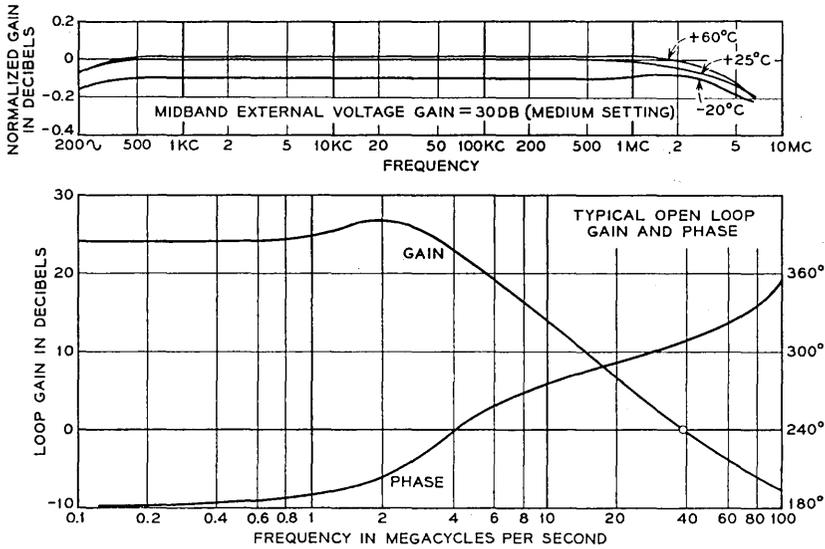
Fig. 23 — Gain-frequency curves — typical transmitter baseband amplifier.

least 54 db and 70 db below the fundamental at 6 mc and full output voltage (4 volts peak).

2.4.8 Squelch Circuit

The squelch threshold level for a typical receiver was measured as a function of temperature. The firing-level setting of −87 dbm drifted to −84 dbm and −85 dbm at −20°C and +60°C, respectively. The hysteresis between turn-on and turn-off was less than 1 db.

2.4.9 AM-to-PM Conversion

The over-all AM-to-PM conversion of a receiver was measured for temperatures ranging from −20°C to +60°C and for IF input levels ranging from −33 to −83 dbm. The worst AM-to-PM conversion was 0.017 radian for a 10 per cent AM index.

III. CONCLUSION AND REMARKS

Certain apparent limitations in the use of solid-state components in a wideband microwave radio relay system have been overcome. The fresh approaches which have been applied have, in some cases, resulted in performance which is superior to that achieved with compara-

ble electron tube designs. This improved performance is over and above that achieved through inherent advantages of solid-state devices over conventional electron tubes, which include reduced power drain, small size, reliability, and potentially low cost.

It has recently come to our attention that others working in the field of microwave radio systems have arrived through parallel efforts at some of the same design techniques described herein.[8] It is hoped that the publication of this paper will help expand the field of application of solid-state devices and will encourage others to design around apparent shortcomings of solid-state devices by refusing to have their thinking completely channeled by what already exists.

IV. ACKNOWLEDGMENTS

The solid-state FM receiver circuits described in this paper are the result of the efforts of many members of Bell Telephone Laboratories. Some of the design concepts were born in the Radio Research Department, which triggered the development of the TL system; and Messrs. L. C. Tillotson, C. L. Ruthroff, N. E. Chasek and W. F. Bodtmann were particularly influential there. The members of the Transmission Division who contributed to the project are numerous, but the efforts of Mr. L. F. Willey on the development of the limiter and discriminator, Mr. J. Gammie's work on the AFC magamp, Mr. G. H. Klemm's equipment design effort, the many helpful suggestions of Mr. F. H. Blecher and the accumulation of several notebooks full of important data by Mr. H. A. Hageman are particularly noteworthy.

APPENDIX

A.1 *Transistor "Low-Pass" IF Amplifiers*

At least three basic configurations are useful in transistor wideband IF amplifiers. These are the common-base stage with a wideband transformer interstage network, the doublet circuit, and the common-emitter stage with frequency-dependent shunt feedback.

A.1.1 *The Common-Base Stage with a Wide-Band Transformer Interstage Network*

Because the current gain of a common-base stage is less than unity, this configuration requires the use of a current step-up interstage network to achieve power gain when a cascade of similar stages is used as a

wideband amplifier. Transformers are available which provide a constant current step-up over a wide band of frequencies[4,5,6] between terminating impedances typical of solid-state circuits. The basic common-base configuration is shown in Fig. 5. It can be shown that to achieve "flat" amplitude response extending to within an order of magnitude of f_T, damping resistor R_2 is required. Use of a transformer having a 1:2 current step-up results in a power gain slightly less than 6 db per stage.

In the TL IF amplifier stages, the transformer turns ratio is much lower than that which would result in maximum gain. This makes the amplifiers quite insensitive to changes in transistor parameters. This implies a very stable transmission characteristic over a wide temperature range and large variations in power supply voltage. Another result is that the circuits accept an extremely wide range of transistor parameters, either due to statistical distribution or to aging; and adjustment of the transmission characteristic is relatively simple.

The input and output impedances are relatively stable with temperature and dc bias and can be represented by simple passive networks. Hence, the common-base stage can be compensated to yield a stable resistive input or output termination over a wide frequency range. This feature makes it particularly useful for connection to passive bandpass filters or other equalizer networks. Since the common-base static characteristics are much more linear than those of other configurations, this configuration also gives superior performance in high-level stages. However, one must look to other configurations, such as the doublet, for the best noise figures in input stages.

A.1.2 The Doublet Circuit

This circuit, shown in Fig. 4, takes advantage of the fact that certain transistor pairs, or doublets, without interstage transforming networks, can provide an over-all gain stage which is more immune to temperature and power supply variations than each transistor considered separately. The reason for this improvement is the fortunate circumstance that undesirable variations on the individual stages tend to cancel for certain configurations. Two combinations which have been shown to exhibit this desirable property are the common-emitter — common-emitter doublet and the common-emitter — common-collector doublet. The gain characteristic, though stable, rolls off smoothly at high frequencies; hence, it is necessary to follow the transistors with an equalizer network, which usually takes the form of a constant-resistance, high-pass filter. The high-pass filter is designed to have a cutoff frequency above the

IF band, and the rolloff of the filter compensates for the rolloff of the transistors.

The gain level of a doublet is a fairly strong function of the f_T of the transistors used; however, the over-all normalized gain-frequency characteristic is stable with temperature and bias variations. Exclusive use of the doublet in a high-gain amplifier would probably dictate either a tight control of the average f_T of the transistors used or a larger dynamic range of automatic gain control. The power gain of the doublet used in the TL radio receiver ranges from 15 to 20 db.

The common-emitter — common-emitter doublet configuration has been found to be the one best suited for use as the input circuit for wideband IF amplifiers. It provides the lowest noise figure of all of the configurations evaluated and, through the use of a simple impedance-matching network, can yield a good input return loss over a wide IF band. The low noise figure is due to the facts that the input of the amplifier is separated by a block of relatively high gain from the remainder of the amplifier and that the natural input impedance of the doublet amplifier needs only minor correction to achieve good input return loss at the desired impedance levels (usually 50 to 125 ohms).

A.1.3 The Common-Emitter Configuration with Frequency-Dependent Shunt Feedback

Of all forms of wideband amplifiers studied, the configuration which most easily yields the broadest bandwidths is the common-emitter stage with frequency-dependent shunt local feedback.[9,10] This circuit, shown in Fig. 24, has a two-terminal RL network connected between base and collector. The effect of the RL network is to reduce the gain of the stage by application of negative feedback. Resistor R_1 determines the low-frequency gain, and inductor L effectively removes the feedback
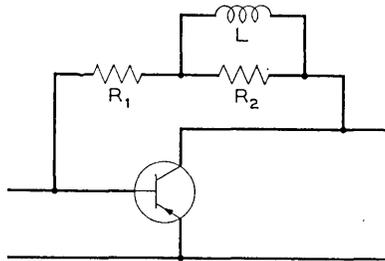

Fig. 24 — Common-emitter stage with shunt local feedback.

at high frequencies and hence is a broadbanding element. Resistor R_2 damps the resonance which occurs between the inductor L and the capacitive reactance presented by the transistor. It has been demonstrated that this configuration is very flexible in that gain and bandwidth can easily be exchanged, and the gain-bandwidth product is approximately given by f_T .[9]

A cascade of common-emitter stages with shunt feedback exhibits only very slight changes in the normalized amplitude response for wide variations in temperature and power supply voltage. However, because the gain level of each stage is highly dependent on f_T and r_b' and on the input impedance of the following stage, the over-all gain level varies considerably. By specifying tight limits on the average values of the parameters for a given set of transistors (usually only the average f_T need be specified), the over-all absolute gain can be kept within close limits. Of course, a moderate amount of gain adjustment may be had by changing the value of R_1 in the feedback network. This configuration cannot compete with the doublet circuit as a low-noise input stage or with the common-base configuration as a low-distortion, high-level stage; however, it appears to be the best configuration to use when extremely large gain-bandwidth products are required.

REFERENCES

1. Hathaway, S. D., Sagaser, D. D., and Word, J. A., The TL Radio Relay System, to be published.
2. Ruthroff, C. L., Amplitude Modulation Suppression in FM Systems, B.S.T.J., **37,** July, 1958, p. 1023.
3. Gucker, G. B., Long-Term Frequency Stability for a Reflex Klystron without the Use of External Cavities, B.S.T.J., **41,** May, 1962, p. 945.
4. Rudenberg, H. G., Distributed Coupling and Amplification of Electric Waves, Ph.D. Thesis in Physics, Harvard University, 1950.
5. Ruthroff, C. L., Some Broadband Transformers, Proc. I.R.E., **47,** Aug., 1959, pp. 1337–1342.
6. Saari, V. R., Coupled Mode Theory with Application to Distributed Transformers, Part 2, 1962 I.R.E. International Convention Record.
7. Houghton, E. W., and Hatch, R. W., FM Terminal Transmitter and Receiver for the TH Radio System, B.S.T.J., **40,** Nov., 1961, pp. 1599–1605.
8. The New Microwave, Parts I and II, The Lenkurt Demodulator, **10,** Sept., Oct., 1961.
9. Ballentine, W. E., and Blecher, F. H., Broadband Transistor Video Amplifiers, Solid-State Circuits Conf., Feb., 1959, Digest, pp. 42–43.
10. Saari, V. R., Kirkpatrick, R. J., Bittmann, C. A., and Davis, R. E., Circuit Applications of a Coaxially-Encapsulated Microwave Transistor, Solid-State Circuits Conf., Feb., 1960, Digest, pp. 64–65.
11. Ballentine, W. E., Saari, V. R., and Willey, L. F., Recent Advances in Wideband FM Receiver Design, Solid-State Circuits Conf., Feb., 1962, Digest, pp. 96–97.

Evaluation of the Net Radiant Heat Transfer between Specularly Reflecting Plates

By V. E. HOLT, R. J. GROSH,† and R. GEYNET

The radiant heat transfer between two parallel infinite plates was determined. The plates were assumed to be specular, anisotropic reflectors and emitters as characterized by the electromagnetic theory for highly polished electrical conductors.

Numerical results are given for specific metals from 4.2 to 1500° K. Also, the results are expressed in generalized form for obtaining the net radiant heat transfer between any two parallel, infinite metal plates given only the temperatures and electrical resistivities.

Total hemispherical and normal emissivities were determined using the same methods. The results were in very good agreement with empirical equations given in the literature. For a contrasting comparison, Christiansen's equation for the net radiant heat transfer between two parallel, diffuse, gray surfaces of infinite extent was evaluated using these emissivities. The values obtained were less than those computed for the net radiant heat transfer between specular plates.

I. INTRODUCTION

Radiative exchange often becomes the controlling mode of heat transfer when systems are found to exist at either low or high temperature levels. In the former case, for instance, it often becomes one of the major heat leaks to cryogenic fluids stored in dewars.

In the following, the net radiant heat transfer between two parallel infinite surfaces is calculated for behavior in all respects as predicted by the electromagnetic theory of radiation for polished electrical conductors.

---

† Head, School of Mechanical Engineering, Purdue University, Lafayette, Indiana.

II. FORMULATION AND SOLUTION

The monochromatic emissivity, absorptivity, and reflectivity are known to be azimuthally symmetric about the normal to a conducting surface. Electromagnetic theory[1,2] indicates that the monochromatic directional emissivity of low-emissivity metals is given by:

$$\epsilon(\theta,\lambda) = \alpha(\theta,\lambda) = 1 - \frac{1}{2}\left[\frac{\dfrac{60\lambda}{re} - 2\sqrt{\dfrac{30\lambda}{re}}\cos\theta + \cos^2\theta}{\dfrac{60\lambda}{re} + 2\sqrt{\dfrac{30\lambda}{re}}\cos\theta + \cos^2\theta}\right.$$
$$\left. + \frac{\dfrac{60\lambda\cos^2\theta}{re} - 2\sqrt{\dfrac{30\lambda}{re}}\cos\theta + 1}{\dfrac{60\lambda\cos^2\theta}{re} + 2\sqrt{\dfrac{30\lambda}{re}}\cos\theta + 1}\right]. \tag{1}$$

Simplified expressions based on electromagnetic theory have been shown to be in agreement with experiment for temperatures as high as 1800°K.[2] However, deviation from experiment is presumed for higher temperatures.

2.1 Radiant Heat Transfer

For the arrangement shown in Figs. 1 and 2, the monochromatic radiation emitted from a unit area of surface 1 into a solid angle $d\omega$ inclined at an angle θ from the normal is

$$\epsilon_1(\theta,\lambda)I(bb,\lambda,T_1)\cos\theta\,d\omega. \tag{2}$$

A fraction $\alpha_2(\theta,\lambda)$ of this is absorbed at surface 2 for the first reflection. For specular reflection, a fraction $\alpha_2(\theta,\lambda)[1 - \epsilon_1(\theta,\lambda)][1 - \alpha_2(\theta,\lambda)]$ is absorbed at surface 2 for the second reflection. Ultimately, the monochromatic radiation emitted from surface 1 in a direction θ that is absorbed by surface 2 is

$$\epsilon_1(\theta,\lambda)\alpha_2(\theta,\lambda)\{1 + [1 - \epsilon_1(\theta,\lambda)][1 - \alpha_2(\theta,\lambda)]$$
$$+ [1 - \epsilon_1(\theta,\lambda)]^2[1 - \alpha_2(\theta,\lambda)]^2$$
$$+ \cdots\}\,I(bb,\lambda,T_1)\cos\theta\,d\omega \tag{3}$$
$$= \frac{\epsilon_1(\theta,\lambda)\alpha_2(\theta,\lambda)I(bb,\lambda,T_1)\cos\theta\,d\omega}{1 - [1 - \epsilon_1(\theta,\lambda)][1 - \alpha_2(\theta,\lambda)]}.$$

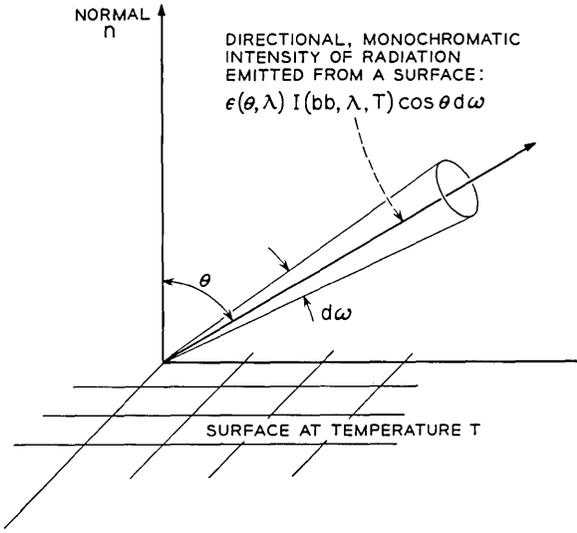Thus, the total radiation emitted from a unit area of surface 1 and

DIRECTIONAL, MONOCHROMATIC
INTENSITY OF RADIATION
EMITTED FROM A SURFACE:

$$\epsilon(\theta,\lambda)\, I(bb,\lambda,T)\cos\theta\, d\omega$$

θ

$d\omega$

SURFACE AT TEMPERATURE T

Fig. 1 — Coordinate system.

RADIATION EMITTED BY
SURFACE 1 AND ABSORBED
BY SURFACE 2

$$\alpha_2(\theta,\lambda)I_1 \qquad\qquad \alpha_2(\theta,\lambda)\left[1-\epsilon_1(\theta,\lambda)\right]\left[1-\alpha_2(\theta,\lambda)\right]I_1$$

SURFACE 2

$I_1 = \epsilon_1(\theta,\lambda)I(bb,\lambda,T_1)\cos\theta\, d\omega$

$\left[1-\alpha_2(\theta,\lambda)\right]I_1$

$\left[1-\epsilon_1(\theta,\lambda)\right]\left[1-\alpha_2(\theta,\lambda)\right]I_1$

$\left[1-\epsilon_1(\theta,\lambda)\right]\left[1-\alpha_2(\theta,\lambda)\right]^2 I_1$

n

θ

SURFACE 1

$$\epsilon_1(\theta,\lambda)\left[1-\alpha_2(\theta,\lambda)\right]I_1$$
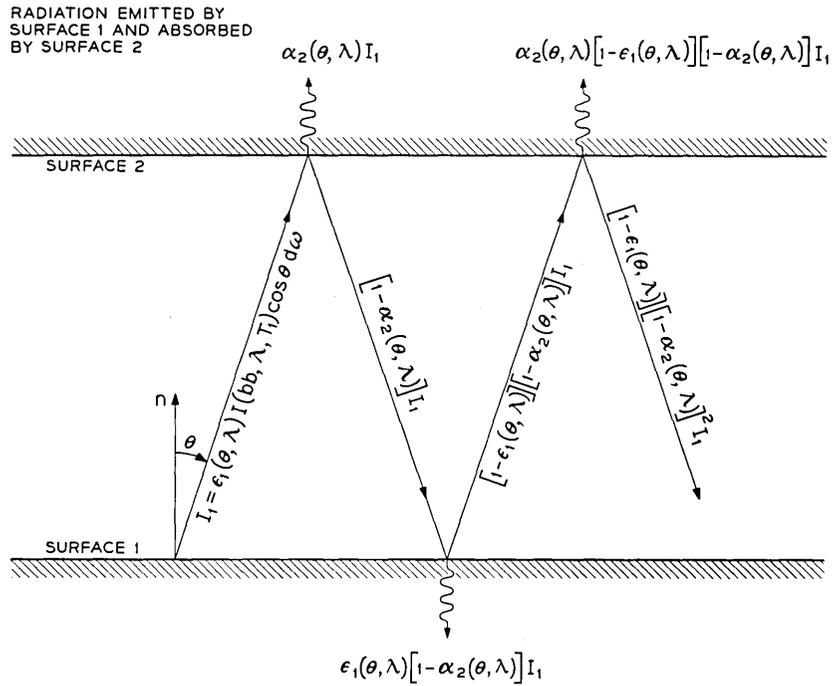
Fig. 2 — Specular radiation between parallel plates.

absorbed by surface 2 is

$$q_{1\to2} = \int_0^\infty \int_0^{\pi/2} \frac{\epsilon_1(\theta,\lambda)\,\alpha_2(\theta,\lambda)}{1 - [1 - \epsilon_1(\theta,\lambda)][1 - \alpha_2(\theta,\lambda)]} \tag{4}$$

$$\cdot E(bb,\lambda,T_1)\,\sin 2\theta\,d\theta\,d\lambda.$$

The net radiation from surface 1 to surface 2 is

$$q_{\text{net}} = q_{1\to2} - q_{2\to1}$$

where $q_{2\to1}$ is evaluated from (4) with the subscripts reversed.

Using the IBM 7090 computer, this equation was evaluated for specific metals and also for various resistances and temperatures. Only a fraction of a minute computation time was required per case. The required resistivity values were obtained from Refs. 3–10.

Specific examples of solutions are given in Table I. In Fig. 3, the radiation $q_{1\to2}$ is graphically expressed in general form in terms of only T_1,

TABLE I — NET RADIATION BETWEEN PARALLEL PLATES —
SPECIFIC EXAMPLES

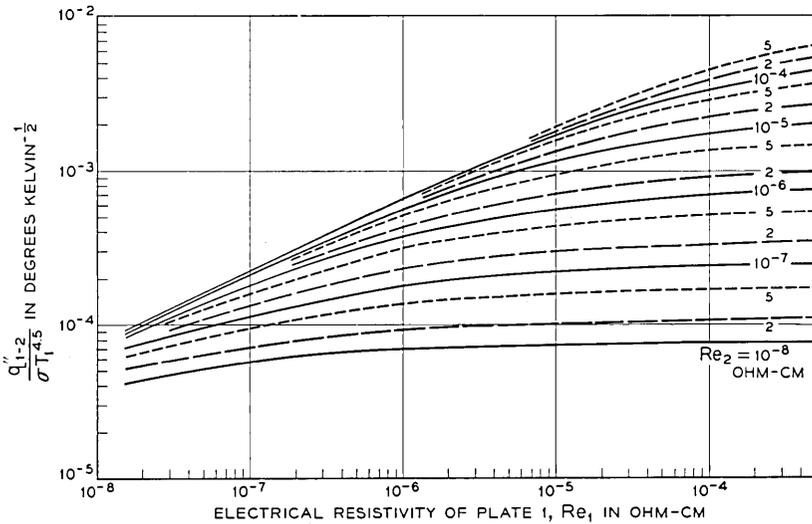| $T_1°$ K	$T_2°$ K	Computed Values — Figure 3			Christiansen's Equation (2)
		$q_{1\to2}$	$q_{2\to1}$	q_{net}	$q_{\text{net}} = \dfrac{\sigma[T_1^4 - T_2^4]}{1/\epsilon_{h_1} + 1/\epsilon_{h_2} - 1}$
BOTH SURFACES GOLD					
77	4.2	1.65×10^{-7}	3.42×10^{-13}	1.65×10^{-7} watts/sq cm	0.442×10^{-7} watts/sq cm
290	77	2.58×10^{-4}	6.65×10^{-7}	2.58×10^{-4}	1.52×10^{-4}
1000	290	0.129	4.97×10^{-4}	0.129	0.0812
BOTH SURFACES IRON					
500	290	1.4×10^{-2}	1×10^{-3}	13×10^{-3}	8.82×10^{-3}
1000	290	0.4	0.0013	0.4	0.195
1000	500	0.44	0.016	0.424	0.322
SURFACE 1 IRON — SURFACE 2 GOLD					
290	77	3.147×10^{-4}	1.2×10^{-6}	3.14×10^{-4}	1.68×10^{-4}
1000	290	0.1733	6.74×10^{-4}	0.172	0.1
SURFACE 1 GOLD — SURFACE 2 STAINLESS 18-8					
290	77	6.35×10^{-4}	10^{-6}	6.34×10^{-4}	5.5×10^{-4}
1000	290	0.258	10^{-3}	0.257	0.22

Fig. 3 — Radiation emitted by plate 1 that is absorbed by plate 2.

re_1, and re_2. As is indicated by the examples in Table I, Fig. 3 can be used to determine the net radiation, $q_{1\rightarrow 2} - q_{2\rightarrow 1}$, between any two similar or dissimilar parallel infinite metal plates. The choice of the ordinate in Fig. 3 was arbitrary. The choice of $\sigma T^{4.5}$ in the denominator removed part of the dependence of emissivity on temperature and resulted in an ordered family of curves.

2.2 Emissivities

An expression similar to (4) can be developed for the total hemispherical emissivity of a perfectly smooth, clean metal surface:

$$\epsilon_h = \frac{1}{E(bb,T)} \int_0^\infty \int_0^{\pi/2} \epsilon(\theta,\lambda) E(bb,\lambda,T) \sin 2\theta \, d\theta \, d\lambda. \qquad (5)$$

This equation was also evaluated for seven metals at various temperatures; the results, depicted in Fig. 4, agree very well with empirical equations (based on electromagnetic theory predictions) that have been applied over specific ranges of reT.[1,2]

Available experimental emittance values for polished metal surfaces are generally from one to three times the computed values. Slight imperfections and oxides on the actual surfaces could account for the variances. Most of the available copious data were taken at pressures above 10^{-6}
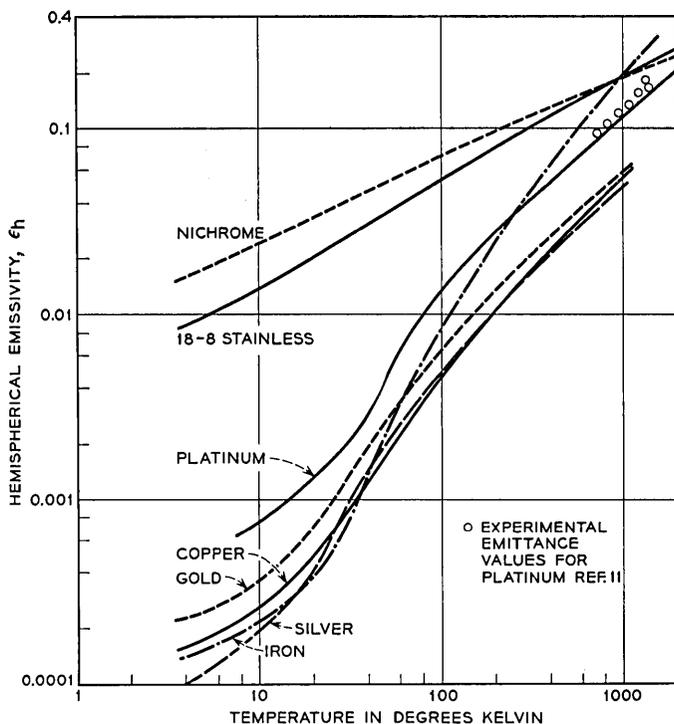
Fig. 4 — Computed total hemispherical emissivities.

Torr, and the samples were not prepared in high vacuum. The results of a recent intensive experimental investigation[11] are in good agreement with the computed values for platinum as shown in Fig. 4. Apparently these investigators chose platinum for their tests because of good surface stability compared with other metals.

The "emittance" of a surface is taken to be equal to the "emissivity" when the surface is opaque, optically flat, and identical to the interior of the material.[11]

Below about 20 degrees K, the resistivity of the materials considered approaches a residual value. This is more noticeable with pure metals than in alloys, and is reflected in the emissivity values in Fig. 4.

The values in Fig. 4 should be applied with qualification to surfaces at very low temperatures, because of the increased importance of the anomalous skin effect which was not considered here. The anomalous skin effect theory indicates that the skin resistance, instead of the bulk resistivity, becomes important in absorption and reflection for the

longer wavelengths (approaching those of diffusely behaving microwaves) that are effective in thermal radiation at extremely low temperatures. At the present time, there is considerable uncertainty concerning the nature of thermal radiation between surfaces below 100°K. This is primarily due to difficulties in taking measurements and to conflicting results. Also, recent evidence suggests that the diffuse or specular nature of a metallic surface at low temperatures may be strongly dependent upon both the temperature of the surface and the wavelength of the incident radiation.[12, 13]

The resistivity of nichrome is nearly constant over the range of temperature considered; thus the slope of the curve for nichrome in Fig. 4 is due only to the temperature dependence of the emissivity in the evaluation that was made. A converse example would be the large change in resistance at a certain temperature during the quantum transition of a superconductor to the superconducting state. The classical expressions solved here predict perfect reflection for the superconducting state, but they would not necessarily be expected to be applicable. In the visible region, no change in reflection has been reported during the superconducting transition; however, an increase in reflection has been reported for frequencies less than the superconducting energy gap frequency (on the order of 3×10^{11} cycles per second).

Equations 4 and 5 can also be readily solved for a particular wavelength or for a particular radiant energy distribution other than the Planckian spectral distribution used here.

Directional and normal emissivity values were also obtained by evaluating (5) for specific values of θ. An exemplary case is given in Fig.

DIRECTIONAL EMISSIVITY, $\epsilon(\theta)$

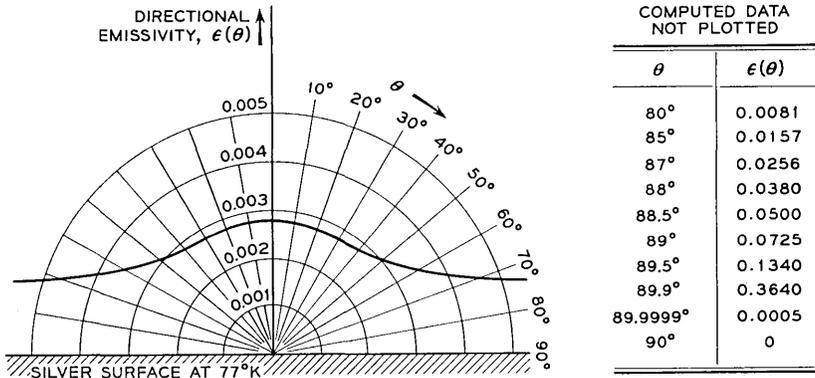| COMPUTED DATA NOT PLOTTED	
θ	$\epsilon(\theta)$
80°	0.0081
85°	0.0157
87°	0.0256
88°	0.0380
88.5°	0.0500
89°	0.0725
89.5°	0.1340
89.9°	0.3640
89.9999°	0.0005
90°	0

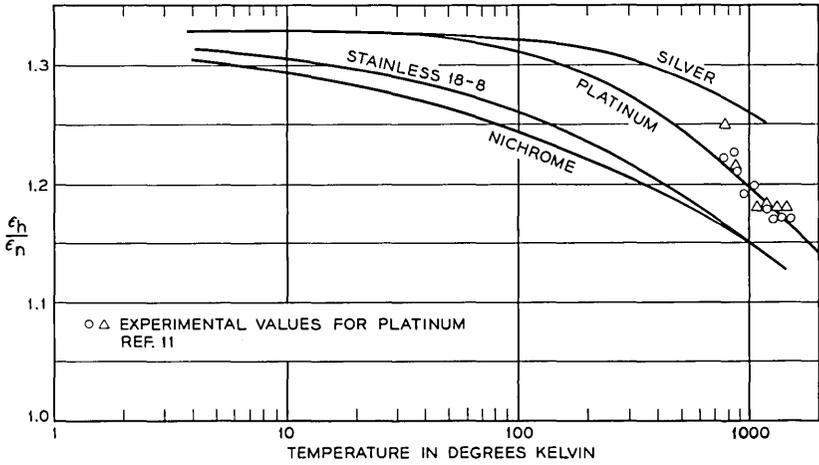Fig. 5 — An example of the directional emissivities computed.

Fig. 6 — Ratio of total hemispherical to total normal emissivity.

5. The ratio ϵ_h/ϵ_n was found to approach the theoretical limiting value of $\frac{4}{3}$ (Ref. 2) using the values computed for the low resistivity metals at very low temperatures, as shown in Fig. 6.

All of the computed values for all of the metals considered are normalized to one curve in Fig. 7. An approximation to the theoretical expression evaluated here and some recent experimental results are included in Fig. 7 for comparison. The departure of a real surface from the
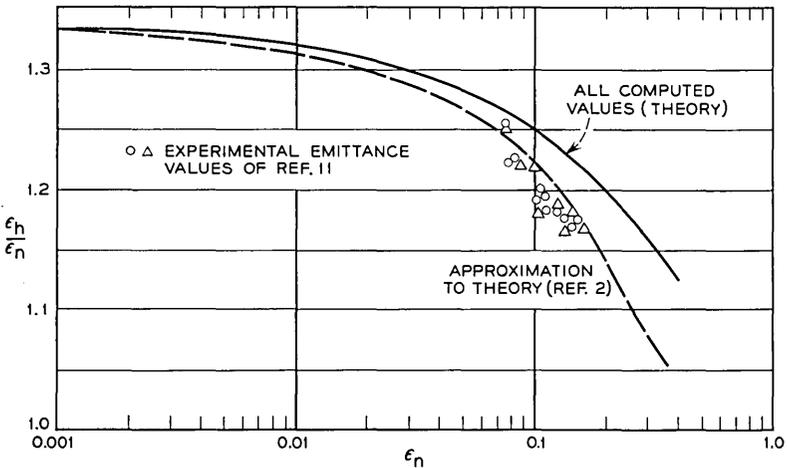

Fig. 7 — Ratio of total hemispherical to total normal emissivity.

ideal optical flat surface and the change in actual surface resistivity from the bulk value would be expected to make the experimentally measured emissivity ratio ϵ_h/ϵ_n lower than would be theoretically predicted.[11]

The computed values of hemispherical emissivity were used in evaluating Christiansen's equation for the net radiant heat transfer between parallel, diffuse, gray surfaces of infinite extent. Christiansen's equation may be written as:[2]

$$q_{net} = \frac{\sigma[T_1{}^4 - T_2{}^4]}{1/\epsilon_{h_1} + 1/\epsilon_{h_2} - 1} .$$

The results for several cases are tabulated in Table I for comparison with the computed examples for net specular radiation. The corresponding values computed for the net specular radiant heat transfer are larger. This may be attributed to the angular and spectral effects. Goodman[14] compared Christiansen's equation with values computed from experimental spectral emissivities for aluminum and Inconel at temperatures of 400°C to 1000°C. The spectral results were 2 per cent to 29 per cent greater than the values predicted by Christiansen's equation.

III. CONCLUSIONS

The radiant heat transfer between any two parallel, specular, infinite, uniform, metal plates was determined and is expressed in terms of only the temperatures and electrical resistivities in Fig. 3. The results exceed the predictions of Christiansen's equation for diffuse radiation between parallel gray plates of infinite extent. Christiansen's equation was evaluated using the computed emissivity values.

Both the radiant heat transfer and the emissivity values presented represent limiting values that can be expected for perfectly clean, smooth metallic surfaces. The results should be very useful in interpreting data and in estimating values where adequate data are lacking.

The solutions presented can be readily evaluated with the aid of a computer to obtain any additional radiant heat transfer and emissivity values that might be of particular interest.

APPENDIX

Nomenclature

$\alpha(\theta,\lambda)$	monochromatic directional absorptivity
$\epsilon(\theta,\lambda)$	monochromatic directional emissivity

ϵ_h total hemispherical emissivity

ϵ_n total normal emissivity

θ direction angle with respect to a normal to the surface

λ wavelength in centimeters

$d\omega$ element of solid angle: $\sin \theta \, d\theta \, d\varphi$ where φ is the azimuth angle

$E(bb,\lambda,T)$ monochromatic emissive power of a black body at temperature T:

$$\frac{3.7404 \times 10^{-12}}{\lambda^5 \left[\exp \left(1.4387/\lambda T\right) - 1\right]} \text{ watts/cm}^2$$

$E(bb,T)$ emissive power of a black body: σT^4 where $\sigma = 5.6699 \times 10^{-12}$ watts/cm^2 °K^4

$I(bb,\lambda,T)$ monochromatic areal radiant intensity of a black body at temperature T:

$$\frac{E(bb,\lambda,T)}{\pi}$$

re electrical resistivity ohm-cm.

REFERENCES

1. Eckert, E. R. G. and Drake, R. M., *Heat and Mass Transfer*, McGraw-Hill, New York, 1959, pp. 355-381.
2. Jakob, M., *Heat Transfer*, Vol. I, John Wiley, New York, 1949, pp. 34-52; also Vol. II, 1959, pp. 3-89.
3. *Advances in Cryogenic Engineering*, Vol. 2, Plenum Press, New York, 1956, paper B1, p. 56, paper B2, p. 62.
4. Scott, R. B., *Cryogenic Engineering*, D. Van Nostrand, Princeton, 1959.
5. *Smithsonian Physical Tables*, 9th ed., 1954, Publ. 4169, Smithsonian Institute, Washington, D. C.
6. *Handbook of Chemistry and Physics*, 40th ed., 1958, Chemical Rubber, Cleveland, pp. 2956-2958.
7. *Advances in Cryogenic Engineering*, Vol. 1, Plenum Press, New York, 1954, paper D3.
8. White, G. K., *Experimental Techniques in Low-Temperature Physics*, Oxford, 1959.
9. *Encyclopedia of Physics*, XV, 1956, p. 191, Springer-Verlag, Berlin.
10. Physical Properties of Metals and Alloys, ASTM special pub. no. 296, Phila, Pa., 1960.
11. Total Normal and Total Hemispherical Emittance of Polished Metals, WADD 61-94. AD 270 470, Nov. 1961.
12. Cline, D., Infrared Wavelength Dependence of the Total Absorptivity of Electroplated Silver, J. Appl. Physics, **33**, 1962, p. 2310.
13. Rayne, J. A., Temperature Dependence of the Absorptivity of Copper in the Near Infrared, Phys. Rev. Letters, **3**, 1959, p. 512.
14. Goodman, S., Radiant-Heat Transfer between Nongray Parallel Plates, Jour. of Res., (N.B.S.), **58**, 1957, p. 37.

Contributors to This Issue

W. E. BALLENTINE studied at Rutgers University and Polytechnic Institute of Brooklyn, and joined Bell Telephone Laboratories in 1954. At Bell Laboratories he has worked on the development of transistor circuits for analog-to-digital converters and on high-speed pulse systems, and has also engaged in the development of a solid-state microwave receiver. More recently he was concerned with the design of the 90-mc IF amplifier used in the experimental Telstar satellite.

L. RAY BOWYER, B.S., 1957, Colorado University; M.E.E., 1959, New York University; Bell Telephone Laboratories, 1957—. Mr. Bowyer was first engaged in work on data processing. Later he worked on automatic data subsets for air line communications. He also was engaged in systems engineering for a communication system for wide-area data service. At present he is in charge of a group responsible for the design of portions of the B1 data trunking system for wide-area data service. Member I.R.E., Tau Beta Pi, Eta Kappa Nu, Sigma Tau.

ROSEMARY GEYNET, A.B., 1947, Pennsylvania State University; Bell Telephone Laboratories, 1953—. Miss Geynet's work has included carrying out computer logic circuit analyses and writing various circuit design programs. At present she is engaged in the solution of various analyses, particularly problems requiring special programming techniques for digital solutions.

RICHARD J. GROSH, B.S., 1950, M.S., 1952, Ph.D., 1953, Purdue University; Head of School of Mechanical Engineering, Purdue University; Bell Telephone Laboratories consultant, 1958—. Mr. Grosh has been engaged in a variety of thermal radiation problems at both high and low temperatures. Sigma Xi Research Society, Pi Tau Sigma, Tau Beta Pi.

WILBUR H. HIGHLEYMAN, B.E.E., 1955, Rensselaer Polytechnic Institute; M.S., 1957, Massachusetts Institute of Technology; D.E.E., 1961, Polytechnic Institute of Brooklyn; Bell Telephone Laboratories, 1958–1962; Data Trends, 1962—. At the Laboratories he first engaged

in the problem of character recognition. More recently, he was concerned with the development of data communication equipment and the study of new devices and techniques for data communication problems. He presently serves as a lecturer at the Polytechnic Institute of Brooklyn. Member Tau Beta Pi, Eta Kappa Nu, Sigma Xi, I.R.E.

VERNON EMERSON HOLT, B.S., 1951, M.S., 1958, and Ph.D., 1960, South Dakota School of Mines, North Carolina State College, and Purdue University; Bell Telephone Laboratories, 1961—. Mr. Holt has been engaged in the development of thin film superconductors for use in high-speed computer circuitry. This work involves low-temperature physics at liquid helium temperatures. Sigma Xi Research Society, Sigma Tau, Pi Tau Sigma, Phi Kappa Phi.

JAY CHIEN-HWAI HSU, B.E.E., 1957, M.E.E., 1958, Ph.D., 1961, Cornell University; Bell Telephone Laboratories, 1961—. Mr. Hsu has been working on a research project on digital-computer controlled systems and is at present also involved with satellite attitude control problems. Member I.R.E., Sigma Xi.

JOHN T. KENNEDY, B.E. in Electrical Engineering, 1949, Yale University. While with the Western Electric Company from 1950–1960 he worked at Bell Telephone Laboratories and with various Air Force wings in bombing-navigational radar system development. In 1960 he joined the staff of Bell Telephone Laboratories, where he has been engaged in development of command radio-guidance systems.

B. K. KINARIWALA, B.S., 1951, Benares University (India); M.S., 1954, and Ph.D., 1957, University of California; Bell Telephone Laboratories, 1957—. He was first engaged in research in circuit theory involving, in particular, active and time-varying networks. More recently, he has been concerned with problems in digital communication systems. Member I.R.E., Sigma Xi.

E. J. MCCLUSKEY, JR., A.B., 1953, Bowdoin College; B.S., 1953, M.S., 1953, and Sc.D., 1956, Massachusetts Institute of Technology; Bell Telephone Laboratories 1955–1959. At Bell Laboratories Mr. McCluskey was engaged in research and consulting in connection with the design of electronic central offices. Member I.R.E., Association for Computing Machinery, Associate Editor, I.R.E. Transactions on Electronic Computers. Presently at Princeton University as Associate

Professor of Electrical Engineering and Director of the University Computer Center.

SPENCER W. ROBERTS, B.S.E. (E.E.) and B.S.E. (Mathematics), 1947, M.S., 1948, University of Michigan; Bell Telephone Laboratories, 1952—. Mr. Roberts is engaged in studies of statistical aspects of quality assurance. Member American Statistical Association, Institute of Mathematical Statistics, Tau Beta Pi, Sigma Xi, Phi Kappa Phi.

J. W. ROSSON, B.S.E.E., 1951, M.S.E.E., 1953, Texas Technological College; Bell Telephone Laboratories, 1953—. Mr. Rosson was first engaged in development work on military data-transmission systems, and also in circuit development work for guided missiles. Later he was engaged in mathematical work using digital and analog computers and on circuit design for missile-borne equipment. At present he is concerned with ICBM and space guidance analysis. Member I.R.E., Kappa Mu Epsilon.

VEIKKO R. SAARI, B.S., 1951, M.S., 1956, University of Minnesota, and M.E.E., 1959, New York University; Bell Telephone Laboratories 1956—. Mr. Saari was first engaged in exploratory development work on transistor multiple-loop feedback amplifiers. He later worked on high-frequency transistor circuitry and low-drift amplifiers, including IF and video amplifiers, compressing amplifiers and dc amplifiers for analog-to-digital encoders. More recently, he has been concerned with the design of solid-state circuitry for the TL microwave system and of the command receiver of the experimental Telstar satellite. Member I.R.E., American Association of Physics Teachers, National Committee of 1963 International Solid-State Circuits Conference.

FRANCIS J. WITT, B.S.E.E., 1953, M.S.E.E., 1955, Johns Hopkins University; Bell Telephone Laboratories, 1954-55, 1957—. At Bell Laboratories Mr. Witt has engaged in active and sampled-data network exploratory research and in solid-state circuit development for short-haul carrier systems. Later he was in charge of a group responsible for the development of some of the solid-state circuits in the Telstar experimental communications satellite. At present he is concerned with the development of digital processing circuitry for a high-speed PCM transmission system. Member I.R.E., National Committee of 1963 International Solid-State Circuits Conference, Tau Beta Pi, Sigma Xi.